Advanced Insights into the Regenerative Limits, Molecular Identities, and Functional Necessity of Vestibular Hair Cell Subtypes in the Adult Mouse Vestibular System

Amanda Nichole Ciani

A dissertation

submitted in partial fulfillment of the

requirements for the degree of

Doctor of Philosophy

University of Washington

2025

Reading Committee:

Jennifer Stone, Chair

James Phillips

David Raible

Program Authorized to Offer Degree:

Speech and Hearing Sciences

University of Washington

Abstract

Advanced Insights into the Regenerative Limits, Molecular Identities, and Functional Necessity of Vestibular Hair Cell Subtypes in the Adult Mouse Vestibular System

Amanda Nichole Ciani

Chair of the Supervisory Committee:

Jennifer Stone

Department of Otolaryngology

Vestibular hair cells are specialized mechanosensory receptors in the inner ear that detect head movements and gravitational forces to support balance, gaze stabilization, and spatial orientation (Hudspeth, 1997; Corey & Hudspeth, 1983; Gillespie & Müller, 2009). In adult mammals, these cells are vulnerable to damage from aging, ototoxic drugs, and genetic mutations, and they have limited regenerative abilities (Forge et al., 1993; 1998; Kawamoto et al., 2009; Golub et al., 2012; Bucks et al., 2017; Sayyid et al. 2019; Hicks et al., 2020; Ciani Berlingeri et al., 2022; Jauregui et al. 2024) compared to those in non-mammalian vertebrates such as birds and fish (Corwin & Cotanche, 1988; Ryals & Rubel, 1988; Ma et al., 2008). It is likely that humans also have some capacity for hair cell regeneration (Taylor et al., 2018). This limited regenerative capacity contributes to persistent vestibular dysfunction and balance impairment following hair cell loss (Agrawal et al., 2009; Hicks et al., 2020). Although a few studies have shown partial recovery of function, the newly formed hair cells do not fully compensate for the loss of vestibular function (Schlecker et al., 2011; Sayyid et al., 2019; Bremer et al., 2014). Many questions arise from these previous results. Why are only some type II hair cells regenerated? What is

needed for functional regeneration? These and many other questions drive my work into the adult vestibular system.

In this thesis, I investigated the molecular, functional, and regenerative properties of vestibular hair cells in adult mice. Using a conditional knockout model, I show that the transcription factor SOX2, previously implicated in sensory development (Kiernan et al., 2005; Neves et al., 2012), is required in adult vestibular supporting cells for the limited regeneration of hair cells following hair cell loss. *Sox2*-deficient supporting cells failed to transdifferentiate into new hair cells, resulting in markedly reduced regeneration across the utricle, saccule, and ampulla (Ciani Berlingeri et al., 2022). Although we now know *Sox2* and *Atoh1* (Hicks et al., 2020) are necessary for the limited number of regenerated hair cells and that these cells come from supporting cells, the lack of regeneration of all the rest of the hair cells does not occur. This led to my exploration into the different types of cells in the adult vestibular sensory epithelia. Maybe there are more cell types than we think.

To define the molecular identity of vestibular hair cell subtypes, I performed single-nucleus RNA-sequencing on adult mouse utricles. This transcriptomic profiling revealed five molecularly distinct hair cell subtypes spanning the classically defined type I and type II hair cell types across different epithelial zones. Markers such as *Calb2, Spp1, Ocm*, *Agbl1, Paqr9,* and others distinguished these subtypes (Xia et al., 2025; Desai et al., 2005; Simmons et al., 2010; Dechesne et al., 1988), and expression patterns were validated through immunolabeling and fluorescent in situ hybridization. The findings expand upon previous efforts by defining hair cell heterogeneity in the adult utricle at single-cell resolution and identifying novel molecular markers specific to regional and subtype identity through analysis of thousands of adult cells (McInturff et al., 2018, Xia et al., 2025). These molecular differences could result in functional differences. Therefore, while analyzing these cells molecularly, I also investigated the functional requirements of one population of vestibular hair cells.

I employed a selective genetic ablation strategy to remove peripheral type I hair cells in all vestibular organs in adult mice while preserving central type I and all type II populations using a recently generated mouse line (McGovern et al., 2022; Hartman et al., 2018). This loss caused severe and lasting deficits in balance and vestibulo-ocular reflex performance, highlighting the unique and non-redundant role of peripheral type I hair cells in dynamic vestibular function.

Altogether, this work identified *Sox2* as a key regulator of supporting cell driven hair cell regeneration, revealed new molecular markers and subtype distinctions in adult vestibular hair cells, as well as identified the critical role of peripheral type I hair cells in maintaining complex vestibular reflexes. These findings add to the foundation for regenerative strategies aimed at restoring vestibular function after injury or degeneration.

Dedications

To my parents, whose unwavering love and curiosity first taught me to ask “why”;
to my partner, Elliot, whose patience and humor kept me balanced when the data did not;
and to every mentor who reminded me that small discoveries, stacked patiently, become insight.

Acknowledgements

This dissertation would not exist without the guidance of my advisor, Dr. Jennifer Stone, and the thoughtful critique of my committee. Their collective wisdom shaped each chapter and sharpened my scientific judgment.

I am deeply grateful to the collaborators who opened both their labs and their minds to this work—Dr. Sarath Vijayakumar, Mi Zhou, Dr. Litao Tao, Dr. Neil Segil, and again Dr. Stone—for the long Zoom calls, shared code, and spirited debates that powered our transcriptomic study. Special thanks to Brandon Cox and Rémy Pujol, whose earlier partnership on Sox2-regeneration experiments laid the foundation for Chapter 2.

Many hands made the science possible day-to-day. I gratefully acknowledge Jialin Shang, Tot Nguyen, Ingrid Bibriesca, Hanna Shin, Irina Omelchenko, Serena Wisner, and Ed Parker at the University of Washington for technical assistance and other contributions, as well as the Tao Lab at Creighton University for our ongoing collaboration. Access to UW’s Core Vision Lab (supported by P30 EY01730) and its JEOL transmission electron microscope was indispensable for ultrastructural work. I also thank Kaley Graves, Chantz Pinder, Luyi Zhou, Jarnail Singh, and Deborah Hamilton at Southern Illinois University School of Medicine for their generous help.

This research was supported by NIH DC014441 (Cox), Office of the Assistant Secretary of Defense for Health Affairs Grant W81XWH-15-1-0475 (Cox), NIH R01 DC013771 (Stone), NIH DC013771-S (Ciani), Auditory Neuroscience Training Grant T32DC005361, F31 DC020060 (Ciani), and Virginia Merrill Bloedel Hearing Research Center Visiting Scholar Awards (Pujol). Additional support came from the Hamilton and Mildred Kellogg Charitable Trust and The Whitcraft Family.

To the members of the Stone Lab and the Bloedel Research Center: thank you for every troubleshooting session, mouse ear, and training technique. The animal-care staff, IACUC coordinators, and the UW Imaging Core kept our experiments humane and our images beautiful; your behind-the-scenes excellence is appreciated daily.

I offer my deepest respect and gratitude to the mice that made this research possible. Their silent contribution, each vestibular system, brain, and behavioral trial, advanced our understanding of balance and hearing in ways words cannot fully capture. Every data point represents a living being whose sacrifice demands that we pursue and apply this knowledge responsibly, always striving to reduce, refine, and replace animal use whenever we can. Their legacy lives on in the insights gained and the future therapies these findings may inspire.

Finally, to my friends and family who cheered each small victory and forgave every missed holiday: your belief in me mattered most. This thesis is as much yours as it is mine.

Table of Contents

Chapter 1: Key Questions About the Vestibular System Addressed in This Thesis

Introduction

In mammals, five vestibular organs sense head motions in a variety of directions and frequencies using specialized mechanosensory receptors called hair cells. The vestibular system includes the otolith organs (utricle and saccule) and cristae ampullari located within the inner ear labyrinths, as well as the vestibular nerve central connections and peripheral mechanisms. The inner ear has ten sensory patches within the vestibular end organs, including the left and right sides. These sensory patches, composed of sensory hair cells and non-sensory supporting cells, are located within the utricles, saccules, and ampullae of the semicircular canals. Together, these sensory organs work harmoniously to provide the brain with information about head position, movement, and spatial orientation, allowing for the coordination of motor responses to maintain balance and stability. Hair bundles are specialized organelles located on the top of each hair cell that defect in response to head motions. Directional deflection elucidates variable potassium entry into the cell, and its membrane voltage (receptor potential) increases, leading to neurotransmission across the hair cell-vestibular ganglion neuron (VGN) synapse, increasing the neuron's firing rate. VGN (afferent) projections to the brainstem and cerebellum alter the activity of neurons in those regions, helping to control the movements of the eyes, neck, and limbs, and enable navigation, balance, and spatial orientation in a variety of conditions.

Hair Cell Damage and Limited Regeneration in the Vestibular System

Vestibular hair cells, like their auditory counterparts, can be lost due to aging, genetic mutations, ototoxic drugs, noise exposure, or infections (Rosenhall & Rubin, 1975; Gleeson & Felix, 1987; Sedó-Cabezón et al., 2015). In humans and other mammals, hair cell loss accumulates with age: studies have documented a progressive decline in vestibular hair cell numbers in older adults (Rauch et al., 2006; Taylor et al., 2015, 2018). Similar age-related hair cell degeneration has been observed in rodents (Park et al., 1987; Nakayama et al., 1994), although strain differences exist, and at least one study reported preservation of hair cells with synaptic changes instead (Wan et al., 2019). The loss of vestibular hair cells correlates with functional deficits such as impaired balance, dizziness, and unstable gaze, and likely contributes to

increased fall risk, particularly in the elderly (Iwasaki & Yamasoba, 2015; Agrawal et al., 2009; Jones & Jones, 2014).

Unlike the inner ears of non-mammalian vertebrates (e.g., birds and fish), which can robustly regenerate lost hair cells, the adult mammalian vestibular system has only a limited capacity for spontaneous hair cell regeneration. When vestibular hair cells are destroyed in adult rodents, only a fraction regenerate over time – on the order of ~20% of the original hair cell population at best (Forge et al., 1993, 1998; Golub et al., 2012; Slowik & Bermingham-McDonogh, 2013). Notably, this natural regeneration in mammals appears to produce exclusively type II hair cells. There is essentially no spontaneous replacement of type I hair cells in adult mice and guinea pigs (Bucks et al., 2017; Hicks et al., 2020; Sayyid et al., 2019; Wang et al., 2019; González-Garrido et al., 2021). Consequently, the limited hair cell recovery that does occur is insufficient to restore normal vestibulo-motor function (Taylor et al., 2018; Hicks et al., 2020). In fact, evidence from other animal studies suggests that regeneration of type I hair cells may be a critical requirement for full functional recovery. In birds, where both type I and II hair cells regenerate, restoring type I hair cells has been shown to be tightly correlated (temporally) with complete recovery of the vestibulo-ocular reflex (VOR), which stabilizes gaze during head motion (Carey et al., 1996; Zakir & Dickman, 2006; Haque et al., 2008). In mammals, recent findings similarly indicate that, when type I hair cells survive an insult or are experimentally preserved, vestibular reflexes like the VOR recover better, whereas the absence of type I cells is associated with persistent deficits (Jáuregui et al., 2024). These observations help explain the poor functional recovery after mammalian vestibular damage: if type I hair cells are not regenerated, certain vestibular functions cannot be regained. This background provides a strong impetus for research aiming to promote regeneration of type I hair cells (in addition to type II) as a strategy to restore vestibular function after injury or in degenerative conditions.

Vestibular hair cell regeneration in adult mammals, though limited, occurs via the transdifferentiation of supporting cells into new hair cells. Supporting cells are the nonsensory epithelial cells that surround hair cells and play crucial roles in maintaining the ionic and structural environment of the sensory organ (Wan et al., 2013; Burns & Corwin, 2014). After hair cell loss, some supporting cells in vestibular epithelia directly convert into hair cells without dividing – a process documented in vestibular organs of mature

rodents (Forge et al., 1993; Kawamoto et al., 2009; Golub et al., 2012, Hicks et al., 2020, Ciani Berlingeri et al., 2022). There is minimal mitotic (proliferative) activity in adult vestibular sensory epithelia in vivo, although limited supporting cell proliferation has been observed under certain conditions, such as in neonatal mice or in cultured organs (Warchol et al., 1993; Burns et al., 2012). The new hair cells generated in adult rodent vestibular organs are produced by these residual supporting cells (Lin et al., 2011; Slowik & Bermingham-McDonogh, 2013; Bucks et al., 2017; Hicks et al., 2020; Ciani Berlingeri et al., 2022). Given that the default regeneration yields only type II-like hair cells, a key question is what molecular factors within supporting cells facilitate the production of new hair cells and particularly whether those factors could be modulated to encourage type I hair cell formation. Understanding the molecular cues that govern supporting cell-to-hair cell conversion is critical for devising therapies to enhance inner ear regeneration. The second chapter of this thesis presents my published work analyzing the requirement of the transcription factor Sox2 in supporting cells for normal levels of type II hair cell regeneration (Ciani Berlingeri et al., 2022). This study provided the first evidence for this critical role of *Sox2* as well as insights into what is needed for the default regeneration that occurs in adult mice.

Molecular Landscape of Vestibular Hair Cells

Despite molecular differences, vestibular hair cells – type I and type II – have been distinguished by their morphology, innervation, and physiology (Eatock & Songer, 2011; Burns & Stone, 2017). Type I hair cells have a flask-like shape and are enveloped by a calyx afferent terminal, supporting rapid, non-quantal synaptic transmission (Contini et al., 2012, 2020; Eatock, 2018), whereas type II hair cells are more cylindrical and contacted by bouton-type afferents and efferent fibers (Desai et al., 2005a, b; Fernández et al., 1988; Goldberg et al., 1990). The distinct functional roles of type I and II hair cells are likely rooted in differences at the molecular level. However, only a few markers, such as calretinin or calbindin 2 (CALB2) for type II cells (Desmadryl and Dechesne, 1992; Leonard and Kevetter, 2002; Desai et al. 2005a, 2005b; Hoffman et al. 2018) and osteopontin (SPP1) for type I cells (McInturff et al. (2018) have been known to distinguish these cell types (Burns & Stone, 2017; Bucks et al., 2017). A comprehensive report of their molecular profiles has been lacking.

Recent advances in genetic sequencing now allow cell-type-specific transcriptomic and epigenomic profiling, offering an opportunity to define the gene expression programs and regulatory DNA elements that distinguish vestibular hair cell types (Jan et al., 2021; Jen et al., 2019; McInturff et al., 2018). I leveraged single-nucleus sequencing approaches to create a molecular atlas of mature vestibular hair cells. Specifically, in collaboration with colleagues from the lab of Dr. Litao Tao, we performed single-nucleus RNA sequencing (snRNA-seq) on adult mouse utricles. This approach captured the transcriptomic landscape of individual hair cells, enabling the identification of cell type specific genes in type I versus type II cells in different regions of the utricle. This dataset will be published in its entirety and provides a valuable resource for understanding gene regulation in vestibular epithelia, offering molecular targets for the generation of tools and regenerative therapies in our field. Overall, this profiling of vestibular hair cells establishes a baseline for comparing normal mature hair cells to those in pathological or regenerating states. Chapter 3 of this thesis presents this investigation into the molecular identities of adult mouse utricular hair cells. Specifically, our study makes available a novel, rigorous snRNAseq dataset for adult mammalian vestibular hair cells, filling a gap from young adult mouse snRNAseq data.

Vestibular Hair Cells: Types and Functional Roles

Within all of the vestibular sensory epithelia (the cristae of the semicircular canals and the maculae of the otolith organs), hair cells are organized into central (striolar) and peripheral (extrastriolar) zones that differ in afferent nerve properties (Desai et al., 2005b; Fernández et al., 1988; Curthoys et al., 2006). Calyx-only afferents innervate mostly central-zone type I cells, tend to fire irregularly at rest, and are particularly sensitive to rapid head movements (Goldberg et al., 1990; Eatock, 2018; Sadeghi et al., 2007). In contrast, bouton-only afferents innervate primarily peripheral-zone type II cells and fire more regularly (Baird et al., 1988; Goldberg et al., 1990). These anatomical and physiological specializations, as well as the molecular differences found in our snRNAseq study, suggest that different subtypes of type I and type II hair cells could play distinct roles in vestibular functions (such as the VOR or tasks that require balance and coordination). However, the specific contributions of each hair cell type have been difficult to parse because most primary vestibular afferents (termed “dimorphic”) contact both cell types (Eatock & Songer,

2011; Burns & Stone, 2017; Jamali et al., 2016). As a result, defining the functional role of each hair cell type has required creative experimental approaches.

Recent studies have begun to address this knowledge gap by selectively targeting hair cell subpopulations. In my work, I focused on determining the specific contributions of peripheral type I hair cells in adult mammalian vestibular organs to motor activities that require the vestibular system. This is the first study to selectively ablate type I hair cells in any sensory organ in adult mice. Previous experimental approaches relied on full vestibular or zone-specific ablation, rather than targeting particular cell types, yielding only general insights into vestibular deficits. Prior studies in mammals induced vestibular hair cell lesions by administering ototoxins such as aminoglycoside antibiotics (Xu et al., 2012; Nagato et al., 2018 ;Kim et al., 2005; Monzack et al., 2015; Kawamoto et al., 2009) and IDPN (iminodipropionitrile- Llorens and Dememes 1994; Zeng et al., 2020; Matrins-Lopes et al., 2019),-cisplatin (Kim et al., 2008; Monzack et al., 2015; Callejo et al., 2017), or injecting diphtheria toxin in *Pou4f3*^{DTR} mice (Golub et al., 2012; Hicks et al., 2020; Ciani Berlingeri et al., 2022) , but these methods cause widespread loss without specifically targeting type I cells in a given zone and also led to type II hair cell destruction. Other studies have disrupted neural activity in the central or striolar zone using another approach beside hair cell killing. For instance, in monkeys, inactivating central calyx-bearing afferents had minimal effect on the VOR (Minor & Goldberg, 1991), whereas in mice, eliminating the central-zone altogether led to significantly increased thresholds of central neural responses to fast head-motions (Ono et al., 2020). These approaches addressed the significance of vestibular hair cells and respective epithelial zones but could not resolve the individual contributions of type I versus type II cells.

To directly test the contribution of type I hair cells, I developed a targeted ablation model using an *Fbxo2*^{CreERT2} driver (McGovern et al., 2022) crossed with a stop-floxed diphtheria toxin A allele to specifically eliminate type I hair cells in the peripheral zones of all vestibular organs in adult mice. Chapter 4 reviews the results of this ablation study. Our results, in combination with previous studies, demonstrate the importance of vestibular hair cells and their subtypes.

Chapter 2: *Sox2* is required in supporting cells for normal levels of vestibular hair cell regeneration in adult mice

Authors: Amanda N. Ciani Berlingeri[1,2], Brandon C. Cox[3], Rémy Pujol[4], Jennifer S. Stone[2]

[1]Department of Speech and Hearing Sciences, University of Washington, Seattle, Washington

[2]Department of Otolaryngology-Head and Neck Surgery and the Virginia Merrill Bloedel Research Center, University of Washington School of Medicine, Seattle, Washington

[3]Departments of Pharmacology and Otolaryngology, Southern Illinois University School of Medicine, Springfield, Illinois

[4] University of Montpellier, INM-INSERM Unit 1298, Montpellier, France

Note: This chapter was published: Ciani Berlingeri, A. N., Pujol, R., Cox, B. C., & Stone, J. S. (2022). Sox2 is required in supporting cells for normal levels of vestibular hair cell regeneration in adult mice. *Hearing Research*, *426*, 108642. https://doi.org/10.1016/j.heares.2022.108642

Abstract

SOX2 is a transcription factor that is necessary in the mammalian inner ear for development of sensory hair cells and supporting cells. Sox2 is expressed in supporting cells of adult mammals, but its function in this context is poorly understood. Given its role in the developing inner ear, we hypothesized that *Sox2* is required in vestibular supporting cells for regeneration of type II hair cells after damage. Using adult mice, we deleted *Sox2* from *Sox9-Cre^{ER}*-expressing supporting cells prior to diphtheria toxin-mediated hair cell destruction and used fate-mapping to assess regeneration. In utricles of control mice with normal *Sox2* expression, supporting cells regenerated nearly 200 hair cells by 3 weeks post-damage, which doubled by 12 weeks. In contrast, mice with *Sox2* deletion from supporting cells had approximately 20 fate-mapped hair cells at 3 weeks post-damage, and this number did not change significantly by 12 weeks, indicating regeneration was dramatically curtailed. We made similar observations for saccules and ampullae. We found no evidence that supporting cells lacking *Sox2* had altered cellular density, morphology, or ultrastructure. However, some Sox2-negative supporting cell nuclei appeared to migrate

apically but did not turn on hair cell markers, and type I hair cell survival was higher. *Sox2* heterozygotes also had reduced regeneration in utricles, but more hair cells were replaced than mice with *Sox2* deletion. Our study determined that *Sox2* is required in supporting cells for normal levels of vestibular hair cell regeneration but found no other major requirements for *Sox2* in adult supporting cells.

1. Introduction

Vestibular hair cells, located in five sensory epithelia in the inner ear, are highly specialized mechanosensory cells that encode head position and motion and modulate activity of the vestibular nerve. Vestibular hair cells degenerate as we age (e.g., Rauch et al., 2006), and they can die earlier as a result of gene mutations, ototoxic drug exposure, or microbial infections (Gleeson and Felix, 1987; Rosenhall and Rubin, 1975; Sedó-Cabezón et al., 2013). In parallel, people experience vestibular deficits that can include imbalance, dizziness, gaze destabilization, and increased risk of falling (e.g., Guinand et al., 2012; Agrawal et al., 2009; Agrawal et al., 2013). Regeneration of vestibular hair cells may help to restore balance function. Some vestibular hair cell replacement seems to occur naturally in humans (Warchol et al., 1993; Taylor et al., 2015; Taylor et al., 2018), but this regeneration is highly limited and insufficient to restore vestibulo-motor function.

Although we understand little about the mechanisms that block hair cell regeneration in humans, studies in mammalian models are providing important insights. Mammals have two types of vestibular hair cell - type I and type II – with distinct morphological, physiological, and molecular features, and different patterns of innervation (reviewed in Eatock and Songer, 2011; Burns and Stone, 2017). When type I and II vestibular hair cells are destroyed in adult guinea pigs or mice, a subpopulation of hair cells is regenerated (Forge et al. 1993; Forge et al., 1998; Kawamoto et al., 2009; Golub et al., 2012; Slowik and Bermingham-McDonogh, 2013). Adult mice replace only ~20% of the hair cell population after complete hair cell destruction (e.g., Golub et al., 2012), and this natural regeneration is limited to type II hair cells (Bucks et al., 2017; Hicks et al., 2020; Sayyid et al., 2019; Wang et al., 2019; Gonzalez-Garrido et al., 2021).

Regenerated vestibular hair cells are derived from supporting cells (e.g., Lin et al., 2011; Slowik and McDonogh, 2013; Bucks et al., 2017), which are non-sensory cells that reside alongside hair cells. In

adult rodents, supporting cells form new vestibular hair cells via a non-mitotic process called direct transdifferentiation (Forge et al., 1993; Kawamoto et al., 2009; Golub et al., 2012), although some supporting cell division has been noted in mature vestibular epithelia after damage *in vitro* (e.g., Warchol et al., 1993) and in neonatal mice *in vivo* (e.g., Burns et al., 2012). Supporting cells serve many functions in the inner ear epithelia (reviewed in Wan et al., 2013). During hair cell damage, in addition to forming new hair cells, supporting cells aid in removal of damaged hair cells and repair of the sensory epithelium (e.g., Monzack et al., 2015; Bucks et al., 2017), similar to microglia in the central nervous system.

Investigators have identified a small number of molecules that regulate vestibular hair cell regeneration in mammals. One is the basic-helix-loop-helix transcription factor *Atoh1* that is required for hair cell development in mice (Bermingham et al., 1999). *Atoh1* directs the expression of many genes necessary for hair cell fate acquisition and differentiation (Cai and Groves, 2015). Deletion of *Atoh1* from supporting cells prior to hair cell damage prevents regeneration from occurring (Hicks et al., 2020). In contrast, ectopic expression of *Atoh1* in supporting cells of rodent utricles induces more new hair cell-like cells to form (Shou et al., 2004; Schleckler et al., 2011; Sayyid et al., 2019).

The SRY box transcription factor *Sox2* functions upstream of *Atoh1* and promotes its transcription during hair cell development (Neves et al., 2012; Kempfle et al., 2016; Puligilla and Kelley, 2016). In mature mice, SOX2 remains highly expressed in vestibular supporting cells and in type II hair cells (Hume et al., 2007; Oesterle et al., 2008). SOX2 serves many functions throughout the body. For instance, it regulates the differentiation of neural progenitor cells (e.g., Graham et al., 2003; Bylund et al., 2003; reviewed in Pevny and Nicolis, 2010), and in combination with other transcription factors, reprograms somatic cells into pluripotent stem cells (e.g., Takahashi and Yamanaka, 2006). During inner ear development, SOX2 specifies pro-sensory cells from non-sensory cells and is required for differentiation of both hair cells and supporting cells (Kiernan et al., 2005; Booker et al., 2006; Dabdoub et al., 2008; Steevens et al., 2019). Therefore, *Sox2* is an interesting candidate regulator of supporting cell-to-hair cell transdifferentiation in mature mammals. In support of this idea, mice that develop with reduced *Sox2* expression regenerate more cochlear hair cells after damage in the neonatal period than do mice with normal *Sox2* expression

(Atkinson et al., 2018). However, a role for SOX2 in mature vestibular epithelia in association with hair cell damage has not been tested.

We used Cre-loxP technology to conditionally delete *Sox2* from supporting cells prior to killing hair cells in adult mice, using diphtheria toxin (DT)-mediated cell death. We determined that *Sox2* is required in supporting cells to achieve normal levels of regenerated hair cells, but it is not essential for supporting cell survival or for maintenance of supporting cell-specific features in damaged vestibular organs.

2. Materials and Methods

2.1. Animals

We purchased *Sox9-CreER*^{T2} mice (stock #18829, Kopp et al., 2011), *Rosa26*$^{loxP\text{-}stop\text{-}loxP\text{-}tdTomato}$ mice (*Rosa26*^{tdTomato}, also called Ai14, stock #7914, Madisen et al., 2010), and *Sox2*^{loxP} mice (stock #13093; Shamham et al., 2009) from The Jackson Laboratory (Bar Harbor, ME). *Pou4f3*^{DTR} mice (Golub et al., 2012; Tong et al., 2015) were acquired from Dr. Ed Rubel at the University of Washington. All mice were primarily on a C57BL/6J background. Both genders were used in the study and displayed similar results.

The Southern Illinois University School of Medicine (Springfield, IL) conducted all animal procedures using approved protocols from their animal care and use committee that conform to standards of the American Veterinary Medical Association and the National Institutes of Health. Tissue samples were shipped to the University of Washington for analysis.

2.2. Drug Treatments

We injected mice at 6 weeks of age intraperitoneally (IP) with tamoxifen (Sigma-Aldrich, St. Louis, MO) at 9 mg/40 g, once a day on two consecutive days spaced 20-24 hours apart to initiate CreER activity in supporting cells. To induce hair cell damage, diphtheria toxin (List Biological Laboratories, Inc., Campbell, CA) at 25 or 50 ng/g was injected intramuscularly at 7 weeks of age (1-week post-tamoxifen) once a day on two days spaced 44-48 hours apart. We selected a DT dose for each experiment based on periodic tests of DT potency, which varied with each lot and diminished over time during storage at -20°C.

2.3. Tissue labeling

After mice were killed using overdose of carbon dioxide, temporal bones were extracted and immersion-fixed in electron microscopy grade 4% paraformaldehyde (Polysciences, Inc., Warrington, PA) overnight at room temperature. Temporal bones were stored in phosphate-buffered saline (PBS) at 4°C prior to being shipped to the University of Washington for analysis.

As described in Bucks et al. (2017), whole utricles were dissected, and the overlying membranes and otoconia were removed. Utricles were immunolabeled in 96 well plates with the following primary antibodies overnight at room temperature: goat anti-Sox2 (1:100; RRID: AB_2286684; #17320; Santa Cruz Biotechnology Inc., Santa Cruz, CA) rabbit anti-myosin VIIa (1:300, RRID:AB_10013626; #25-6790; Proteus Biosciences Inc., Ramona, CA); rabbit anti- tubulin ßIII (Tubb3; 1:500, RRID:AB_291637; #PRB-435P; Covance, Ann Arbor, MI); mouse anti- tubulin ßIII (Tubb3; 1:300; gift from Anthony Frankfurter, University of Virginia); rabbit anti-calretinin (Calb2; 1:500, RRID:AB_2068506, #AB5054; EMD Millipore, Burlington, MA); and rabbit anti-Pou4f3 (1:300; RRID:AB_2878872; #21509-1-AP; Proteintech, Rosemont, IL). Primary antibodies were labeled using Alexa Flour-conjugated secondary antibodies (1:400, Invitrogen, Carlsbad, CA) applied at room temperature for 3 hours.

To label nuclei, we used 4',6'-diamidine-2-phenylindole (DAPI; Sigma-Aldrich, St. Louis, MO) at 1 µg/mL in 10 mM PBS. Utricles were whole-mounted on slides in Fluoromount-G (Southern Biotech, Birmingham, AL) or Prolong Gold (Thermo Fisher Scientific, Waltham, MA).

2.4. Tissue Imaging, Criteria for Cell-Typing, Quantitative Analysis, and Statistics

We acquired fluorescent images of whole-mount utricles using a FV-1000 laser scanning confocal microscope (Olympus, Center Valley, PA). Using a 60x oil objective, Z-series images of the entire sensory epithelium were taken from the lumenal surface of the epithelium through the first few microns of the stroma. Olympus files were imported into Fiji (http://fiji.sc/) for qualitative analyses, and cells were counted using Fiji's Cell Counter plugin.

To confirm *Sox2* deletion from supporting cells, we examined Sox2 immunolabeling in utricles of *Sox2* (wildtype) WT and conditional knockout (CKO) mice at 1 or 2 weeks post-tamoxifen. Sampling 20% of the

epithelium including the striola, medial extrastriola, and lateral extrastriola, we scored each tdTomato-labeled supporting cell as Sox2-postive or Sox2-negative. Data from all regions were averaged.

To test the requirement for *Sox2* in supporting cells during hair cell regeneration, we counted hair cells in utricles, saccules, and horizontal ampullae from *Sox2* CKO and *Sox2* WT mice at 3 weeks and 12 weeks post-DT. Every hair cell was scored as type I or type II and as tdTomato-positive or tdTomato-negative. Hair cells were distinguished from supporting cells by their immunoreactivity for myosin VIIa (Hasson et al., 1997). To define hair cells as type I or II, we used morphological criteria that have been described previously (Rüsch et al., 1998; Bucks et al., 2017; Pujol et al., 2014). Briefly, type II hair cells have a thick neck and heavy myosin VIIa labeling in the cytoplasm around the nucleus and in the basolateral processes (Desai et al., 2005; Oesterle et al., 2008; Pujol et al., 2014). The type II hair cell nucleus is oval and larger than the type I hair cell nucleus. For some samples, we confirmed type II identify using antibodies to Calb2, a type II hair cell marker (Desai et al., 2005). Type I hair cells have thin necks, small, round nuclei, very little perinuclear myosin VIIa labeling, and no basolateral processes. Type I hair cells have an afferent nerve terminal called a calyx that labels with antibodies to Tubb3 and appears as a tdTomato-negative (black) space between the myosin VIIa-labeled type I hair cell body and the surrounding tdTomato-positive cells.

To assess cell-autonomous effects of *Sox2* deletion from supporting cells, we performed several analyses using confocal microscopy to survey the utricular epithelia. We assessed supporting cell morphology and counted supporting cell nuclei by sampling 20% of the entire epithelium and averaging data from all regions.

Fiji and Adobe Photoshop CS4 (San Jose, CA) were used to make figures. Prism6 (GraphPad Software, San Diego, CA) was used for statistical analysis and graph generation. Differences between conditions were considered statistically significant if $p \leq 0.05$. Data are expressed as mean ± 1 standard error of the mean (SEM) unless otherwise indicated. The “n” value is the number of mice per experiment and is included in each Figure Legend. We performed counts on one utricle per animal for a given experiment. Statistical results are provided in Results, Figure Legends, and Tables.

2.5. Transmission electron microscopy (TEM)

We analyzed two utricles from *Sox2* WT and *Sox2* CKO mice using TEM. Utricles were prepared as described in Gonzalez-Garrido et al. (2021). Briefly, temporal bones were isolated and fixed in 2.5% glutaraldehyde in 0.2M cacodylate buffer, rinsed and post-fixed with 2% osmium tetroxide in cacodylate buffer. Utricles were dissected and embedded in Eponate (Ted Pella Inc. #18010). Transverse ultrathin (80-90 nm) sections were taken through the extrastriolar and striolar zones imaged using a JEOL 1230 transmission electron microscope equipped with an AMT XR80 digital camera.

Results

3.1. Conditional deletion of *Sox2* from supporting cells prior to hair cell damage prevents normal levels of vestibular hair cell regeneration

Mammals have five vestibular sensory organs (**Fig. 1A**): two otolithic organs (utricle and saccule) that sense gravity, and three cristae ampullae (horizontal, anterior, and posterior) that detect head rotations. Our study focused on the utricle (**Fig. 1B**) but included analysis of the saccule and horizontal ampulla. Mature vestibular sensory epithelia are composed of type I and type II hair cells and supporting cells; type I hair cells are surrounded by a neural calyx (**Fig. 1C**). Type I and II hair cells, as well as supporting cells and neural processes, are distributed throughout the utricular epithelium in mice (Desai et al. 2005a; Li et al. 2008).

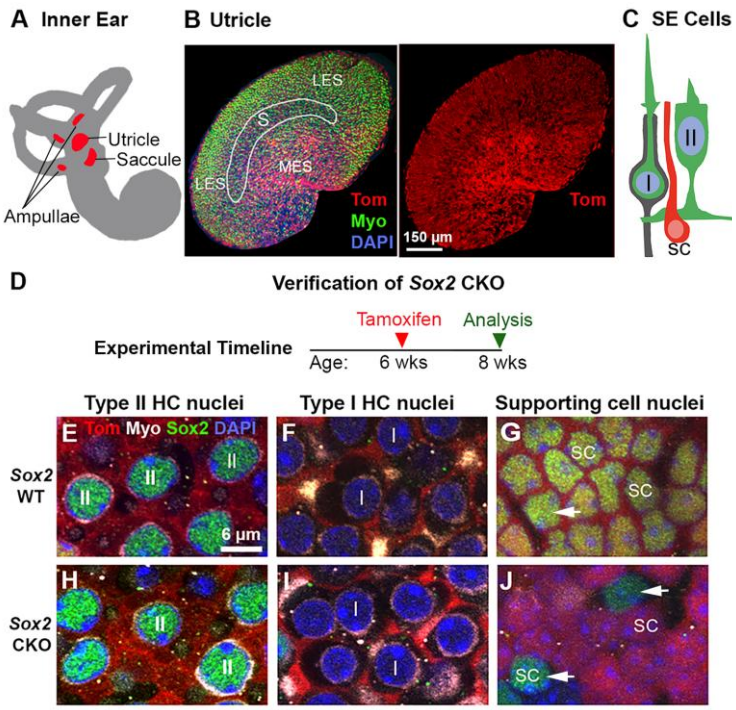

Figure 1. Using *Sox9-CreER*^{T2} mice to drive *Sox2* deletion from supporting cells.

A. Diagram of inner ear labyrinth (gray) with the five vestibular sensory organs (red). **B, left panel.** Low magnification horizontal slice (xy, parallel to the lumen) of an undamaged utricle with its three zones labeled. Tomato (Tom) labeling of supporting cells is red, myosin VIIa (Myo) labeling of hair cells is green, and DAPI labeling of nuclei is blue. LES, lateral extrastriola; S, striola; MES, medial extrastriola. White line approximates the location of the striola. **B, right panel.** Same image as in B, left, except showing only Tom. Scale bar in B, right panel applies to both images in B. **C.** Schematic of sensory epithelial (SE) cells from the undamaged utricle including type I hair cells (I), type II hair cells (II), and supporting cells (sc). Note the cell layers and the neural calyx (gray) around the type I hair cell body. **D.** Experimental timeline for verifying *Sox2* deletion from supporting cells in *Sox2* CKO mice. **E-J.** Horizontal slices from different cell layers from the lateral extrastriolar region of undamaged utricles from *Sox2* WT and *Sox2* CKO mice. Tom labeling is red, Myo labeling is white, Sox2 labeling is green, and DAPI labeling is blue. Each panel shows one plane of focus through each nuclear layer. Arrows in G,J point to Sox2-positive supporting cells (sc). Scale bar in E applies to E-J.

We tested the requirement for *Sox2* during hair cell regeneration in adult mouse vestibular organs using CreER-loxP technology by deleting *Sox2* from supporting cells prior to hair cell damage. We targeted CreER expression to supporting cells using *Sox9-CreER*^{T2} transgenic mice, in which tamoxifen given at 6 weeks of age induces CreER activity in 87% of supporting cells and 4% of hair cells under normal physiological conditions (Stone et al., 2018, **Fig. 1B**). We previously showed that *Sox9-CreER*^{T2}-expressing supporting cells regenerate hundreds of type II hair cells after damage (Hicks et al., 2020). We generated *Pou4f3*$^{DTR/+}$*:Sox9-CreER*$^{T2/+}$:*Rosa26*$^{tdTomato/+}$:*Sox2*$^{loxP/loxP}$ (*Sox2* CKO), which allowed deletion of one or both copies of the *Sox2* coding region and also enabled expression tdTomato (Tomato) in the nucleus and cytoplasm of *Sox9*-expressing supporting cells for fate-mapping. *Pou4f3*$^{DTR/+}$*:Sox9-CreER*$^{T2/+}$:*Rosa26*$^{tdTomato/+}$:Sox2$^{+/+}$ (*Sox2* WT) mice were used as controls.

To determine if *Sox2* is required in vestibular supporting cells for hair cell regeneration in adult mice, we used *Sox2* WT and *Sox2* CKO mice that included the *Pou4f3*^{DTR} allele, which enabled hair cell ablation upon injection of diphtheria toxin (DT) (Golub et al., 2012; Tong et al., 2015). We injected 6-week-old mice with tamoxifen, and one week later, we administered DT (**Fig. 2A**). We chose this timeline because we thought that 1) *Sox2* deletion would occur by one week post-Tam and 2) supporting cell transdifferentiation would begin around one week post-DT (or 2 weeks post-Tam) due to our finding that *Atoh1* is upregulated between one and 4 weeks post-DT (Hicks et al., 2020). To verify this approach, we injected *Sox2* WT and *Sox2* CKO mice (**n=3 or 4** for each genotype) at 6 weeks of age with tamoxifen and labeled utricles with anti-Sox2 antibodies (**Fig. 1D**). In *Sox2* WT mice, Sox2 protein was detected in type II hair cell nuclei (**Fig. 1E**) but not in type I hair cell nuclei (**Fig. 1F**), as expected (Oesterle et al., 2008). Of supporting cells, **140 ±62** (mean ±standard deviation, or SD) per 10,000 um^2 were Tomato-labeled, and all of them had Sox2-positive nuclei (**Fig. 1G**), as expected (Oesterle et al., 2008). In *Sox2* CKO mice, the vast majority of Tomato-labeled supporting cells lacked Sox2 immunoreactivity (**Fig. 1J**), indicating that *Sox2* had been deleted. Specifically, only **8 ±8** supporting cells per 10,000 um^2 expressed Sox2, which was equal to **5%** of the Tomato-labeled supporting cell population. Sox2 was maintained in type II hair cells (**Fig. 1H**), which was expected because most type II hair cells lacked CreER expression, and in the few supporting cells that lacked CreER (Tomato) expression (**Fig. 1J**). Similar to *Sox2* WT mice, Sox2 was not detected in type I hair cells in *Sox2* CKO mice (**Fig. 1I**).

To explore the impact of *Sox2* deletion from supporting cells on hair cell regeneration, we labeled utricles at 3 weeks post-DT with antibodies to myosin VIIa, which is present in all hair cells (Hasson et al., 1997), calbindin 2 (Calb2), a type II hair cell-specific marker (Desai et al., 2005), and/or tubulin β3 (Tubb3), which is abundant in the calyceal afferent nerve terminal surrounding type I hair cells (e.g., Stone et al., 2021). Adult mice normally have approximately 3,700 myosin VIIa-labeled hair cells per utricle (Golub et al., 2012). At 3 weeks post-DT, there was significant hair cell loss from both *Sox2* WT and CKO mice (compare **Fig. 1B** with **Fig. 2B,F**). There were also signs of hair cell regeneration in *Sox2* WT mice: 171 ±4 (mean± SEM) hair cells per utricle were Tomato-positive (**Fig. 2B,C1,C2,H, Table 1**), indicating they were derived from Tomato-positive (CreER-expressing) supporting cells. All Tomato-positive hair cells were deemed to be type II by several criteria: they had heavy myosin VIIa labeling and at least one basolateral process emanating from the cell body (arrows in **Fig. 2C1,C2)**, which are features of type II hair cells (Pujol et al., 2014; Bucks et al., 2017); they were Calb2-positive (**Fig 2D1-D4**); and they lacked a Tubb3-positive calyx terminal that is unique to type I hair cells (**Fig 2E1-E4**). In contrast to *Sox2* WT mice, very few hair cells per utricle (19 ±5) were Tomato-positive in *Sox2* CKO mice at 3 weeks post-DT (**Fig. 2F,G1,G2,H; Table 1**), indicating that regeneration of type II hair cells was inhibited in the majority of supporting cells that lacked *Sox2*.

We were surprised to see any Tomato-positive type II hair cells at 3 weeks post-DT. One potential explanation for this finding is that supporting cells began to transdifferentiate into hair cells before two weeks post-tamoxifen, and some of those cells had retained sufficient Sox2 protein to enable them to complete transdifferentiation. In support of this interpretation, we found that **23%** of Tomato-positive supporting cells in *Sox2* CKO mice retained Sox2 protein at one week post-tamoxifen. Specifically, **130 ±40** (mean± SD, n=3 mice) supporting cells per 10,000 μm^2 were Tomato-positive, and **25 ±17** were Tomato-positive and Sox2-positive This observation indicated that *Sox2* deletion from supporting cells took longer than one week, and it may explain why some Tomato-positive supporting cells were able to regenerate type II hair cells in our study.

To determine if transdifferentiation of supporting cells into type II hair cells was simply delayed in *Sox2* CKO mice, we examined utricles at a later recovery time: 12 weeks post-DT. We selected this time

because new hair cells continue to be added to utricles up to 10 weeks after DT-mediated hair cell damage but there appears to be no new hair cell addition after that point (Golub et al., 2012; Hicks et al., 2020). In *Sox2* WT mice, numbers of Tomato-positive type II hair cells per utricle (323 ±34) were higher at 12 weeks post-DT than at 3 weeks (**Fig. 2H; Table 1**), as expected. Conversely, *Sox2* CKO mice had only 58 ±4 Tomato-labeled hair cells per utricle at 12 weeks post-DT (**Fig. 2H; Table 1**), which represented no significant difference from 3 weeks post-DT for this group. This finding shows that type II hair cell regeneration was significantly curtailed in *Sox2* CKO mice as late as 12 weeks after damage.

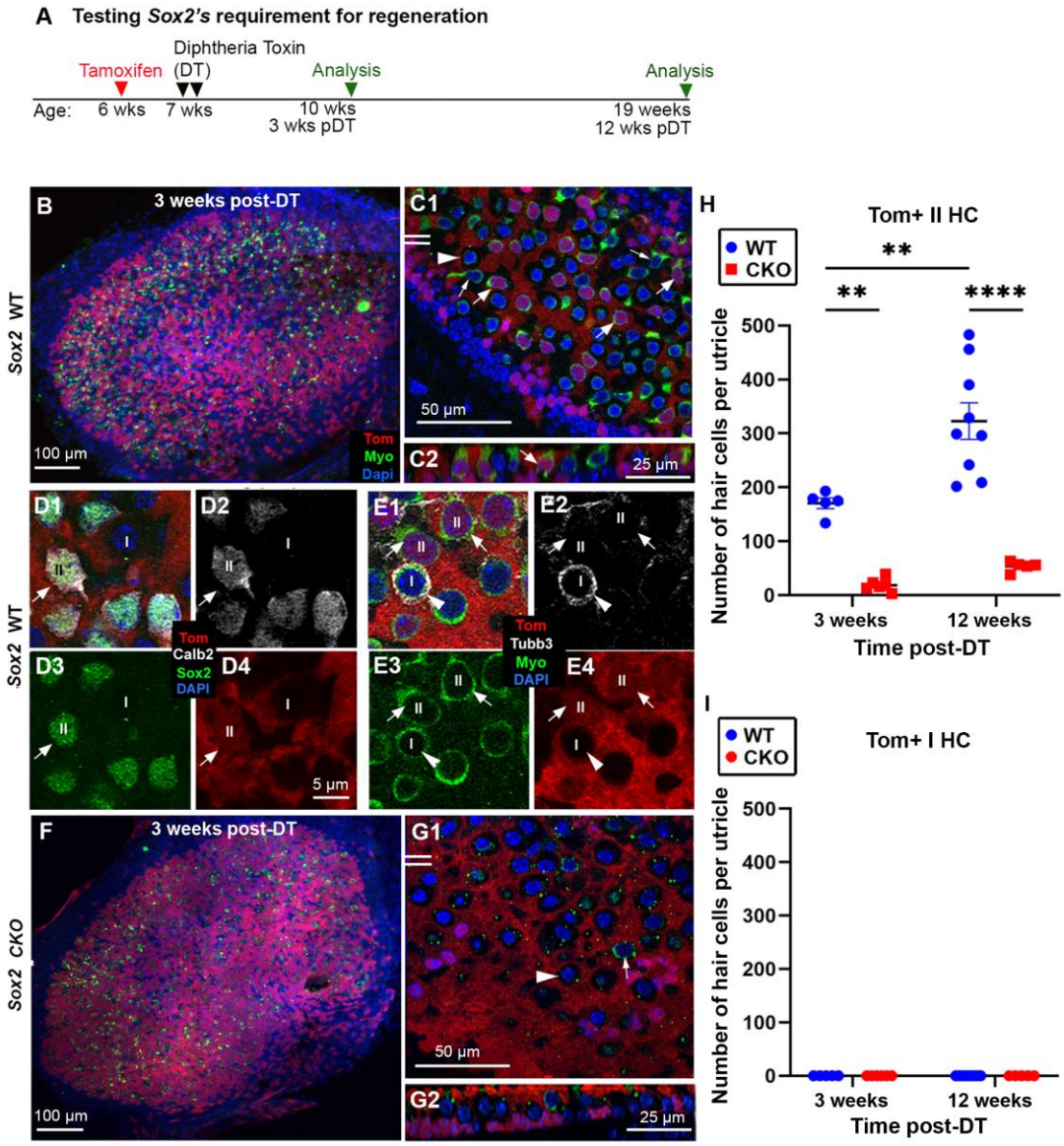

Figure 2. *Sox2* is required in supporting cells for normal levels of type ll hair cell regeneration in adult mice. **A.** Experimental timeline for testing the requirement of *Sox2* in supporting cell transdifferentiation into hair cells after damage. **B-G2.** All images are derived from single confocal slices through the hair cell layer or from Z-stacks through the whole sensory epithelium, with molecular labels indicated in appropriately colored text. **B.** Low magnification horizontal slice (xy) image of a *Sox2* WT utricle at 3 weeks post-DT. Organ orientation is similar to Fig. 1B. **C1.** Horizontal slice of the lateral extrastriola of a *Sox2* WT utricle. Arrows with wide ends point to Tomato (Tom)-positive, regenerated type II hair cells; arrows with narrow ends point to Tom-negative type II hair cells; and the arrowhead points to a Tomato-negative type I hair cell**. C2.** Cross-sections (xz slice) of C1, at the level of the double white lines, left side of C1. Arrow points to a regenerated Tom-positive type II hair cell. **D1-4.** Horizontal slice of a *Sox2* WT utricle showing Calb2 labeling of type II hair cells; D1 shows all channels; D2-4 show individual channels. Arrow points to one exemplary Calb2-positive type II hair cell (II). A type I hair cell (I) is also shown. **E1-4.** Horizontal slice of a *Sox2* WT utricle showing Tubb3 labeling of neural elements. E1 shows all channels; E2-4 show individual channels. Arrows point to two exemplary type II hair cells lacking a Tubb3-positive calyx; arrowhead points to an exemplary type I hair cell with a Tubb3-positive calyx. **F.** Low magnification horizontal slice of a *Sox2* CKO utricle at 3 weeks post-DT. **G1.** Horizontal slice of the lateral extrastriola of a *Sox2* CKO utricle. Arrowhead points to a Tomato-negative type I hair cell; arrow points to a Tom-negative type II hair cell. **G2.** Cross-section of G1, at the level of the double white lines, left side of G1. Scale bar in D4 applies to D1-E4. **H,I.** Graphs show numbers per whole utricle of Tomato-labeled type II (**H**) and type I (**I**) hair cells in *Sox2* WT and CKO mice. Each dot/square represents the data for one mouse; each error bar shows mean ± SEM. Sample size = 5-9 mice per group. Horizontal lines over bars and asterisks indicate significant difference from control per a two-way ANOVA with Tukey's multi-comparisons post-hoc test. p values: **≤.0.01, ****≤.0001.

In all utricles (**Fig. 2I**), we detected only rare Tomato-positive type I hair cells. This finding was consistent with other studies demonstrating that type I hair cells are not naturally regenerated in utricles, saccules, or horizontal ampullae in adult rodents (e.g., Forge et al., 1998; Kawamoto et al., 2009; Hicks et al., 2020; Gonzalez-Garrido et al., 2021).

We also examined hair cell regeneration in horizontal ampullae and saccules. Similar to utricles, there were significantly fewer Tomato-positive type II hair cells at 3 weeks after *Sox2* CKO than in *Sox2* WT mice at the same time (**Fig. 3A-F; Table 2A,B**), and we identified no Tomato-positive type I hair cells.

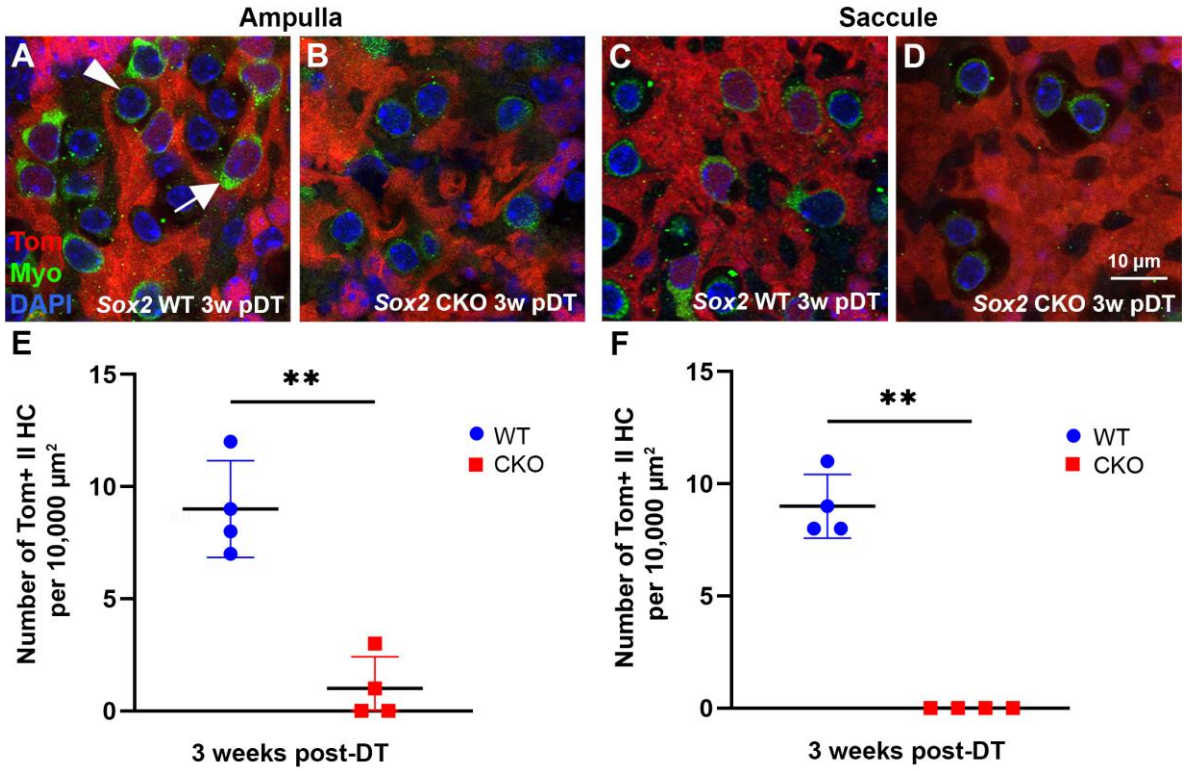

Figure 3. *Sox2* is required for normal levels of type ll hair cell regeneration in saccules and horizontal ampullae. A-D. Horizontal confocal slices (xy) through the hair cell layer, with molecular labels indicated in appropriately colored text in A. **A.** Slice from the peripheral region of a *Sox2* WT ampulla at 3 weeks (w) post-DT. Arrow points to a Myo-positive, Tomato-positive regenerated type II hair cell; arrowhead points to a Tomato-negative type I hair cell**. B.** A slice from the peripheral region of a *Sox2* CKO ampulla at 3 weeks (w) post-DT. Note the absence of Tomato-positive hair cells. **C,D.** Slices through the lateral extrastriolar region of a *Sox2* WT saccule (C) and a *Sox2* CKO saccule (D). Scale bar in D applies to A-D. **E,F.** Graphs show density of Tomato-positive type II hair cells for horizontal ampullae (E) and saccules (F). Each dot/square represents the data for one mouse; each error bar shows mean ± SEM. Sample size = 4 mice per group. Horizontal lines over bars and asterisks indicate significant difference from control per one-way ANOVA with Tukey's multi-comparisons post-hoc test. p value **≤.0.01.

3.2. Deletion of *Sox2* from supporting cells did not alter supporting cell density or appearance in utricles

Next, we explored whether, in addition to preventing normal levels of hair cell regeneration, *Sox2* deletion from supporting cells caused other changes. First, we counted supporting cell nuclei, which were small and round and located nearest the basal lamina (**Fig. 4A,B**). There was a significant decrease in the density of Tomato-labeled supporting cells over time in the *Sox2* WT mice (**Fig. 4C**), which likely occurs

as supporting cells transdifferentiate into hair cells. However, there was no significant difference in the density of Tomato-labeled supporting cells between *Sox2* WT and *Sox2* CKO mice at either time post-DT, nor a change in Tomato-labeled supporting cell density in *Sox2* CKO mice between 3 and 12 weeks post-DT (**Fig. 4C; Table 3**).

Then, we used transmission electron microscopy (TEM) to determine if ultrastructural changes in supporting cells were evident in utricles at 12 weeks after *Sox2* deletion. In *Sox2* WT mice (**Fig. 4D**), as anticipated based on a recent study (Gonzalez et al., 2021), we saw new type II hair cells and surviving type I hair cells with nuclei located in the apical-most half of the epithelium. The nuclei of supporting cells were present along the basal lamina, and their cell bodies extended to the lumenal surface. In utricles from *Sox2* CKO mice (**Fig. 4E**), it was significantly more challenging to identify hair cells, which was expected given the lack of regeneration. Most sections that we examined had no hair cells (**Fig. 2, Fig. 4E**). Supporting cells had a similar cell shape, and their nuclei had a basal localization and comparable density, as *Sox2* WT mice. Analysis of high-magnification images revealed that both the apex and the base of supporting cells from *Sox2* CKO mice had normal features. At their apex, supporting cells from *Sox2* WT mice had the characteristic electron-dense material (**Fig. 4F**) and cell-cell junctions (**Fig. 4G**; desmosome-like junctions are shown). Both of these features were preserved in *Sox2* CKO mice (**Fig. 4H,I**). At their base, supporting cells from *Sox2* WT mice had close membrane apposition with adjacent supporting cells, and their cytoplasm enwrapped nearby afferent neurites (**Fig. 4J,K**). The basal portion of supporting cells from *Sox2* CKO mice had a similar appearance (**Fig. 4L,M**). The nucleus of supporting cells had comparable features in both *Sox2* WT and *Sox2* CKO mice (**Fig. 4J,L**). In conclusion, we found no difference in supporting cell ultrastructure following *Sox2* deletion as late as 12 weeks after hair cell damage.

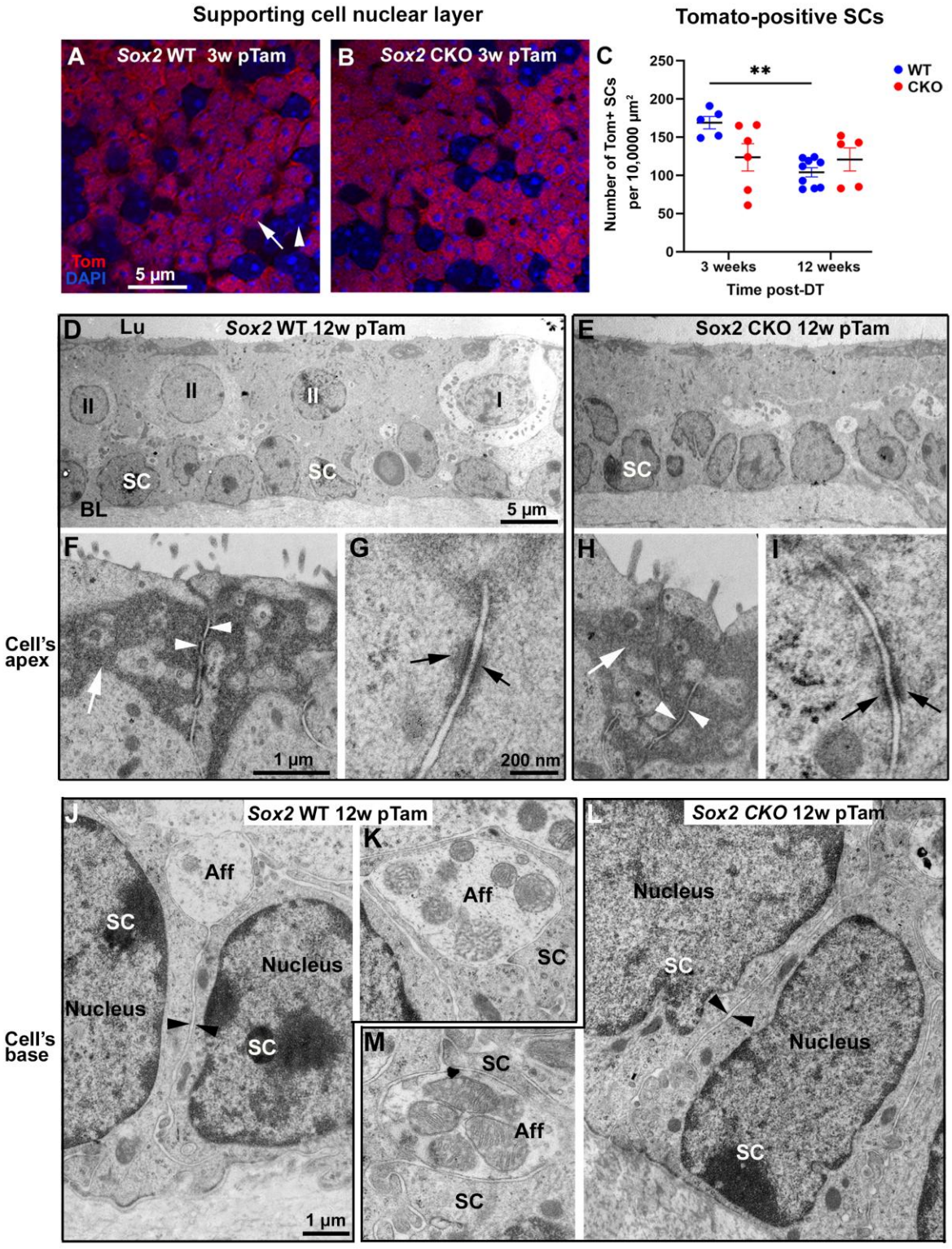
Supporting cell nuclear layer
Tomato-positive SCs
A
Sox2 WT 3w pTam
Tom
DAPI
5 μm
B
Sox2 CKO 3w pTam
C
**
WT
CKO
Number of Tom+ SCs per 10,0000 μm²
250
200
150
100
50
0
3 weeks
12 weeks
Time post-DT
D
Lu
Sox2 WT 12w pTam
II
II
II
I
SC
SC
BL
5 μm
E
Sox2 CKO 12w pTam
SC
F
G
H
I
Cell's apex
1 μm
200 nm
J
Sox2 WT 12w pTam
Aff
SC
Nucleus
Nucleus
SC
K
Aff
SC
M
SC
Aff
SC
Cell's base
1 μm
L
Sox2 CKO 12w pTam
Nucleus
SC
Nucleus
SC

Figure 4. *Sox2* deletion from supporting cells did not alter their cell density or their morphology in the utricle. A,B. Horizontal slices (xy) of the lateral extrastriola of a *Sox2* WT utricle (**A**) and a *Sox2* CKO utricle (**B**) at 3 weeks post-DT. Arrow points to Tomato-positive supporting cell; arrowhead points to a Tomato-negative supporting cell. **C.** Graph showing density of Tomato-positive supporting cells (SCs) in *Sox2* WT and CKO mice. Data are expressed as mean ± SEM. Each dot represents data from one mouse. Sample size = 5-9 mice per group. Two-way ANOVA with Tukey's multi-comparisons post-hoc test showed that *Sox2* WT mice at 12 weeks post-DT had significantly fewer Tomato-positive supporting cells than at 3 weeks post-DT. p value **≤.0.01. **D,E.** Low-magnification transmission electron micrographs of the lateral extrastriolar region of utricles from a *Sox2* WT mouse (D) and a *Sox2* CKO mouse (E), both at 12 weeks post-DT and taken perpendicular to the lumen. Note the similar appearance and density of the supporting cell (SC) nuclei in the *Sox2* CKO mouse (D) relative to the *Sox2* WT mouse (E). Type II and I hair cells are present in the *Sox2* WT mice. BL = basal lamina. Lu = lumen. **F-I.** Higher-magnification images of the apex of supporting cells in a *Sox2* WT mouse (F,G) and a *Sox2* CKO mouse (H,I) at 12 weeks post-DT. Arrowheads point to apical supporting cell-supporting cell junctions, near the lumen, and arrows indicate the electron-dense material present in the apex of supporting cells. Note the similar appearances of the junctions including desmosomes (black arrows in G,I), and the electron-dense material between the *Sox2* WT and CKO sections. **J-M.** Higher-magnification images of the supporting cell base in *Sox2* WT (J-M) and a *Sox2* CKO (L,M) mice at 12 weeks post-DT. Arrowheads in J,L point to the cell-cell junction between two supporting cells. Note the similar appearance of the cell-cell junctions and the close wrapping of afferent

3.3. *Sox2* CKO caused an increase in supporting cell nuclei in the apical epithelial layer at 12 weeks post-DT

In the normal, undamaged utricle, the nucleus of each supporting cell is positioned deep in the sensory epithelium, near the basal lamina, and the nucleus of each type II hair cell is located apically, near the lumen (**Fig. 5A, left panel**). Unlike hair cells, the supporting cell body extends from the basal lamina to the lumen. As a supporting cell transdifferentiates into a type II hair cell during regeneration, its nucleus undergoes basal-to-apical translocation (**Fig 5A, middle panel**). After transdifferentiation is complete, the nucleus of the regenerated hair cell remains in the apical compartment (**Fig. 5C, right panel**). In *Sox2* WT and *Sox2* CKO utricles at 3 weeks post-DT, we noted that some Tomato-positive nuclei positioned in the apical compartment lacked the hair cell marker (myosin VII) (**Fig. 5B1-3**). In *Sox2* WT mice, numbers of these apical non-hair cells (presumed supporting cells) decreased between 3 and 12 weeks post-DT, resulting in significantly fewer apical supporting cells than *Sox2* CKO at the later timepoint (**Fig. 5C; Table 4**). In contrast, there were similar numbers of apically located supporting cells in *Sox2* CKO mice at both times (**Fig. 5C; Table 4**). These observations suggested that many supporting cells whose nuclei migrate

into the apical compartment during regeneration in *Sox2* WT mice acquire a hair cell fate within 12 weeks, while supporting cells with *Sox2* deletion initiate nuclear migration but fail to complete the transdifferentation process (e.g., they become stalled).

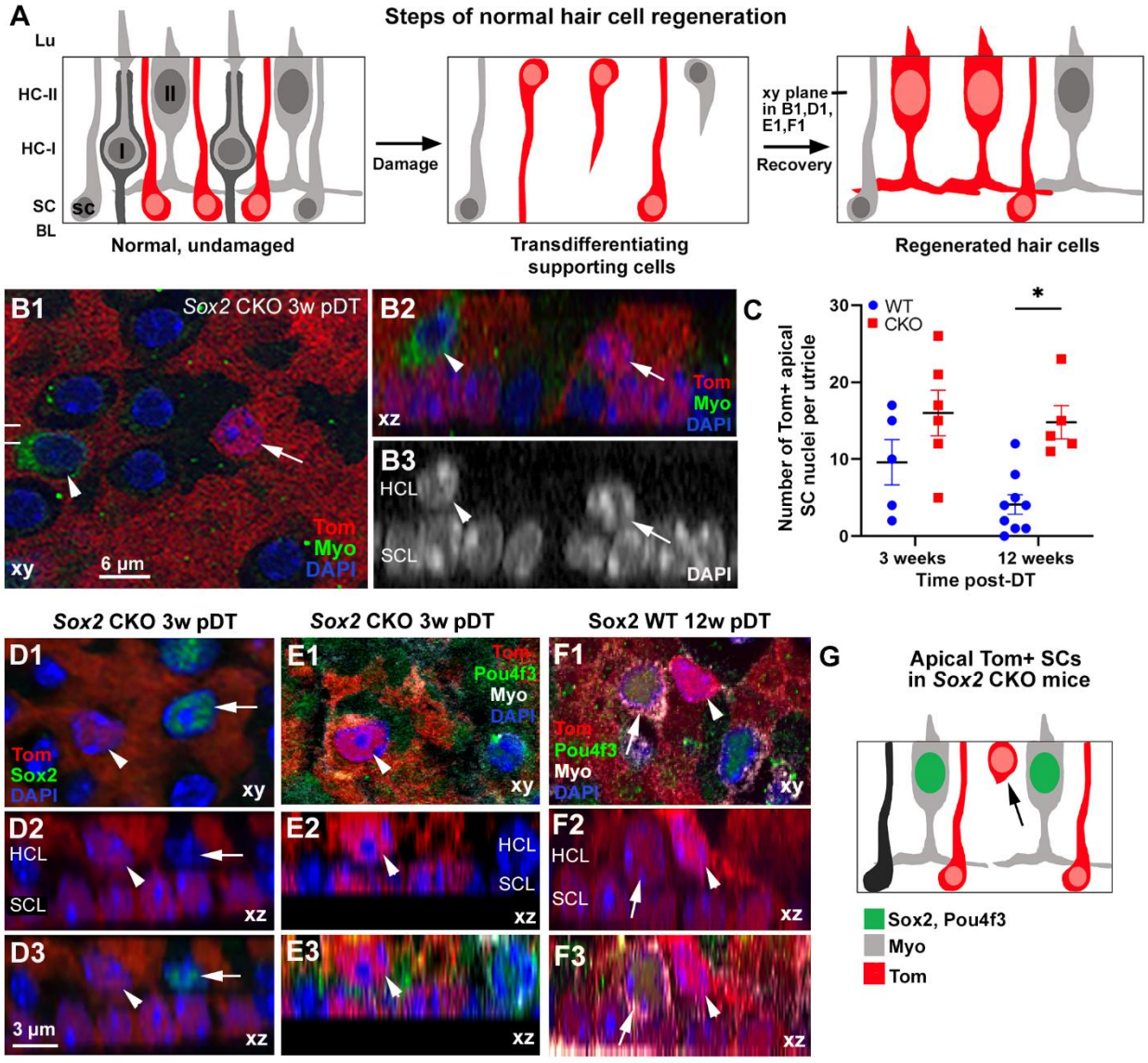

Figure 5. A. Diagram of the positions of hair cell and supporting cell nuclei in normal undamaged conditions (left panel), during the early phase of hair cell regeneration (middle panel), and once regeneration of type II hair cells is complete (right panel). Lumen (Lu), basal lamina (BL), type I hair cell (HC-I), type II hair cell (HC-II), supporting cell (SC). **B1**. Horizontal slice (xy) of the lateral extrastriola of a utricle from a *Sox2* CKO utricle at 3 weeks (w) post-DT, focused on the hair cell nuclear layer (apical compartment, plane of section shown in A, right panel). Arrow points to a Tomato-positive nucleus in a cell lacking labeling for the hair cell marker myosin VIIa (Myo), a presumed supporting cell. Arrowhead points to a Tomato-negative Myo-positive type II hair cell, for reference. **B2.** Cross-sections (xz slice) through the area shown in B1, taken at the site indicated by two white lines on left edge of B1. Arrowhead and arrow point to the same cells as in B1. **B3.** Same image as B2 but with DAPI only. Scale bar in B1 applies to B1-B3. Hair cell layer (HCL); supporting cell layer (SCL). **C.** Graph showing the number of Tomato-positive nuclei that lack Myo labeling (presumed supporting cells) per utricle in *Sox2* WT and *Sox2* CKO mice. Each dot/square represents the data for one mouse, and each error bar shows mean ± SEM. Sample size = 5-9 mice per group. Horizontal line over bar and asterisk indicates significant difference from control determined using a two-way ANOVA with Tukey's multi-comparisons post-hoc test. *, $p \leq 0.05$. **D1-3** show immunolabeling for Sox2 (green) in a utricle from a *Sox2* CKO mouse at 3 weeks post-DT. Tom and DAPI are also shown. D1 shows a horizontal slice through the apical compartment (plane of section shown in A, right panel). The arrowhead indicates a Tomato-negative/Sox2-negative nucleus, while the arrow shows a Tomato-negative/Sox2-positive nucleus (positive control for Sox2 labeling). D2 and D3 show cross-sections through the same cells as in D1, with D2 showing only Tom and DAPI and D3 showing all 3 labels. **E1-3** show immunolabeling for Pou4f3 (green) and Myo (white) in a utricle from a *Sox2* CKO mouse at 3 weeks post-DT. Tom and DAPI are also shown. E1 shows a horizontal slice through the apical compartment (plane of section shown in A, right panel). The arrowhead points to an apical nucleus that is Tom-positive in a cell that lacks both Pou4f3 and Myo labeling. E2 and E3 show cross-sections through the same cell as in E1, with E2 showing only Tom and DAPI and E3 showing all 4 labels. **F1-3** show immunolabeling for Pou4f3 (green) and Myo (white) in a utricle from a *Sox2* WT mouse at 12 weeks post-DT. Tom and DAPI are also shown. F1 shows a horizontal slice through the apical compartment (plane of section shown in A, right panel).The arrowhead points to an apical nucleus that is Tom-positive in a cell that lacks both Pou4f3 and Myo labeling, while the arrow points to a Tom-positive cell that is Pou4f3-positive/Myo-positive. F2 and F3 show cross-sections through

In a qualitative analysis, we further characterized the Tomato-positive cells with apical nuclei in *Sox2* WT and CKO mice at 3 or 12 weeks post-DT (n=2-3 mice per group). First, we confirmed that such cells lacked nuclear Sox2 immunolabeling (**Fig. 5D1-D3**), indicating that their failure to express myosin VIIa could not be attributed to unsuccessful *Sox2* deletion. Second, we determined that the transcription factor Pou4f3, which is abundant in the nucleus of hair cells but not supporting cells in mature mice (e.g., Sung et al., 2022), was not detected in myosin VIIa-negative, Tomato-positive cells with an apical nucleus in *Sox2* CKO mice at either 3 or 12 weeks post-DT (**Fig. 5E1-E3**, 3 weeks is shown). While some Tomato-positive cells with apical nuclei in *Sox2* WT mice lacked Pou4f3 immunolabeling, we found many examples of many such cells were double-labeled for both myosin VIIa and Pou4f3 in *Sox2* WT mice at 3

weeks and at 12 weeks pDT (**Fig. 5F1-F3**,12 weeks post-DT is shown). These observations support the interpretation that, while some supporting cells lacking *Sox2* can migrate up to the apical compartment after hair cell damage, few appear to differentiate hair cell properties, at least within the timeframe that we examined. **Fig. 5G** summarizes these findings.

3.4. Hair cell regeneration is also significantly reduced in reduced *Sox2* heterozygotes

A previous study showed that hair cell regeneration in the neonatal cochlea was increased in mice with only one copy of *Sox2* (Atkinson et al., 2018). Thus, we also examined vestibular hair cell regeneration in *Sox2* heterozygous (*Pou4f3*$^{DTR/+}$*:Sox9-CreER*$^{T2/+}$*:Rosa26*$^{tdTomato/+}$*:Sox2*$^{loxP/+}$) mice. At 3 weeks post-DT, numbers of Tomato-positive type II hair cells in *Sox2* heterozygotes were not statistically different from either *Sox2* WT or *Sox2* CKO mice (**Fig. 6A,B; Table 5A**). In contrast, at 12 weeks post-DT, *Sox2* heterozygotes had significantly fewer regenerated hair cells than *Sox2* WT mice and significantly more than *Sox2* CKO mice. Thus, there were fewer hair cells regenerated over time in adult mice when supporting cells had only one copy of *Sox2*.

Like both *Sox2* WT and *Sox2* CKO mice*, Sox2* heterozygotes had no Tomato-labeled type I hair cells (data not shown), indicating that type I regeneration was not enhanced when *Sox2* levels were reduced. We also found no difference in supporting cell density amongst *Sox2* WT, heterozygous, and CKO mice at either time post-DT, nor a change in Tomato-labeled supporting cell density in *Sox2* heterozygotes between 3 and 12 weeks post-DT (**Fig. 6C; Table 5B**). Finally, similar to *Sox2* CKO mice, mice lacking one copy of *Sox2* had significantly higher numbers of Tomato-positive, myosin VIIa-negative apical supporting cells at 12 weeks post-DT than *Sox2* WT mice (**Fig. 6D,E; Table 5C**), suggesting that fewer supporting cells completed transdifferentiation into type II hair cells when Sox2 levels were reduced.

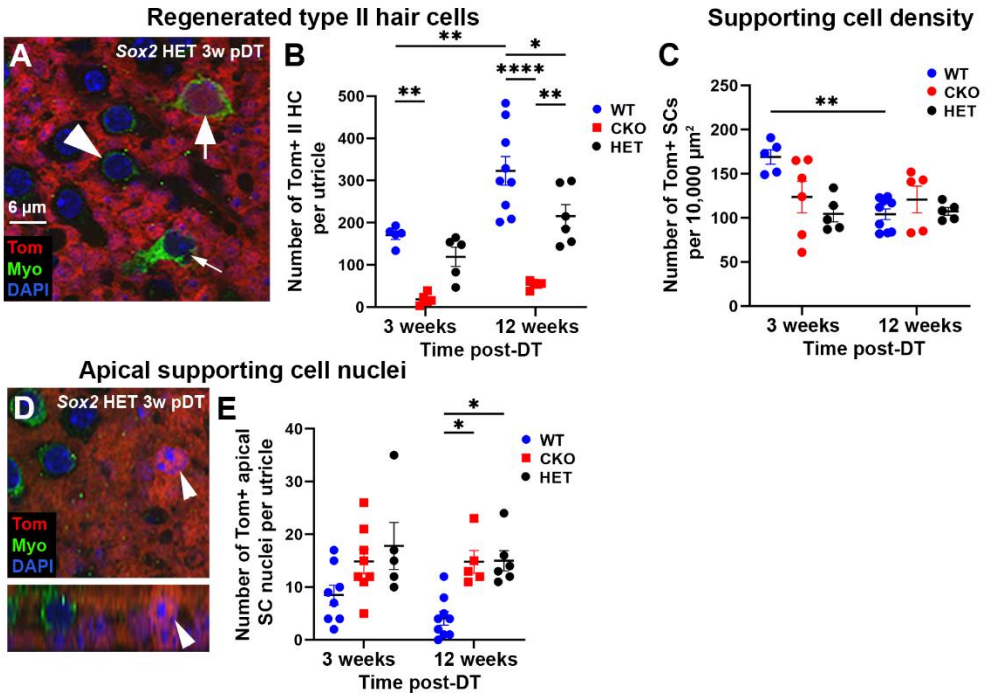

Figure 6. *Sox2* heterozygosity in supporting cells significantly curtailed hair cell regeneration but did not impact supporting cell density in the utricle. A. Horizontal slice (xy) through the hair cell layer of a utricle from a *Sox2* heterozygote (HET) at 3 weeks post-DT, with each label indicated in the appropriate color. Thick arrow points to a Tomato (Tom)-positive type II hair cell; thin arrow points to a Tom-negative type II hair cell; and arrowhead points to a Tomato-negative type I hair cell. Scale bar in A applies to A,D. **B.** Graph showing number of Tomato-positive (regenerated) type II hair cells per utricle. Sample size = 5-9 mice per group. **C.** Graph showing number Tomato-positive supporting cells per 10,000 µm^2. Sample size = 5-9 mice per group. **D.** Horizontal slice through the hair cell layer of a utricle from a *Sox2* heterozygote (HET) at 3 weeks post-DT. Arrowhead points to a Tomato-positive supporting cell in the hair cell layer (the apical-most part of the epithelium). **E.** Graph showing number Tomato-positive apical supporting cell nuclei (SC) per utricle. Sample size = 5-9 mice per group. For all graphs, each dot/square represents the data for one mouse, and each error bar shows mean ± SEM. Horizontal lines over bars and asterisks indicate significant difference from control per two-way ANOVA with Tukey's multi-comparisons post-hoc test. p value *≤.0.05, **≤.0.01, ****≤.0.0001.

3.5. Analysis of Tomato-negative cells

We examined Tomato-negative hair cells (myosin VIIa-positive) in utricles from all *Sox2* WT and *Sox2* CKO mice at 3 and 12 weeks post-DT which included hair cells that survived the DT ablation as well as regenerated hair cells formed from Cre-negative supporting cells. Many Tomato-negative type II hair cells

were identified (**Fig. 7A,B; Table 6A**). Numbers of Tomato-negative type II hair cells did not change over time in either *Sox2* WT or *Sox2* CKO mice. e.

We also detected Tomato-negative type I hair cells in utricles of all *Sox2* WT and *Sox2* CKO mice (**Fig. 7A,C; Table 6B**). Because no type I hair cells regenerate in adult mice after damage (Golub et al., 2012; Bucks et al., 2017; Hicks et al., 2020), these cells must have survived DT treatment. Surprisingly, there were significantly more Tomato-negative type I hair cells in *Sox2* CKO mice at 12 weeks post-DT compared to the *Sox2* WT mice, suggesting that Sox2 expression in supporting cells may be required for normal clearance of type I hair cells after damage.

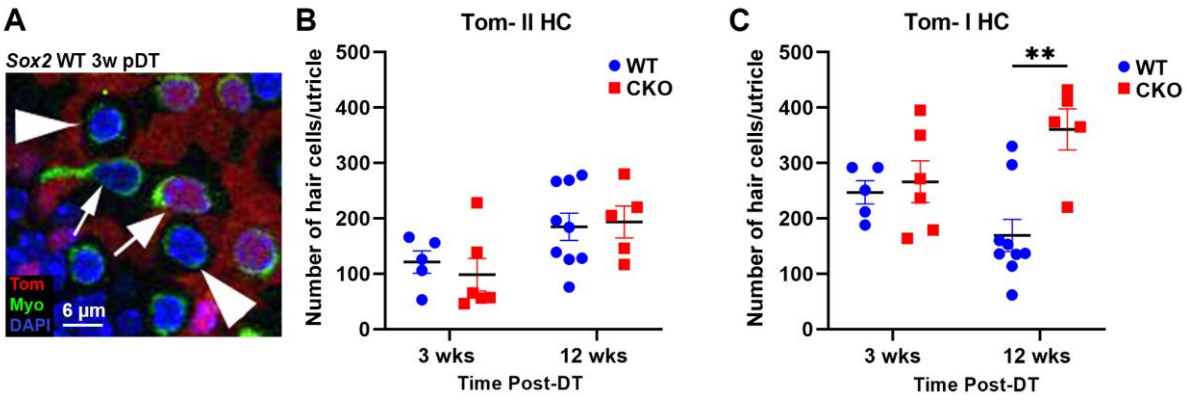

Figure 7. Analysis of Tomato-negative hair cells. A. Horizontal slice (xy) through the hair cell layer of a utricle from a *Sox2* WT mouse at 3 weeks (w) post-DT, with each label indicated in the appropriate color. Thick arrow points to a Tomato (Tom)-positive type II hair cell; thin arrow points to a Tom-negative type II hair cell; and arrowheads point to two Tomato-negative type I hair cells. **B.** Graph showing number of Tomato-negative (regenerated) type II hair cells per utricle. Sample size = 5-9 mice per group. **C.** Graph showing number Tomato-negative supporting cells per 10,000 µm^2. Sample size = 5-9 mice per group. For both graphs, each dot/square represents the data for one mouse; each error bar shows mean ± SEM. Horizontal lines over bars and asterisks indicate significant difference from control per two-way ANOVA with Tukey's multi-comparisons post-hoc test. p value **≤.0.05.

4. Discussion

Our study revealed heretofore unknown roles for *Sox2* in vestibular supporting cells during hair cell damage and hair cell regeneration in adult mice. We determined that *Sox2* is necessary in supporting cells for their full transdifferentiation into type II hair cells and to achieve normal levels of regenerated hair cells after damage. In addition, utricles with *Sox2* deletion from supporting cells had more surviving type I

hair cells after the damaging treatment, suggesting that supporting cells promote or enable type I hair cell death and/or clearance in a *Sox2*-dependent manner. In contrast, *Sox2* does not seem to be required for supporting cell survival or maintenance of the normal supporting cell phenotype, at least in the context of hair cell damage.

4.1. *Sox2* is required in mature supporting cells for normal levels of type II hair cell regeneration in mature mammals

Sox2 is required for development of both hair cells and supporting cells (Kiernan et al., 2005), but its role in hair cell regeneration in mature mammals has not been examined. To test *Sox2*'s requirement in supporting cells for vestibular hair cell regeneration in adult mice, we conditionally deleted *Sox2* from supporting cells, destroyed most hair cells one week later, and fate-mapped supporting cells using Tomato labeling. In *Sox2* CKO mice, there were relatively few Tomato-positive type II hair cells in the utricle or other vestibular organs (saccule and horizontal ampulla), even after 12 weeks of recovery from damage, indicating that regeneration was significantly curtailed during that period. Although not significant, there was an increase in the very small number of type II hair cells that were Tomato-positive between 3 and 12 weeks post-DT in *Sox2* CKO mice. This finding raises the possibility that *Sox2* deletion from supporting cells did not completely block hair cell regeneration but rather delayed it. This possibility seems unlikely, however, because addition of new hair cells is normally completed by 10 weeks post-DT (Golub et al., 2012) and therefore positive signals for regeneration likely do not persist after that time. It seems more plausible that a small number of Tomato-positive supporting cells in *Sox2* CKO mice retained Sox2 protein and that these cells generated new hair cells between 3 and 12 weeks post-DT. Consistent with this, we found that some Tomato-positive supporting cells retained Sox2 at 1 week post-Tam. If we had injected mice with DT at 2 weeks post-tamoxifen instead of at 1 week, we predict there would have been very few Tomato-positive type II hair cells in *Sox2* CKO mice.

There are also other explanations for why Tomato-labeled type II hair cells were present in *Sox2* CKO mice at both time points. Because tamoxifen induces Tomato labeling in ~138 hair cells per utricle in adult *Sox9-CreER*^{T2} mice, most of which are type II (Stone et al., 2018), it is possible that some of the Tomato-labeled type II hair cells we saw had survived DT treatment. Alternatively, Tomato-labeled type II hair cells

may have been regenerated by a subpopulation of supporting cells that did not delete both copies of Sox2 or by a subpopulation that do not require *Sox2* to transdifferentiate. Nonetheless, our observations demonstrate that *Sox2* is necessary in supporting cells for the normal timing and level of type II hair cell regeneration in adult mice.

Our finding that *Sox2* is required for normal levels (and perhaps timing) of hair cell regeneration is similar to a study that determined *Sox2* is required for regeneration of hair cells in the inner ears of larval zebrafish (Millimaki et al., 2010). It is important to note that Millimaki and colleagues found that in zebrafish, unlike mice, *Sox2* is not required for the initial development of inner ear hair cells. Thus, this study highlights important differences in molecular regulation of hair cell formation during development and after damage across ages and species.

We detected Tomato-negative type II hair cells in *Sox2* WT and *Sox2* CKO mice. Some of these hair cells were likely regenerated by Tomato-negative supporting cells, which comprise about 13% of the supporting cell population in the *Sox9-CreER*^{T2} mouse line (Stone et al., 2018). Additional Tomato-negative type II hair cells may have survived the damage regimen. A previous study showed that approximately 6% of vestibular hair cells persist in *Pou4f3*$^{DTR/+}$ mice after DT treatment (Golub et al., 2012).

We detected only rare Tomato-positive type I hair cells in any mice in this study. This finding was expected because, although overall numbers of hair cells increase in mouse utricles after hair cell destruction, most of the cells at later times of recovery are type II-like (Kawamoto et al., 2009; Golub et al., 2012; Sayyid et al., 2019. Gonzalez-Garrido et al., 2021), and only type II hair cells have been fate-mapped from supporting cells after damage (e.g., Bucks et al., 2017; Hicks et al., 2019; Sayyid et al., 2019). The rare Tomato-positive type I hair cells that we saw had probably survived the DT treatment.

As each supporting cell transdifferentiates into a type II hair cell, its nucleus migrates from the basal layer to the apical layer of the epithelium, where hair cell nuclei normally reside. We identified small numbers of Tomato-labeled nuclei in both *Sox2* WT and *Sox2* CKO mice that were positioned in the apical compartment, near the lumen. These cells did not express the hair cell marker myosin VIIa, suggesting they were supporting cells that were still in the process of undergoing transdifferentiation. At 12 weeks post-DT (but not 3 weeks), *Sox2* CKO mice had significantly more of these cells than *Sox2* WT mice.

These observations suggest that, in at least some supporting cells, *Sox2* is not required for the apical migration of their nuclei during transdifferentiation. Consistent with this, we confirmed that such apically located supporting cell nuclei lacked Sox2 protein. Our findings further suggest that, in *Sox2* CKO mice at 12 weeks post-DT, many supporting cells had become stalled and had accumulated in the apical compartment, whereas in *Sox2* WT mice at that time, supporting cells had proceeded to turn on hair cell markers (myosin VIIa and Pou4f3). It is also possible that the nuclei of supporting cells lacking *Sox2* cycle from the basal to apical compartments for extended periods as a consequence of *Sox2* deletion, increasing the likelihood of detecting them near the lumen. It is also possible that transdifferentiation of supporting cells is delayed in *Sox2* CKO mice, such that higher numbers of supporting cells had migrated into the apical compartment at 12 weeks than at 3 weeks post-DT. However, the later hypothesis seems unlikely because, in *Sox2* WT mice, very new type II hair cells are formed after 10 weeks post-DT (Golub et al., 2012; Hicks et al., 2020), suggesting that signals promoting supporting cell transdifferentiation may have dwindled by that time.

4.2. Hair cell regeneration is also curtailed in supporting cells missing one copy of *Sox2*

Deletion of a single *Sox2* allele did not significantly alter the number of regenerated hair cells relative to *Sox2* WT mice at 3 weeks post-DT, but at 12 weeks, *Sox2* heterozygotes had significantly fewer new hair cells. This finding contrasts with a study by Atkinson et al. (2018), which determined that *Sox2* heterozygosity augmented regeneration in the neonatal mouse cochlea. The reasons underlying these different observations are not clear, but a few possibilities are evident. In developing inner ear epithelia, *Sox2* serves as a necessary transcriptional activator of the pro-hair cell factor, *Atoh1* (Kiernan et al., 2005; Ahmed et al., 2012; Neves et al., 2012; Kempfle et al., 2014; Puligilla and Kelley, 2016). However, *Sox2*'s role is not simple; it can also antagonize *Atoh1* expression (Dabdoub et al., 2008), in some cases by promoting expression of *Atoh1* inhibitors, which limits the period when *Atoh1* is expressed (Neves et al., 2012; Neves et al., 2013). Therefore, one potential explanation for the findings by Atkinson et al. (2018) is that decreased levels of *Sox2* in the cochlea actually stimulated *Atoh1* transcription, increasing the likelihood that a cell acquired the hair cell fate. Alternatively, the differing results may have stemmed from the timing of *Sox2* heterozygosity, which occurred at fertilization in Atkinson et al. (2018) and during

adulthood in our study. It is evident that the manners in which *Sox2* regulates hair cell fate are different in vestibular versus cochlear organs, but further studies are needed to fully understand the divergent observations in our study and in the paper by Atkinson and colleagues.

4.3. *Sox2* is not required for survival or maintenance of supporting cell-specific features in adult mice but it may be required for hair cell clearance after DT-mediated damage

Although deletion of *Sox2* from supporting cells prior to hair cell damage significantly curtailed transdifferentiation into hair cells, it did not alter the density of supporting cells, their gross appearance, or their ultrastructure. These findings are consistent with the interpretation that supporting cells that fail to transdifferentiate into hair cells because they lack *Sox2* persist over time and that *Sox2* is not required to maintain the supporting cell phenotype, at least following hair cell damage.

We also found that numbers of Tomato-negative type I hair cells decreased over time in *Sox2* WT mice, which was expected based on prior studies (e.g., Golub et al., 2012). However, unlike *Sox2* WT mice, numbers of Tomato-negative type I hair cells in *Sox2* CKO mice were not altered over time. At the latest survival time we analyzed (12 weeks post-DT), there were significantly more Tomato-negative type I hair cells in *Sox2* CKO than in *Sox2* WT mice. Inner ear supporting cells aid in removing damaged vestibular hair cells and in repairing the sensory epithelium (e.g., Monzack et al., 2015; Bucks et al., 2017; reviewed in Hirose et al., 2017). Our findings suggest that hair cell death and clearance are regulated in some manner by *Sox2* in supporting cells, which could constitute a new role for this transcription factor. However, it is also possible that the higher numbers of Tomato-negative type I hair cells in *Sox2* CKO mice occurred because of variations in DT efficacy amongst *Pou4f3*^{DTR} mice.

4.4. Potential mechanisms by which SOX2 regulates transdifferentiation of vestibular supporting cells into hair cells

How does Sox2 regulate transdifferentiation of supporting cells into hair cells? As discussed in Section 4.1, Sox2 regulates gene transcription in inner ear hair cell progenitors, as both an activator and a repressor. Sox2 also acts as a pioneer transcription factor, modifying the structure of both chromatin and DNA and recruiting other transcriptional regulators to specific DNA loci (e.g., Amador-Arjona et al., 2014;

Vanzan et al., 2020; Zaret et al., 2020). Through its actions, Sox2 can reprogram cells by altering the activities of genetic networks. In vestibular supporting cells in mammals, Sox2 likely plays critical roles in initiating and directing hair cell regeneration, in particular through its regulation of *Atoh1*. Upregulation of *Atoh1* expression in supporting cells is one of the earliest steps in hair cell regeneration in several types of animals including birds, fish, and mice (e.g., Cafaro et al., 2007; Ma et al., 2008; Wang et al., 2010; Lin et al., 2011). *Atoh1* is essential for both hair cell development (Bermingham et al., 1999) and regeneration (Hicks et al., 2020). *Atoh1* expression and activity require Sox2 in some contexts (Neves et al., 2012; Kempfle et al., 2014; Puligilla and Kelley, 2016). We were not able to assess whether *Atoh1* upregulation still occurs in supporting cells lacking *Sox2*.

4.5. Summary

Hair cells of the vestibular system respond to motion and relay information about our head's position relative to gravity to the brain, providing us with a sense of balance. The transcription factor Sox2 is required for the development of these sensory hair cells and supporting cells (e.g., Kiernan et al., 2005). Our study shows that *Sox2* is also required in supporting cells of mature vestibular organs in mice to achieve normal levels of hair cell regeneration via direct transdifferentiation into type II hair cells after damage. Future studies will identify targets of Sox2 in supporting cells to further understand the mechanisms by which supporting cells form new type II hair cells and perhaps to identify clues as to why type I hair cells fail to regenerate in adult mammals.

TABLE 1

Table 1. Two-way ANOVA for Figure 2H. Number of Tomato-positive type II hair cells per utricle	
3w Sox2 WT n=5 3w Sox2 CKO n=6 12w Sox2 WT n=9 12w Sox2 CKO n=5	
Time Effect	f (1, 21) = 12.58 p=0.0019
Genotype Effect	f (1, 21) = 63.69 p<0.0001
Multi-comparisons	
3w WT vs 12w WT	s, p = .0018 **
3w CKO vs 12w CKO	ns, p = .8050
3w WT vs 3w CKO	s, p = .0041 **
12w WT vs 12w CKO	s, p < .0001 ****

TABLE 2

Table 2A. Welch's t-test for Figure 3E. Number of Tomato-positive type II hair cells per horizontal ampulla	
3w Sox2 WT n=4	3w Sox2 CKO n=4
3w WT vs 3w CKO	s, p=.0014 **

Table 2B. Welch's t-test for Fig 3F. Number of Tomato-positive type II hair cells per saccule	
3w Sox2 WT n=4	3w Sox2 CKO n=4
3w WT vs 3w CKO	s, p=.0010 **

TABLE 3

Table 3. Two-way ANOVA for Figure 4C. Density of Tomato+ supporting cells	
3w Sox2 WT n=5	3w Sox2 CKO n= 6
12w Sox2 WT n=9	12w Sox2 CKO n=5
Time Effect	f (2, 21) = 7.788 p=.0110 *
Genotype Effect	f (1, 21) = 1.392 p=.2513
Multi-comparisons	
3w WT vs 12w WT	s, p = .0038 **
3w CKO vs 12w CKO	ns, p = .9985
3w WT vs 3w CKO	ns, p = .0826
12w WT vs 12w CKO	ns, p =.7428

TABLE 4

Table 4. Two-way ANOVA for Figure 5C. Tomato-positive apical supporting cells	
3w Sox2 WT n=5	3w Sox2 CKO n=6
12w Sox2 WT n=9	12w Sox2 CKO n=5
Time Effect	f (1,21) = 2.136 p=.1586
Genotype Effect	f (1, 21) = 13.94 p=.0012 **
Multi-comparisons	
3w WT vs 12w WT	ns, p=.4671
3w CKO vs 12w CKO	s, p =.9840
3w WT vs 3w CKO	ns, p =.2576
12w WT vs 12w CKO	s, p =.0119*

TABLE 5

Table 5A. Two-way ANOVA for Figure 6B. Regenerated type II hair cells in heterozygotes		
3w Sox2 WT n=5	3w Sox2 CKO n=6	3w Sox2 Het n=5
12w Sox2 WT n=9	12w Sox2 CKO n=5	12w Sox2 Het n=6
Time Effect	f (1, 30) = 19.22 p =.0001***	
Genotype Effect	f (2, 30) = 33.01 p = .0001****	
Multi-comparisons		
3w WT vs 12w WT	s, p = .0020 **	
3w CKO vs 12w CKO	ns, p = .9403	
3w WT vs 3w CKO	s, p = .0051 **	
3w WT vs 3w Het	ns, p = .7932	
3w CKO vs 3w Het	ns, p = .1208	
12w WT vs 12w CKO	s, p < .0001 ****	
12w WT vs 12w Het	s, p =.0329 *	
12w CKO vs 12w Het	s, p = .0026 **	

Table 5B. Two-way ANOVA for Figure 6C. Density of Tomato+ supporting cells in heterozygotes	
Time Effect	f (1, 30) = 6.206 p = .0185 *
Genotype Effect	f (2, 30) = 4.97 p = .0229 *
Multi-comparisons	
3w WT vs 12w WT	s, p = .0013 **
3w CKO vs 12w CKO	ns, p > .9999
3w WT vs 3w CKO	ns, p = .0714
3w WT vs 3w Het	s, p = .0056 **
3w CKO vs 3w Het	ns, p = .8215
12w WT vs 12w CKO	ns, p = .8557
12w WT vs 12w Het	ns, p > .9999
12w CKO vs 12w Het	ns, p = .9325

Table 5C. Two-way ANOVA for Figure 6E. Number of Tomato-positive apical supporting cells per utricle in heterozygotes	
Time Effect	f (1, 30) = 2.230 p = .1458
Genotype Effect	f (2, 30) = 8.63 p = .0011**
Multi-comparisons	
3w WT vs 12w WT	ns, p = .6156
3w CKO vs 12w CKO	ns, p = .9995
3w WT vs 3w CKO	ns, p = .5424
3w WT vs 3w Het	ns, p = .3216
3w CKO vs 3w Het	ns, p = .9966
12w WT vs 12w CKO	s, p = .0456 *
12w WT vs 12w Het	s, p = .0259 *
12w CKO vs 12w Het	ns, p > .9999

TABLE 6

Table 6A. Two-way ANOVA for Figure 7A Tomato- type II hair cells	
3w Sox2 WT n=5	3w Sox2 CKO n=6
12w Sox2 WT n=9	12w Sox2 CKO n=5
Time Effect	f (1, 21) = 8.310 p=0.0089 **
Genotype Effect	f (1, 21) = .06557 p=0.8004
Multi-comparisons	
3w WT vs 12w WT	ns, p = .3478
3w CKO vs 12w CKO	ns, p = .1181
3w WT vs 3w CKO	ns, p = .9401
12w WT vs 12w CKO	ns, p = .9952

Table 6B. Two-way ANOVA for Figure 7B Tomato- type I hair cells	
Time Effect	f (1, 21) = 0.06248 p=0.8050
Genotype Effect	f (1, 21) = 9.842 p=0.0050 **
Multi-comparisons	
3w WT vs 12w WT	ns, p =. 4763
3w CKO vs 12w CKO	ns, p = .3503
3w WT vs 3w CKO	ns, p = .9993
12w WT vs 12w CKO	s, p = .0024 **

w = weeks, WT = wildtype, CKO = conditional knockout, Het = heterozygote, s = significant; ns = not significant

Chapter 3: Transcriptomic characterization of vestibular hair cells in adult mice

Authors: Amanda Ciani Berlingeri, Dr. Sarath Vijayakumar, Mi Zhou, Dr. Litao Tao, Dr. Neil Segil, Dr. Jennifer Stone

Note: This chapter is "In Progress" for publication. Tables that will be used for this publication are not presented here due to dissertation formatting requirements/restrictions.

Abstract

The sensory organs in the mammalian vestibular system house specialized mechanosensory hair cells that detect head movements. These hair cells are currently classified into two types, I and II, that differ in shape, molecular markers, physiology, and innervation. There is limited knowledge regarding the actual genetic diversity of mature vestibular hair cells and the regulatory mechanisms that control this diversity. Defining gene expression patterns in each distinct hair cell type in vestibular organs will inform on their unique features and functions and on strategies to drive functional hair cell regeneration. Single nucleus RNAseq sequencing was performed on utricles from adult C57BL/6 mice using 10x Genomics in the lab of our collaborator, Litao Tao, at Creighton University. I analyzed the transcriptomes of vestibular hair cells in mice at 6, 7, 10, 14, and 22 weeks of age using Seurat Library, creating cell clusters based on transcriptional similarities and verifying them using known marker genes. Genes of interest (>2x enriched in each subtype) were explored using data from other RNAseq datasets via the gEAR portal. I validated some genes of interest using fluorescent in situ hybridization. The analysis revealed five transcriptionally distinct hair cell clusters: three for type I hair cells, and two for type II hair cells. Further analysis showed two of the type I clusters were extrastriolar specific. I defined new candidate markers for each of the 5 hair cell subtypes and used high-resolution in situ hybridization chain reaction (HCR-FISH) to confirm the mRNA expression of 10 subtype-specific novel genes of interest (GOI) within each hair cell subtype: *Bmp2, Paqr9, Dlk2, Mgat4c, Agbl1, Cntnap5b, Lmo3, Irx2, Isl1,* and *Lin28b*. This work establishes a rigorous, integrated molecular atlas of adult utricular hair cells in mice, providing new insights into the

transcriptional identity of cell-type and region-specific specialization in the utricle. These findings have broad implications for understanding vestibular function and its decline with aging or disease. They also offer a foundation for future regenerative strategies aimed at selectively restoring distinct hair cell populations using gene- or region-specific therapeutic approaches.

Introduction

Vestibular hair cells are mechanoreceptors that sense head position and motion. They are located in the sensory organs of the inner ear: the utricle and saccule in the vestibule and the ampullae of the semicircular canals. Mammalian hair cells have two types of hair cells, type I and type II, that differ in morphology, physiology, and synaptic architecture. These differences have been determined using microscopy, histology, and electrophysiology. Type I hair cells synapse upon a cup-shaped (calyx) afferent terminal to generate short latency receptor potentials in response to hair bundle deflection, using quantal (glutamate-mediated) transmission, as well as faster, non-quantal (electrical) transmission (Holt et al., 2007; Songer and Eatock 2013; Contini et al., 2017; Contini et al., 2024; Dememes et al., 1995). In contrast, type II hair cells synapse upon small bouton afferent terminals, generate slower receptor potentials, and utilize only quantal transmission. Due to their rapid depolarization and calyx synapses, type I hair cells are thought to be better suited than type II hair cells to encode fast or sudden head motions.

Mammalian vestibular epithelia are clearly organized into specialized regions that support distinct functional roles. In the otolithic organs—the utricle and saccule—the sensory epithelium includes a central striolar zone surrounded by an extrastriolar region. The cristae of the semicircular canals show an analogous division into central and peripheral zones. These zones are distinguished not only by location but by structural and molecular differences among their hair cells. For example, Li et al. (2008) found that hair bundle morphology in the mouse utricle varies between these regions, with striolar hair cells exhibiting shorter kinocilia and lower kinocilium-to-stereocilium ratios. This difference likely confers greater stiffness and tuning to rapid head motion signals. Molecular markers also define these zones: for example, striolar type I hair cells are enriched for oncomodulin (OCM) and calbindin (CALB1) proteins (McInturff et al., 2018; Hoffman et al., 2018). Further zonal distinctions are evident in afferent innervation

of hair cells. Vestibular ganglion neurons innervating striolar zones fire irregularly at rest and respond preferentially to rapid, high-frequency motion, producing phasic bursts that encode the onset of acceleration (Baird et al., 1988; Goldberg et al., 1990; Eatock & Songer, 2011; Goldberg, 2000). Regular afferents, found most commonly in the peripheral/extrastriolar zone, have linear, proportional responses to graded head velocity and are well suited for rate coding (e.g., encoding the magnitude of head motion) (Sadeghi et al. 2007). Furthermore, type I hair cells in the striolar zone are uniquely innervated by calyx-only afferents, which terminate on either one or multiple hair cells (Fernández et al., 1988; Lysakowski and Goldberg, 1997).

Although we are aware of these many differences amongst hair cells and others, we do not know how many molecularly distinct subtypes of hair cells exist in adult mice or how development and maintenance of these subtypes are regulated. Exploring the molecular signatures that vary between type I and type II hair cells in the different zones using single cell transcriptomics will identify unique markers for each subtype and inform on unique functional specializations in adult hair cells, as well as the genes that regulate their form and function. Although some studies have examined the transcriptomic profiles of vestibular hair cells in mice (Jen et al., 2019; McInturff et al. 2018; Jan et al., 2021), they were conducted in relatively immature stages with only small cell numbers, leaving a gap in our understanding of transcriptional and regulatory specialization of mature vestibular organs. We performed an integrated analysis of single-nucleus RNA sequencing (snRNAseq) of utricles of adult mice from 6-22 weeks of age. Through my analysis of this transcriptomic data, I defined 5 subtypes of utricular hair cells that vary by hair cell type and location, and I generated an atlas of gene expression across these subtypes.

Methods

Mice

All procedures were approved by the Institutional Animal Care and Use Committee (IACUC) at Creighton University and the University of Washington, in accordance with NIH guidelines. Mice were euthanized in accordance with protocols in accordance with American Veterinary Medical Association guidelines. Mice

had a mixed genetic background composed most highly of C57BL/6J. Both sexes were used for all experiments.

Sample Collection and Preparation

To capture the mature utricular transcriptome across a range of adult ages, the lab of Litao Tao at Creighton University collected samples from mice at 6, 7, 10, 14, and 22 weeks of age. A subset of mice (n=4) received tamoxifen administration because they are being used as controls for a separate study involving a CreER driver line. For these mice, tamoxifen (Sigma-Aldrich, T5648) was dissolved in corn oil at 20 mg/mL and administered intraperitoneally at 75 mg/kg body weight once daily for 2 consecutive days. To assess whether tamoxifen administration itself altered gene expression, additional control mice (n=3) did not receive tamoxifen. Differential gene expression analyses incorporated tamoxifen treatment status as a covariate to account for potential transcriptional effects of tamoxifen exposure.

Inner-ear labyrinths were dissected from each mouse, and utricles were rapidly transferred to ice-cold DPBS. Tissue was enzymatically dissociated with trypsin, mechanically triturated to a single-cell suspension, filtered (40 µm), and pelleted by low-speed centrifugation. Cells were washed once in DPBS/0.04 % BSA and assessed for viability.

For nuclei isolation, cells were lysed in Nuclei EZ buffer on ice, diluted with the 10x Genomics wash buffer, and re-pelleted. Nuclei were rinsed in diluted Nuclei Buffer (10x Genomics), recentrifuged, and gently resuspended to the concentration recommended for Chromium Single-Cell 3′ v3.1 library preparation.

Single-Nucleus RNA-seq Library Preparation and Sequencing

Single nuclei were prepared for RNA sequencing in the Tao lab using the 10x Genomics Chromium platform. Nuclei were partitioned into Gel Beads in Emulsion (GEMs), where barcoding and reverse transcription occurred, followed by cDNA amplification and library construction. Libraries were sequenced on an Illumina NovaSeq. Sequenced libraries were processed using the Cell Ranger pipeline (10x Genomics) to demultiplex reads, align them to the mouse genome (mm10), and generate the gene–cell count matrix for downstream analysis. Quality control measures included the assessment of library size,

the distribution of read lengths, and the evaluation of mitochondrial gene expression to exclude degraded or low-quality samples.

Data Analysis

I analyzed the sequencing data from Tao lab as follows. The gene-cell count matrix (the primary data table from RNA-seq: rows list genes, columns list individual cells, and each cell in the table holds the raw number of sequencing reads mapped to that gene in that sample) was examined using the Seurat R package (v4.0) for downstream single-cell analytics. First, I conducted quality control filtering to remove low-quality nuclei and potential doublets. Nuclei with very high or very low unique molecular identifier (UMI) counts, or with >5% of reads mapping to mitochondrial genes, were excluded. Unsupervised clustering was applied using the Louvain algorithm in Seurat, yielding an initial set of transcriptomic clusters. Data were normalized and log-transformed, and I identified highly variable genes for clustering. Principal component analysis (PCA) was performed using Seurat on the variable gene matrix, and the top principal components were used to embed cells in a two-dimensional UMAP(Uniform Manifold Approximation and Projection) space for visualization. Integration using CCA (canonical correlation analysis) was used to combine each timepoint.

Clusters of cells were characterized based on expression of known marker genes within each cluster, and differential expression analysis was performed to characterize the transcriptional profiles specific to each identified cell cluster. Hair cells were identified by the expression of canonical markers such as *Pou4f3, Myo7a,* and *Otof* and exclusion of known markers for other cell types in the sensory epithelium, such as *Sox9 and Otog* for supporting cells. Clusters that had robust hair cell marker expression and lacked expression of supporting cell markers were retained (subset) for further analysis; all other clusters (supporting cells, glial cells, etc.) were excluded from further analysis. Hair cell nuclei were re-clustered to resolve hair-cell-intrinsic heterogeneity. Differential expression analysis compared each cluster to all others to find significantly upregulated genes, with an FDR < 0.05 threshold. We cross-referenced DEGs against the gEAR database to check for known expression patterns and validate novelty. Independent analyses performed by two investigators yielded consistent and reproducible results.

Validation of gene expression in situ

Expression of a selection of genes in each putative subtype (cluster) was validated using hybridization chain reaction-fluorescent in situ hybridization (HCR-FISH). Custom probes were designed by Molecular Instruments for 9 select genes showing more than two-fold enrichment in specific cell subtypes and baseline read counts/expression level.

After mice were euthanized using overdose of carbon dioxide, temporal bones were extracted and immersion-fixed in electron microscopy grade 4% paraformaldehyde (Polysciences, Inc., Warrington, PA) for between 2-3 hours at room temperature. Temporal bones were rinsed in phosphate-buffered saline plus .4%Tween (1XPBT). Whole utricles and horizontal, anterior, and/or posterior ampullae were removed from the temporal bone, and the membranes and/or otoconia overlying the organs were manually removed or blown off with syringe. Tissue was dehydrated through a series of graded steps to 100% methanol for storage in -80°C prior to HCR-FISH protocol. The hybridization protocol followed instructions by the manufacturer, Molecular Instruments

After HCR-FISH, some organs were immunolabeled in 96 well plates with the following primary antibodies overnight at room temperature: rabbit anti-calretinin (CALB2; 1:500, RRID:AB_2068506, #AB5054; EMD Millipore, Burlington, MA); goat anti-calretinin (CALB2; 1:500, RRID:AB_5054, Chemicon); goat anti-oncomodulin (OCM; 1:200, Santa Cruz Biotechnology, catalog #SC-7446, RRID:AB_2267583). Primary antibodies were labeled using Alexa Flour-conjugated secondary antibodies (1:400, Invitrogen, Carlsbad, CA) applied at room temperature for 2-3 hours.

To label cell nuclei, vestibular organs were incubated in 4’,6’-diamidine-2-phenylindole (DAPI; Sigma-Aldrich, St. Louis, MO) at 1 µg/mL in 10 mM PBS. Organs were mounted on slides in Fluoromount-G (Southern Biotech, Birmingham, AL) or Prolong Gold (Thermo Fisher Scientific, Waltham, MA) with a glass coverslip.

Tissue Imaging

I acquired fluorescent images of the labeled sensory epithelium with a FV-1000 laser scanning confocal microscope (Olympus, Center Valley, PA). Using 20x air, and 60x oil objectives, Z-series images at 0.25 or 0.5 μm steps were taken within each zone of the sensory epithelium from the lumenal surface through the first few microns of the stroma.

Results

Single-nucleus sequencing reveals five distinct hair cell clusters in the adult utricle.

The Tao lab performed single-nucleus RNA sequencing on adult mouse utricles across multiple age points (6–22 weeks) to map transcriptional profiles at mature stages (Fig. 1A). After quality control filtering, including removal of cells with high mitochondrial transcript proportions or abnormal gene/UMI counts, we retained high-quality nuclei for bioinformatic analysis. Integrating all cells from all timepoints using Seurat's integration workflow to minimize batch effects, I analyzed 16,079 cells. I applied normalization and PCA, selecting the top ~20 principal components based on elbow plots for integration and clustering. These data revealed diverse cell types within the utricle, including hair cells, supporting cells, transitional epithelial cells, and glial cells, with each type characterized by established marker gene expression at all timepoints (Fig. 1B,C,D,E,F,G, Supplemental Fig. 1A,). With every cluster represented in each dataset, including the no tamoxifen and tamoxifen timepoints, our data also showed that injection of tamoxifen did not alter transcriptional activity or change the relative abundance of any subtype (Supplemental Fig. 1A,C). The average number of genes detected per cell was 1,282. I initially identified four major clusters of hair cells in the global analysis (Fig. 1B,E,F,G-gray circle). These cells showed high expression in known hair cell genes *Pou4f3* (Fig. 1E), *Otof* (Fig. 1F), *Myo7a* (Fig. 1G).

Next, I extracted hair cell nuclei and re-clustered this subset to resolve hair-cell-intrinsic heterogeneity. This resulted in 2,814 cells being used for hair cell analysis. My analysis yielded five distinct clusters, replicated across age groups, and identifiable by unique combinations of known and novel marker genes (Fig. 2,3, Supplemental Fig. 1C,D,E,F). Cluster 1 consistently contained the greatest number of hair cells across all timepoints while the last two clusters (4 and 5) had the least number of cells (Fig. 2 and Supplemental Fig. 1C,D).

The hair cell clustering mostly paralleled the classical distinctions of type I versus type II hair cells and their striolar versus extrastriolar localization (Fig. 2C). There were striolar type I and type II hair cells, clusters 4 and 5 respectively, as well as clusters that represent extrastriolar type II (2) and type I hair cells (1,3). However, I determined that two clusters (1,3) corresponded to *extrastriolar type I hair cells*: these clusters lacked expression of *Sox2, Calb2, Mapt* and *Anxa4* (Fig. 2B,D,H), which in protein form have been defined as type II-specific markers (Desai et al. 2005a; Oesterle et al., 2008; McInturff et al., 2018). Furthermore, these two clusters shared high expression of *Spp1* (Fig. 2B,E,I), a marker for extrastriolar type I hair cells (McInturff et al., 2018), and they lacked transcripts for *Ocm* (Fig. 2E,F,I,J), which as a protein, is confined to the striola (Simmons et al. 2010). I called such cells *Spp1+, Ocm-.* One of these two *Spp1+/Ocm-* type I hair cell clusters (1) showed elevated expression of novel genes including *Mgat4c* (Fig. 3D) and the other cluster (3) showed high expression of *Tshz3* (Fig. 3F), suggesting a slightly different transcriptomic signature from each other. Although there were fewer hair cells in the second *Spp1+* cluster (cluster 3), this cluster was identified in each timepoint (Supplemental Fig. 1C). The existence of two *Spp1+/Ocm-* subclusters indicated that mature extrastriolar type I hair cells are not homogeneous and likely reflect subtypes with distinct gene expression profiles. In contrast, the striolar type I hair cell cluster (cluster 4) exhibited minimal *Spp1* expression and high expression of *Ocm (Spp1-, Ocm+*) (Fig. 2B, I). OCM protein has been localized mostly in striolar type I hair cells but has also been detected in a few striolar type II hair cells (Simmons et al. 2010; Hoffman et al. 2018). Cluster 4 consistently had a low number of cells to analyze (Supplemental Fig. 1, Fig. 1C).

The two type II clusters (2,5) had low *Spp1* expression and were enriched for transcripts previously associated with type II identity, such as *Sox2, Calb2* (Fig. 2B,H), *Mapt* and *Anxa4* (Bucks et al., 2017; McInturff et al., 2018). I hypothesized that one type II cluster was striolar and one was extrastriolar. In support of this, I found that, although two clusters of cells in my dataset expressed *Ocm* (4,5), only one of them (5) also expressed *Calb2* (Fig. 2B,H,J) and *Sox2*. Therefore, because cluster 5 was *Calb2+, Ocm+*, I distinguished it as a *striolar type II cluster* (Fig. 2B,H,J). The other type II cluster (2) lacked *Ocm* expression and highly expressed *Calb2* and *Sox2* (*Calb2+, Sox2+, Ocm-)*, so I designated it an *extrastriolar type II cluster* (Fig. 2B,H,J).

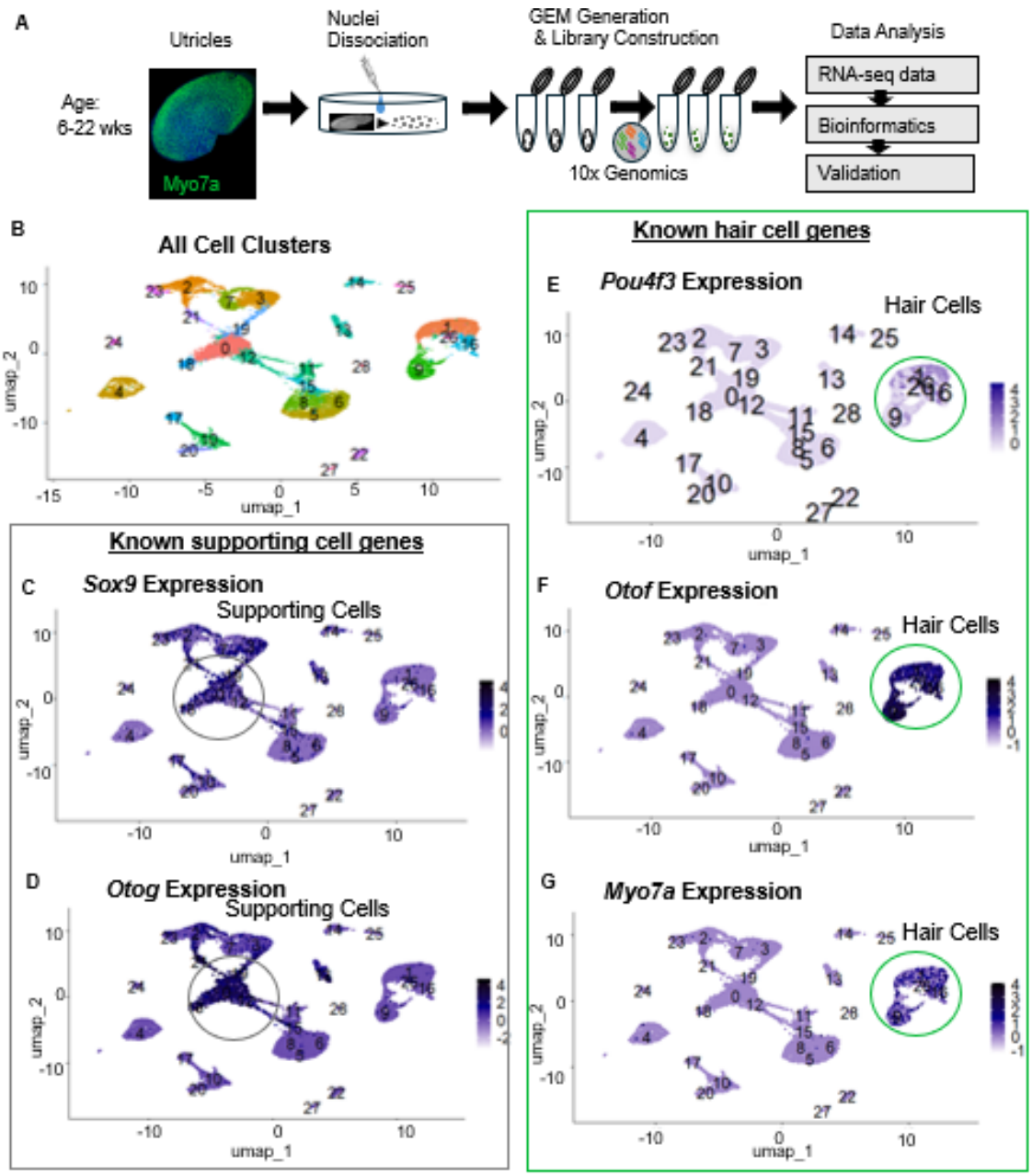

Figure 1. Single-nucleus RNA sequencing of adult mouse utricles identifies major cell classes and hair cell populations.

(A) Schematic outline of RNAseq process. (B) UMAP embedding of all nuclei (n=16,079) from adult mouse utricles aged 6–22 weeks, colored by unsupervised cluster assignment. Clusters include hair cells (HC), supporting cells (SC), and other cell populations. Each dot represents a cell. (C,D) Feature plots of known supporting cell markers, outlined and circled in gray (e.g., *Sox9* (C), *Otog* (D)) in distinct non-hair cell clusters confirm cluster identity. The darker the shading, the higher the expression. (E,F,G) Feature plots of known hair cell genes, outlined and circled in green (e.g., *Pou4f3* (E), *Otof* (F), *Myo7a* (G)) highlight the separation of hair cell clusters based on marker expression.

Based on the observations described above, my final annotation of the five putative hair cell subtypes based on their marker gene profiles and known spatial distribution in the utricle was as follows (see Fig. 2G):

Cluster 1: Extrastriolar Type I Hair Cells, type A (*Spp1+, Ocm–)*

Cluster 2: Extrastriolar Type II Hair Cells (*Calb2+, Ocm–)*

Cluster 3: Extrastriolar Type I Hair Cells, type B (*Spp1+, Ocm–)*

Cluster 4: Striolar Type I Hair Cells, type unknown (*Spp1+, Ocm+)*

Cluster 5: Striolar Type II Hair Cells (*Calb2+, Ocm+)*

Marker genes and differential expression in each cluster

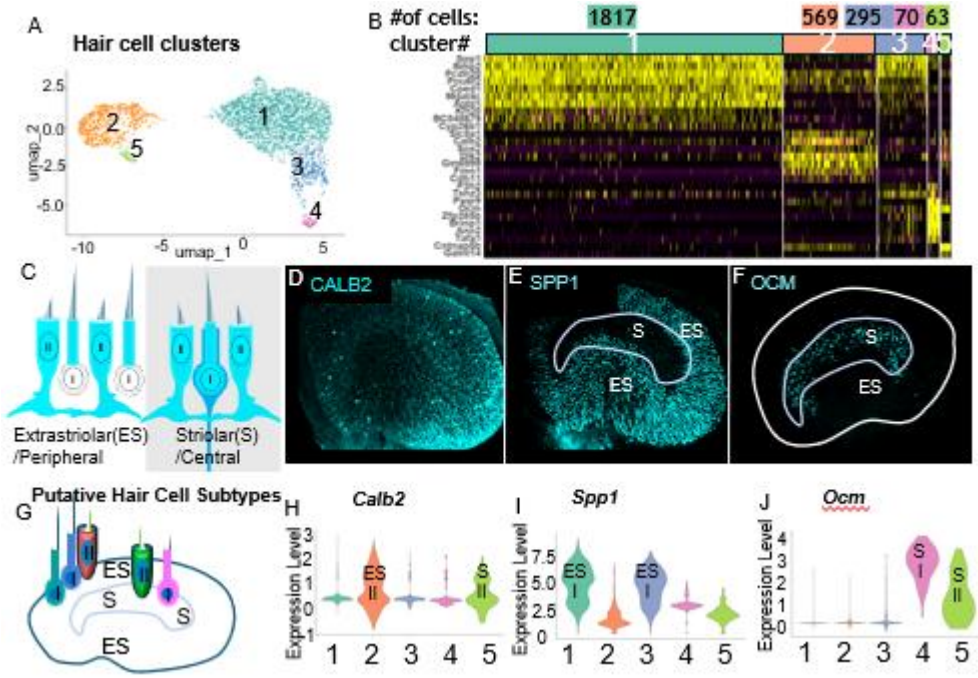

Figure 2. Resolution of five transcriptionally distinct hair cell subtypes in the adult utricle. (A) UMAP plot of hair cell-only nuclei (n=2,814) reveals five reproducible clusters. Each dot is one cell. (B) Heatmap of top differentially expressed genes (DEGs) per cluster shows unique marker profiles. (C) Diagram of hair cell types based on known marker expression and known spatial domains: I=type I HC, II=type II HC. (D-F) Low magnification confocal images of whole-mount utricle preparations labeled with antibodies of representative known marker genes (e.g., CALB2 (D), SPP1 (E), OCM (F)). ES= extrastriola, S= striola, drawn lines distinguish these regions. (G) Annotation of hair cell clusters into hypothesized subtypes based on marker expression and known spatial domains: Extrastriolar type I A (Cluster 1), Extrastriolar type II (Cluster 2), Extrastriolar type I B (Cluster 3), Striolar type I (Cluster 4), and Striolar type II (Cluster 5). (H,I,J) Violin plot visualizations of the same known marker gene expression from D-F, confirm region- and subtype-specific enrichment.

To quantify how distinct these transcriptomic identities are, I performed cluster-specific differential gene expression (DEG) analysis using Wilcoxon rank-sum tests (FDR < 0.05). This revealed varying degrees of transcriptional specialization (Supplemental Fig. 1D,E,F). Type II hair cells (clusters 2 and 5) exhibited the highest DEG counts (~165 and ~120 DEGs respectively) with average log2 fold changes of ~2.6–2.9, indicating considerable transcriptional variability. In contrast, extrastriolar type I clusters (1 and 3) showed lower DEG counts (<30 DEGs each) with average log2 fold changes ~2.1–2.2, suggesting a more stable transcriptome. Striolar type I cells (cluster 4) displayed intermediate DEG counts (~85 DEGs) but had the highest average fold change (~3.1), reflecting strong differential expression of a small, specific gene set.

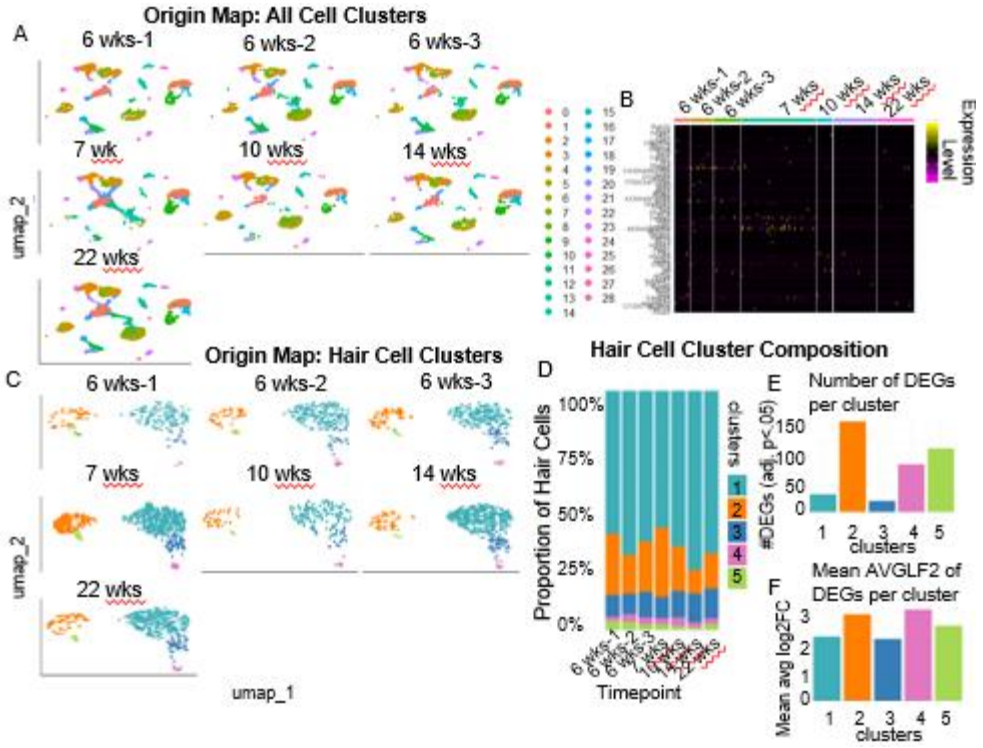

Supplemental Figure 1. Quality control, cluster origin mapping, and timepoint distributions. (A) UMAPs of all clusters isolated from each time point (6, 7, 10, 14, 22 weeks). (B) Heatmap showing the lack of time point-specific genes of interest in each cluster, demonstrating consistent cluster identification. (C) UMAPs of all hair cell only clusters isolated from each time point (6, 7, 10, 14, 22 weeks). (D) proportion of cells per cluster at each time point reveals a stable representation across adult stages. (E, F) Number of DEGs per cluster (E) and mean log2 fold change of DEGs per cluster (F) demonstrate variation in

A heatmap of top differentially expressed genes helped me to further visualize these distinctions (Fig. 2B). Novel genes of interest such as *Bmp2* and *Mgat4c* were enriched in the type I hair cell clusters (1,3;1 respectively), while *Dlk2*, *Calb2*, and *Sox2* defined the type II hair cell clusters (2,5). *Paqr9* (4) and *Cntnap5b* (5) stood out as highly regionally specific to the striolar zone, supporting their utility as new markers for striolar subtypes. The genes are *Bmp2* (Bone morphogenetic protein 2), *Mgat4c* (Mannosyl α-1,3-glycoprotein β-1,4-N-acetylglucosaminyl-transferase C), *Dlk2* (Delta-like non-canonical Notch ligand 2), *Calb2* (Calbindin 2 / calretinin), *Paqr9* (Progestin and adipoQ receptor family member 9), *Cntnap5b* (Contactin-associated protein-like 5B). *Agbl1*, recently identified to be expressed in some extrastriolar type I hair cells in Xia et al. (2025), was also expressed in one of our extrastriolar type I hair cells clusters (1) (Fig. 2B).

I examined the average log-normalized expression of marker genes across five hair cell clusters. Values presented below for each gene (in parentheses) are average log-normalized expression per cluster, computed as natural-log-transformed normalized counts. *Bmp2* was highly expressed in clusters 1 (1.19) and 3 (1.19), with moderate expression in cluster 4 (0.69), and minimal expression in clusters 2 (0.05) and 5 (0.03). This pattern supports its role as a selective marker for type I hair cells. *Mgat4c* showed strong enrichment in cluster 1 (1.59) and was nearly absent in other clusters, indicating specificity for a subset of type I cells with distinct glycosylation-related gene expression.

Dlk2 mRNA expression was highest in cluster 2 (1.12) and cluster 5 (0.66), while remaining low in clusters 1 (0.11), 3 (0.11), and 4 (0.08). This distribution aligns with a role as a type II hair cell marker. *Cntnap5b* displayed marked enrichment in cluster 5 (1.17) with minimal expression in other clusters (<0.05), suggesting it is a highly specific marker for striolar type II hair cells. *Paqr9* mRNA was almost exclusively detected in cluster 4 (1.67), with minimal expression in all other clusters (<0.13), highlighting its utility in defining an *Ocm+* striolar type I hair cell subtype. *Tshz3* was enriched in clusters 3 (0.77) and 4 (0.63), with much lower expression in clusters 1 (0.19), 2 (0.04) and 5 (0.12), indicating its potential as a marker for distinct type I subpopulations.

Violin plots showing differential expression levels provided another way to assess if known hair cell markers segregated appropriately to a given cluster. This analysis for 6 genes validated my prediction of

five transcriptionally distinct clusters of hair cells (Fig 3). Violin plots also facilitated identification of novel transcripts in each cluster. *Bmp2*, was almost exclusively expressed in type I clusters and was essentially absent from type II clusters (Fig. 3A). In contrast, *Dlk2* was detected in virtually all type II hair cells (Fig. 3B). *Mgat4c* and *Tshz3* both show differential mRNA expression in clusters 1 and 3 respectively (Fig. 3D, F). *Paqr9* was almost exclusively expressed in the striolar type I cluster (Fig. 3C), while *Cntnap5b* was enriched in striolar type II hair cells, suggesting subtype- and region-specific expression (Fig. 3E).

Spatial validation of hair cell subtypes by in situ hybridization:

I performed HCR-FISH on adult mouse utricles (whole-mounts) to detect transcripts of interest *in situ*. My goals were to validate the putative cluster identities and their putative spatial localization, as predicted by our single-cell RNA-seq analysis. To help me distinguish the different zones during my analysis, utricles were post-labeled with antibodies including anti-CALB2, which selectively labels type II hair cells throughout the utricle as well as calyx-only afferents confined to the striola, and anti-OCM antibody to label type I and II hair cells in the striola. Other antibodies such as SPP1 would have been desirable to use but did not work following HCR.

I found that *Bmp2* mRNA was enriched in all type I hair cells and absent from type II cells (Fig. 3A1-4), consistent with its snRNAseq expression pattern. *Bmp2* transcripts did not co-localize with the CALB2, the type II marker, further supporting its specificity for type I cells. *Paqr9* mRNA expression was restricted to the striolar region and was only detected in type I hair cells, as confirmed by the OCM antibody (Fig. 3C1-4). *Paqr9* did not co-localize with CALB2 but co-labeled for OCM in the striola as well as with type I hair cells surrounded by CALB2+ calyces, supporting its identity as a novel marker of striolar type I hair cells and could be functionally relevant in the hair cells that have calyx only innervation (Fig. 3C3,C4). *Dlk2* mRNA was detected in all CALB2+, type II hair cells in both striolar and extrastriolar zones (Fig. 3B1-3), confirming its classification as a type II marker. The *Cntnap5b* mRNA also co-localized with CALB2 as well as with the lighter OCM-labeled hair cells in the striola, consistent with a role as a striolar type II marker (Fig. 3B4). Together, these results provide spatially resolved, single-cell-resolution validation of the cluster-specific marker gene expression patterns predicted by our transcriptional analysis.

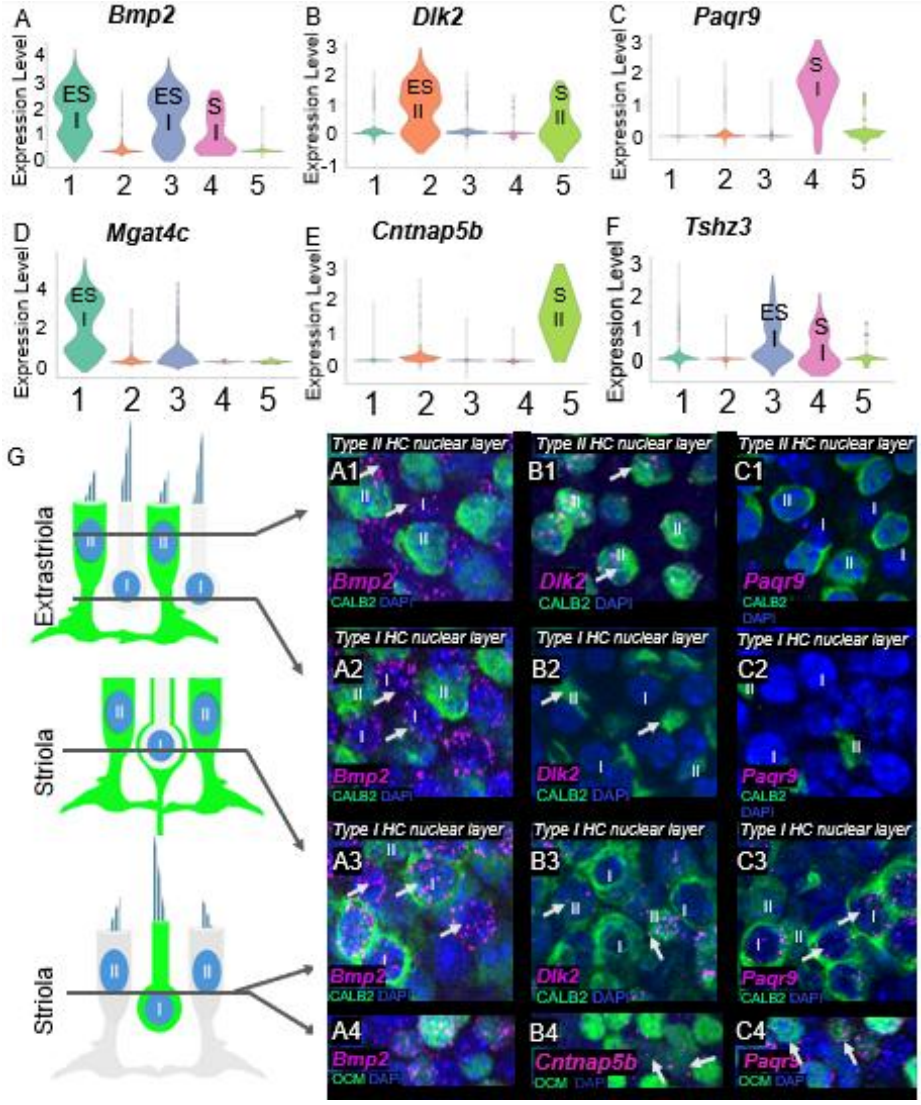

Figure. 3 Validation of novel markers within each hair cell subtype. A,B,C,D,E,F,G, violin plots of novel genes of interest for each cluster; *Bmp2 (A), Dlk2 (B), Paqr9 (C), Mgat4c (D), Cntnap5b (E), Tshz3 (F).* G, diagrams of hair cells in each region shown in A1-C4, gray arrows point to the representative regions and show the image layer. A1-C4, High magnification confocal images of whole-mount utricle preparations labeled with HCR-FISH probes for novel marker genes (e.g., *Bmp2, Paqr9, Dlk2, Cntnap5b* mRNA probes in magenta) and immunostaining with known antibodies (CALB2 and OCM in green). A1, A2, B1, B2, C1, C2, are all examples from the extrastriolar region and are co-labeled with CALB2. A3, A4, B3, B4, C3, C4 are all examples from the striolar region. A3, B3, C3, are all co-labeled with CALB2. A4, B4, C4 are all co-labeled with OCM. I=type I hair cell, II=type II hair cell. White arrows point to representative hair cells.

Discussion

A Transcriptional Atlas of Mature Vestibular Hair Cells

This study presents a novel transcriptional atlas of mature vestibular hair cells in the adult mouse utricle. I identified five distinct hair cell populations based on single-nucleus RNA sequencing, including type I and type II hair cell clusters from central (striolar) and peripheral (extrastriolar) zones. This study expands upon previous efforts by defining hair cell heterogeneity in the adult utricle at single-cell resolution and identifying novel molecular markers specific to regional and subtype identity via analyzing thousands of cells. Our findings also show that these zonal markers remain robustly segregated even in mature adults up to 22 weeks, reflecting a stable regional specialization of hair cells well into adulthood

Validation of Canonical Zonal Markers and Regional Specialization

I confirmed that canonical markers such as *Spp1* and *Calb2* differentiated type I from type II hair cells, respectively, consistent with earlier reports (McInturff et al., 2018; Hoffman et al., 2018; Desmadryl and Dechesne, 1992; Leonard and Kevetter, 2002; Desai et al., 2005a, 2005b; Hoffman et al., 2018). Notably, *Ocm* expression was observed in subsets of both type I and type II hair cells located within the striola, in agreement with immunolabeling studies indicating that OCM protein is not exclusive to a single hair cell type, but rather, to a specific zone (Simmons et al., 2010; Hoffman et al., 2018). This dual expression pattern supports the hypothesis that striolar hair cells, regardless of type, share a distinct molecular profile that may be related to their functional specialization (Ono et al., 2020a,b; Minor and Goldberg et al., 1991, Eatock and Songer et al., 2011). Our findings are consistent with functional and anatomical studies. For instance, Li et al., (2008) showed clear hair bundle difference in length and orientation between extrastriolar and striolar zones. This difference suggests distinct zonal mechanotransduction properties.

Intrinsic Heterogeneity Among Hair Cell Subtypes

Our analysis also revealed significant heterogeneity within hair cell subtypes. Among type I hair cells, two extrastriolar subclusters were distinguishable based on differential expression of genes such as *Mgat4c, Agbl1,* and *Tshz3,* with *Paqr9* enriched in striolar type I hair cells and suggesting functional and/or

developmental divergence. Similarly, type II hair cells were divided into striolar and extrastriolar subtypes: *Cntnap5b* was enriched in striolar type II hair cells, while *Dlk2* was expressed in all type II hair cells. This heterogeneity was not resolved in earlier single-cell work, likely because of age differences or limited cell recovery in neonatal or early postnatal samples (McInturff et al., 2018; Jen et al., 2019). Our results suggest that hair cell identity is defined not only by zonal location but also by transcriptional expression, in line with anatomical studies showing regional differences in afferent innervation and synaptic organization (Desai et al., 2005a,b), bundle height (Li et al., 2008), and function and physiology (Goldberg and Fernández 1977; Baird et al. 1988; Goldberg et al. 1990; Lysakowski et al. 1995; Sadeghi et al. 2007; Ono et al., 2020a,b).

Stability of Hair Cell Identity in Adult Mice

Comparative analysis of tamoxifen-treated and untreated mice revealed similar hair-cell clusters with compatible within-cluster variability. Thus, the tamoxifen injections did not introduce measurable transcriptional changes or alter the relative abundance of any subtype. Also, our data align with morphological evidence that hair cell phenotypes remain stable through mid-life even though synaptic loss can occur with aging (Wan et al., 2019). Our data add evidence that, in adult mice, hair cell identity is also preserved at the level of the transcriptome. This could indicate that age-related vestibular decline may involve changes at the synaptic level instead of loss of hair cell subtype identity. Recently, Xia et al. (2025) used single-nucleus sequencing to examine aging-related transcriptomic changes in the mouse inner ear, including the utricle. They showed clear transcriptomic changes, especially in one of their type I hair cell groups, as animals aged from 6 – 24 months (Xia et al., 2025). Our study, focusing on the young adult window (6-22 weeks), does not finding any strong evidence of age-related shifts in marker expression or cluster proportions, although we did not analyze this in great detail. Interestingly, many of our genes of interest within each hair cell cluster were not the differentially expressed genes of interest that Xia et al. identified as important genes for aging. Thus, the genes we selected to analyze here could be stable hair cell identifiers, even in old mice. Similar to Xia et al., our data suggest that major aging-associated transcriptomic reprogramming likely emerges later in life, after a period of relative stability.

Identification of Novel Subtype-Specific Marker Genes

We identified novel candidate markers for subpopulations, including *Dlk2*, which was highly enriched in all type II cells. Additional differentially expressed genes, such as *Bmp2, Paqr9,* and *Cntnap5b,* provide further evidence of discrete molecular programs within utricular hair cells and serve as valuable entry points for studying subtype-specific function or regeneration. Multiple studies have shown that adult mice can regenerate a limited number of type II hair cells (Wang et al., 2024, Lahlou et al., 2024; Jauregui et al. 2024; Gonzalez-Garrido et al., 2021; Forge et al., 1993; 1998; Kawamoto et al., 2009; Golub et al., 2012; Bucks et al., 2017; Sayyid et al. 2019; Hicks et al., 2020; Ciani Berlingeri et al., 2022), but whether such regeneration generates normal, mature hair cells with their zonal specificity remains unclear. Our data serve as a reference map to help evaluate naturally regenerated type II hair cells, as well as inform on new regenerative strategies for promoting regeneration of type I hair cells, by providing transcriptional markers for each hair cell type, in each zone. Our data can also provide new insights into how mature vestibular hair cells encode regional and subtype-specific identities. In future studies, these profiles can be referenced by others who wish to track lineage relationships, assess transcriptional changes after injury, or develop strategies for subtype-directed reprogramming.

Summary

In summary, our single-nucleus RNA-seq analysis defined five distinct hair cell subtypes in the adult mouse utricle. These clusters reflect molecularly distinct type I and type II hair cells in both striolar and extrastriolar zones, including two subpopulations of extrastriolar type I hair cells. Each population displayed a unique transcriptomic identity, supporting functional specialization and offering molecular targets for subtype-specific regeneration (Jan et al., 2021; Bucks et al., 2017). Our work confirms and extends previous findings on zonal molecular identity, an addition to providing novel markers: *Dlk2, Bmp2, Cntnap5b*, and *Paqr9*, for subtype specific studies, and established a benchmark for evaluating regeneration in aging and disease. Our transcriptomic analysis demonstrated that adult utricular hair cells comprise stable yet molecularly distinct populations defined by both cell type and spatial domain. These results highlight the complexity of hair cell identity in the vestibular system and provide a foundation for

future functional and regenerative studies. Future work should assess how these adult states change after injury or following pro-protection or pro-regeneration therapies.

Chapter 4: Testing the requirement for peripheral type I hair cells on motor behaviors in adult mice

Authors: Amanda Ciani Berlingeri, Dr. Noah Druckenbrod, Dr. Joe Burns, Dr. Brandon Cox, Dr. James Phillips, Dr. Jennifer Stone

Note: This paper chapter will be submitted for publication in fall 2025

Abstract

The mammalian vestibular system has two types of sensory receptor (hair cell), type I and type II, that have distinct morphological and physiological characteristics. Understanding the specific functions of each hair cell type is challenging, in part because most primary afferent neurons receive inputs from both cell types. To investigate the role of type I hair cells in vestibular functions, we ablated primarily type I hair cells from the peripheral zone of vestibular epithelia in young adult *Fbxo2*^{CreERT2}*::Rosa*^{DTA} mice (experimentals) and assessed the impact of this loss on motor behaviors and on nuclear CFOS expression in vestibular nucleus neurons evoked by off-axis centrifugation. Control mice, which lacked the *Rosa*^{DTA} *a*llele and had no hair cell ablation, underwent the same tests. In experimental mice, over 90% of peripheral type I hair cells were ablated in all vestibular organs by 1 week after tamoxifen injection, with no significant changes in cell numbers over time. Numbers of central type I and type II hair cells were unchanged up to 8 weeks after tamoxifen. Experimental mice, like controls, exhibited no circling or head-bobbing behavior, and no differences in home-cage locomotor activity were detected up to 6 weeks post-ablation. Stimulus-evoked CFOS expression in vestibular nucleus neurons was nearly abolished at 1 week after ablation. At this point, mice struggled to remain on the balance beam or rotarod for more than a few seconds, and their horizontal vestibulo-ocular reflex (hVOR) gains at 0.3 and 1.0 Hz were about half of control levels. No improvements were seen in balance beam performance or VOR gains out to 8 weeks, but some mice regained the ability to remain on the rotarod by 4 weeks, which based on our observations, they likely achieved by their leaning against the apparatus' wall. Middle-aged mice had

poorer baseline performance on the rotarod than young mice and, unlike young adults, did not recover any rotarod performance over time after ablation. These results show that peripheral type I hair cells are essential for maintaining hVOR gains and for certain motor behaviors requiring balance and coordination, but they are not necessary for normal locomotion.

Introduction

In mammals, five vestibular organs sense head motions in a variety of directions and frequencies using specialized mechanosensory receptors called hair cells. Head motions cause a specialized organelle located atop each hair cell (the hair bundle) to deflect. When this deflection occurs in a certain direction, potassium enters the cell, and its membrane voltage (receptor potential) increases, leading to neurotransmission across the hair cell-vestibular ganglion neuron (VGN) synapse and increasing the neuron's firing rate. VGN (afferent) projections to the brainstem and cerebellum alter the activity of neurons in those regions, helping to control the movements of the eyes, neck, and limbs, that enable navigation, balance, and spatial orientation in a variety of conditions.

Mammals have two types of vestibular hair cell, type I and type II. Type I hair cells generate short latency receptor potentials in response to hair bundle deflection, and they synapse upon a cup-shaped (calyx) afferent terminal using quantal (glutamate-mediated) transmission, as well as faster, non-quantal (electrical) transmission (Holt et al., 2007 ; Songer and Eatock 2013 ; Contini et al., 2017 ; Contini et al., 2024; Dememes et al., 1995). In contrast, receptor potentials take longer to form in type II hair cells, and they synapse upon small bouton afferent terminals using only quantal, glutamatergic, transmission (Lysakowski & Goldberg, 1997; Holt et al., 2006). Due to their rapid depolarization and calyx synapses, type I hair cells are thought to be better than type II hair cells at encoding fast head motions.

Type I and II hair cells are distributed throughout two zones called *peripheral* and *central* in the horizontal, anterior, and posterior ampullae, which sense angular acceleration, and *extrastriolar* and *striolar* in the utricle and saccule, which sense linear acceleration (**Figure 1**). Although we do not understand the specific roles of each hair cell type in each zone, we do know some important aspects about the afferent fibers that innervate hair cells there. Afferent fibers terminating in the central/striolar zone display irregular firing

patterns at rest, while those innervating peripheral/extrastriolar hair cells have more regular firing patterns (Baird et al., 1988; Goldberg et al., 1990). Irregular afferents exhibit high sensitivity to high-frequency, fast-changing stimuli; they fire bursts of action potentials at the onset of head acceleration, enabling short-latency, phasic encoding of sudden movements (Eatock and Songer, 2011; Goldberg, 2000; Baird et al., 1988; Goldberg et al., 1990). As such, irregular afferents are thought to act as timing detectors. Consistent with this, Ono et al. (2020) showed that the striolar zone is required to detect jerk stimuli, which have rapid onset and acceleration (Ono et al., 2020). This makes them essential for reflexes requiring rapid communication of movement onset, such as the vestibulo-ocular reflex (VOR), which stabilizes gaze during high frequency head movements. In contrast, regular afferents, found most commonly in the peripheral/extrastriolar zone, have linear, proportional responses to graded head velocity and are well suited for rate coding (e.g., encoding the magnitude of head motion) (Sadeghi et al. 2007). Their tonic and sustained firing makes them well suited to convey information about slow or constant head movements, such as posture and tilt (Sadeghi et al., 2007; Goldberg & Fernandez, 1971). Although irregular afferents are highly responsive to sudden jerk stimulus and lack of a defined striolar zone causes loss of vestibular evoked potentials, reversible ablation experiments by Minor and Goldberg in 1991 showed that these irregular afferents are not strictly required for vestibular-occular reflex measured in squirrel monkeys. Using selective galvanic silencing of irregular canal fibers, the VOR gain and phase remained unchanged, indicating that regular afferents can sustain the reflex under these conditions. These two studies suggest a division of labor: regular (peripheral/extrastriolar) inputs provide the steady, linear velocity signal that forms the backbone of the VOR, while irregular (central/striolar) afferents excel at detecting brief, high-acceleration transients and sharpening reflex timing when head-movement frequencies exceed the bandwidth of routine tests. Collectively, these observations suggest that afferents terminating on peripherally located hair cells may selectively encode more stable motor states, while those synapsing with central hair cells may enable high-fidelity detection of sudden changes (Goldberg and Fernández 1977; Baird et al. 1988; Goldberg et al. 1990; Lysakowski et al. 1995).

The extent to which hair cells influence firing patterns in vestibular afferents is not well understood (Eatock & Songer, 2011; Goldberg, 2000). Furthermore, the vast majority of afferent neurons seem to have both calyx and bouton terminals and therefore, receive synaptic input from both type I and type II hair cells

(Fernandez et al., 1988; Goldberg 2000; Lysakowski and Goldberg 1997, 2008), so it is challenging to infer the specific roles of each hair cell type in motor functions that rely on the vestibular system. To begin to address this, we ablated nearly all type I hair cells in the peripheral zone of all vestibular organs of adult mice. Our findings revealed that peripheral type I hair cells are essential for normal motor coordination, balance, and the sensitivity of the vestibulo-ocular reflex (VOR), shedding new light on the zone-specific contributions of vestibular hair cell types to sensorimotor function.

Materials and Methods

1. Animals

We obtained *Fbxo2^{CreERT2}* mice from Andrew Groves at Baylor College of Medicine, whose lab modified them (McGovern et al., 2022) after they were generated in Stefan Heller's lab at Stanford University (Hartman et al., 2018). To validate *Fbxo2^{CreERT2}* expression in sensory organs and brains, we used *Rosa26$^{loxP\text{-}stop\text{-}loxP\text{-}tdTomato}$* reporter mice (also called Ai14, stock #7914, Madisen et al., 2010) mated with *Fbxo2^{CreERT2}* mice. We refer to these mice as *Fbxo2^{CreER}::Rosa^{TOM}* mice. To ablate hair cells, we used *Rosa26$^{loxP\text{-}stop\text{-}loxP\text{-}DiphtheriaToxinA}$* (*Rosa^{DTA}*) mice that were purchased from The Jackson Laboratory (#009669). Experimental mice were heterozygous for both *Fbxo2^{CreERT2}* and *Rosa^{DTA}* alleles. We refer to these mice as *Fbxo2^{CreER}::Rosa^{DTA}* mice. For most controls, we used *Fbxo2^{CreER}* mice with no DTA allele, either with and without tamoxifen. For additional controls, we used *Fbxo2^{CreER}::Rosa^{DTA}* mice without tamoxifen. In each cohort of similarly aged mice, experimental and control mice were studied simultaneously.

All mice had a mixed genetic background that was enriched for C57Bl6/J. Both male and female mice were included in all experiments. Sex differences were not examined due to different numbers of each sex across experimental and control mice. We studied two different age groups of mice: *younger mice*, which were 3-6 months at the start of the experiment and *middle-aged mice, which were* 16 months when the experiment started. Mice were housed with free access to food and water. Experiments were approved by the Institutional Animal Care and Use Committee of the University of Washington School of Medicine (Seattle, WA) and adhered to standards of the American Veterinary Medical Association.

2. Tamoxifen injections

To activate Cre expression in hair cells, adult mice were injected intraperitoneally (IP) with tamoxifen (Sigma-Aldrich, St. Louis, MO) at 3.5 - 4.5 mg/20g, once a day on two consecutive days spaced 20-24 hours apart. Similar amounts and spatial patterns of hair cell loss were seen with each dose.

3. Vestibular Function Assessment

Mice in the younger age group underwent behavioral and/or physiological testing before tamoxifen and/or at 1, 3, 4, 6, and/or 8 weeks (wks) post-tamoxifen. While most mice were tested at all time points, some mice were tested at only a few timepoints due to our desire to verify hair cell ablation in each cohort of mice. For mice in the older age group, we tested only two post-tamoxifen timepoints: 1 and 4 weeks.

3A) Behavioral testing

Most control and experimental mice in the study were subjected to a battery of tests across time, before and after tamoxifen injection, described below. All testing occurred during daylight hours, usually mid-day.

3A.1) Horizontal vestibulo-ocular reflex (hVOR)

The hVOR, which reflects horizontal crista function, was assessed in dark conditions in mice with head movement restricted during rotation in the horizontal plane. Gains (eye velocity/head velocity) were measured at 0.3, 0.5, 0.7, and 1.0 Hz. Similar to Jáuregui et al. (2024), control and experimental mice underwent testing in a custom, silent linear servo-driven apparatus that rotated each mouse *en bloc* about an earth-vertical axis intersecting the interaural axis in the mid-sagittal plane. In the current experiments, the head was minimally restrained with a restrictive collar. Prior to testing, mice were anesthetized with isoflurane and placed in a plastic restraining tube that encircled their body. After about 5 minutes of recovery, the tube was mounted on a rate table inside a light-tight enclosure equipped with a high-magnification infrared (IR) CCD camera. Each mouse was oriented in the stereotaxic plane, and head and eye motions were video-recorded. Sinusoidal rotation (±10◦) about an earth-vertical axis was performed in complete darkness at frequencies from 0.3 to 1.0 Hz. From the videos, we measured eye position during epochs of stable head position relative to the rotator, and we calculated slow-phase eye

velocity from filtered, de-saccaded traces using custom software. Gain values (eye velocity/head velocity) were derived via a least-squares sine-wave fit of eye and head velocity for each cycle, averaged over multiple rotation cycles. Results were confirmed by directly comparing the amplitude of sinusoidal eye movements (during saccade-free cycles) to the constant amplitude of head rotation.

3A.2) Rotarod

To assess balance and neuromuscular coordination, mice were tested under either normal room light or relative darkness (red light) following methods described by Tung et al. 2014; Luong et al., 2011)). The apparatus consisted of a 3.5 cm thick cylinder that rotates up to 40 rpm at a gradually accelerating rate with grip indentations on the rod (Accelerating Rotarod**,** Economex (Columbus Instruments, Columbus, OH)). Before testing, each mouse was placed on the stationary rod for approximately 30 seconds, after which the rod began to move and accelerate. During testing, the time (in seconds) that each mouse remained on the rod was recorded with a timer after each run. Mice underwent up to 10 trials per session, with 30 seconds of rest in between each trial. Each trial lasted until mice fell from the rod onto a soft padded surface about 18 inches below or the trial was ended by the experimenter (at 5 minutes after the start of the trial).

3A.3) Balance Beam

To further assess balance and motor coordination, mice were subjected to a balance beam task. Mice traversed a 3-foot-long, ½-inch-diameter aluminum rod inclined at an angle of approximately 5.7° above horizontal toward a small (13 cm × 22 cm) and dark housing unit (goal box) that was positioned approximately 60 cm above the ground. A net was placed under the bar to catch the mice if the fell off. Testing was conducted under ambient lighting conditions, encouraging mice to seek shelter in the dark goal box, which is a natural behavior. Each trial recorded the time it took for the mouse to traverse the beam. Mice underwent up to six trials per session, each separated by at least a 1-minute interval. Before official trials, mice were gradually introduced to the beam with progressively increasing distance from the goal box, until they could traverse it independently. We considered the mouse's ability to remain on the bar and the speed of passage as measures of motor function on this test.

3A.4) Locomotion and exploration in a novel environment

We monitored each mouse's motor activity for 5 minutes in a clean cage under ambient room lighting. Mice were videotaped in the cage using a video camera on a tripod and QuickTime Player video capture software. Parameters such as total distance traveled, velocity, acceleration, and numbers of full body rotations (spinning in place) were determined using Ethovision software to identify any changes in general activity or vestibular dysfunction. On videos, we also looked for evidence of head-bobbing in the horizontal or vertical planes, which has been reported in mice after near-complete hair cell loss (e.g., Golub et al. 2012).

3B) Physiological testing: Assessing CFOS upregulation in vestibular nucleus neurons following off-axis sinusoidal centrifugation

Mice were placed in a 500 mL beaker at the periphery of a 28 cm-radius rate table and subjected to sinusoidal centrifugation about an earth-vertical axis (0.01 Hz, pk-pk 600°/s) for 10 minutes. Because the mice were unrestrained, they experienced acceleration and deceleration in multiple planes, likely activating several vestibular organs and modulating both rotational and linear acceleration afferents. After 45 minutes of recovery with access to food and water, mice were deeply anesthetized with ketamine (100 mg/kg) and xylazine (5 mg/kg) delivered intraperitoneally. Cardiac perfusion was then performed with saline for a few seconds, followed by 4% paraformaldehyde (Sigma-Aldrich).

4) Tissue labeling of vestibular organs and brain sections

After mice were killed using an overdose of carbon dioxide, temporal bones were extracted and immersion-fixed in electron microscopy grade 4% paraformaldehyde (Polysciences, Inc., Warrington, PA) for 2-5 hours at room temperature on a nutator. Temporal bones were rinsed in phosphate-buffered saline (PBS) and stored at 4°C prior to dissection of the vestibular end organs.

Whole vestibular organs (utricles, saccules, as well as horizontal, anterior, and posterior ampullae) were removed from the temporal bone, and the membranes and/or otoconia overlying the organs were

manually removed. Organs were immunolabeled in 96 well plates with the following primary antibodies overnight at room temperature: mouse anti-secreted phosphoprotein 1 (SPP1; 1:300, RRID:AB_2194997, catalog #sc-21742, Santa Cruz Biotechnology); rabbit anti-ßIII tubulin (TUBB3; 1:500, RRID:AB_291637; #PRB-435P; Covance); mouse anti-ßIII tubulin (TUBB3; 1:300; gift from Anthony Frankfurter, University of Virginia); rabbit anti-calretinin (CALB2; 1:500, RRID:AB_2068506, #AB5054; EMD Millipore); goat anti-calretinin (CALB2; 1:500, RRID:AB_5054, Chemicon); goat anti-oncomodulin (OCM, 1:200, Santa Cruz Biotechnology, catalog #SC-7446, RRID:AB_2267583); rabbit anti-myosin VIIa, MYO7A, 1:300, RRID:AB_10013626; #25-6790; Proteus Biosciences Inc.). The following primary antibodies overnight at 37˚C: mouse anti-CTBP2 IgG class1 (CTBP2; 1:300, RRID:61204, BD Biosciences); mouse anti-GLUR2, class 2a (GLUR2, 1:300, MAB397, Millipore Sigma, Burlington, MA). Primary antibodies were labeled using Alexa Flour-conjugated secondary antibodies (1:400, Invitrogen) applied at room temperature for 3 hours. To label cell nuclei, organs were labeled with 4',6'-diamidine-2-phenylindole (DAPI; Sigma-Aldrich) at 1 µg/mL in 10 mM PBS. Organs were mounted on slides in Fluoromount-G (Southern Biotech) or Prolong Gold (Thermo Fisher Scientific) with a glass coverslip.

For immunohistochemical labeling of CFOS in vestibular nuclei, brains were mounted in agar gel, and 50 µm coronal sections through the entire vestibular nucleus (VN) complex were generated using a vibratome (Leica), starting at the caudal edge of the fourth ventricle (Bregma −7.08 mm) and ending around Bregma −5.68 mm. Sections were stored in PBS at 4°C until immunohistochemical labeling using rabbit anti-phospho-CFOS (RRID:AB_2106617; Cell Signaling Technology #4384) and the DAB immunostaining method, as described in Jauregui et al. (2024). Then, sections were mounted on Superfrost Plus slides (Fisher Scientific, #22-037-246) with DPX media (Electron Microscopy Sciences, #13512) and coverslipped.

To assess CreER activity in the central vestibular pathway, we prepared sections of brains from *Fbxo2*^{CreERT2}*::Rosa*^{Tom} mice at 4 weeks post-tamoxifen and examined TOM fluorescence.

5. Imaging of vestibular organs and brain sections

We acquired images of fluorescent labeling in the vestibular organ or the brain using a FV-1000 laser scanning confocal microscope (Olympus, Center Valley, PA). For vestibular organs, we used a 20x or 60x oil objective to generate Z-series images of the entire sensory epithelium at 0.5 or 1.0 μm steps starting at the lumenal surface (top of the sensory epithelium) and ending in the stroma underlying the sensory epithelium. Olympus files were imported into Fiji (http://fiji.sc/), and cells in experimental and control groups were counted using Fiji's Cell Counter plugin.

6. Quantitative analysis of vestibular organs and brain sections

For assessing hair cell ablation using acquired images, 100 μm x 100 μm regions of each zone in the maculae were assessed in organs labeled for CALB2, SPP1, OCM, and/or TUBB3. 20% of each utricle was sampled. For ampullae, ~50% of each epithelial zone (central or peripheral) was sampled using several 100 μm x 100 μm regions. Experimenters performing cell-counting were blind to the experimental groups. Average hair cell density (cells/10,000 μm^2) was calculated for each specific region. Fiji and Adobe Photoshop CS4 were used to make figures.

For quantifying presynaptic and postsynaptic elements in sensory epithelia, confocal images (60x immersion oil, 3x zoom) were taken of the lateral extrastriolar and peripheral zones of utricles and horizontal ampullae that were immunolabeled for CTBP2, GLUA2, and MYOVIIA antibodies. We identified the basolateral processes of hair cells using MYO7A and counted the number of CTBP2 puncta and dyads of CTBP2 and GLUA2 (González-Garrido et al., 2021; Pujol et al., 2014), for 10 control type II hair cells and 60 experimental type II hair cells at 4 weeks post-tamoxifen.

For quantifying CFOS, we examined every third brain slice for phospho-cFos immunoreactivity using a conventional room-temperature protocol. Vestibular nuclear neurons (VNNs) expressing cFos after centrifugation were visualised in bright-field on a Zeiss Axioplan with 4×–20× objectives. Images were acquired with SlideBook software (Intelligent Imaging Innovations, Denver, CO). Neuronal counts were made at 20× magnification using a 10 × 10 eyepiece reticle grid. Immunostained slices spanning the rostro-caudal extent of the vestibular complex was examined. Within each section containing the medial

(MedVNu) or spinal (SpVNu) vestibular nuclei, neurons displaying robust nuclear cFos signal were counted and then averaged.

7. Statistics

Prism6 (GraphPad Software, San Diego, CA) was used for statistical analysis and graph generation. Data are expressed as mean ± 1 standard error of the mean (SEM). Mouse numbers (n) are reported in each Figure Legend. Every symbol on the graph represents one mouse. For cellular analyses, each data point corresponds to one sensory organ deriving from either the left or right side of the mouse. We considered differences for all comparisons to be statistically significant if $p \leq 0.05$.

Results

Ablation of peripheral type I hair cells was induced by tamoxifen in adult *Fbxo2^{CreERT2}::Rosa^{DTA}* mice

The goal of this project was to selectively ablate type I hair cells located in the periphery of each vestibular epithelium in order to test the requirement of these cells for various vestibular functions. The sensory epithelium of each organ has two distinct zones specified by anatomic location, morphological and physiological features of its afferent innervation, and other features (**Fig. 1A-D**, utricle and horizontal ampulla are shown). In the macula-type epithelium of otolithic organs (utricle and saccule), which sense linear acceleration and head position, the two zones are 1) a centrally located striola (S) and 2) a peripherally located extrastriola (ES), which surrounds the striola (**Fig. 1B,D**). In the crista-type epithelium of the horizontal, anterior, and posterior ampullae, which detect head rotations, there is a central (C) zone and a peripheral (P) zone (**Fig. 1C,D**). The central and peripheral zones of the cristae are in many ways analogous to the striola and extrastriola of the maculae.

To test the requirement for type I hair cells in peripheral or extrastriolar zones of the vestibular organs, we administered tamoxifen to young adult mice *Fbxo2^{CreERT2}::Rosa^{DTA}* mice. Before doing so, we verified that tamoxifen induces CreER in the majority of peripheral type I hair cells in adult *Fbxo2^{CreERT2}::Rosa^{Tom}* mice, as described by McGovern et al. (2022), injecting tamoxifen to 6 week old mice and examining organs at

1 week after tamoxifen (**Fig. 1H).** Although we examined all five vestibular organs and found comparable results (see **Table 1**), we performed rigorous quantitative analyses in only the utricle and horizontal crista. Similar to McGovern et al. (2022), tamoxifen induced a high level of tdTomato reporter (TOM) expression in over 90% of extrastriolar type I hair cells and 30% of type II hair cells in the utricle (**Fig. 1E,G, Table 1**). While 30% of striolar type I cells also had TOM labeling, it was very light compared to extrastriolar type I hair cells. In horizontal cristae, we detected strong TOM labeling in 95% of peripheral type I hair cells and 25% of type II hair cells; only light TOM labeling was seen in central type I hair cells (in about 28% of the population)

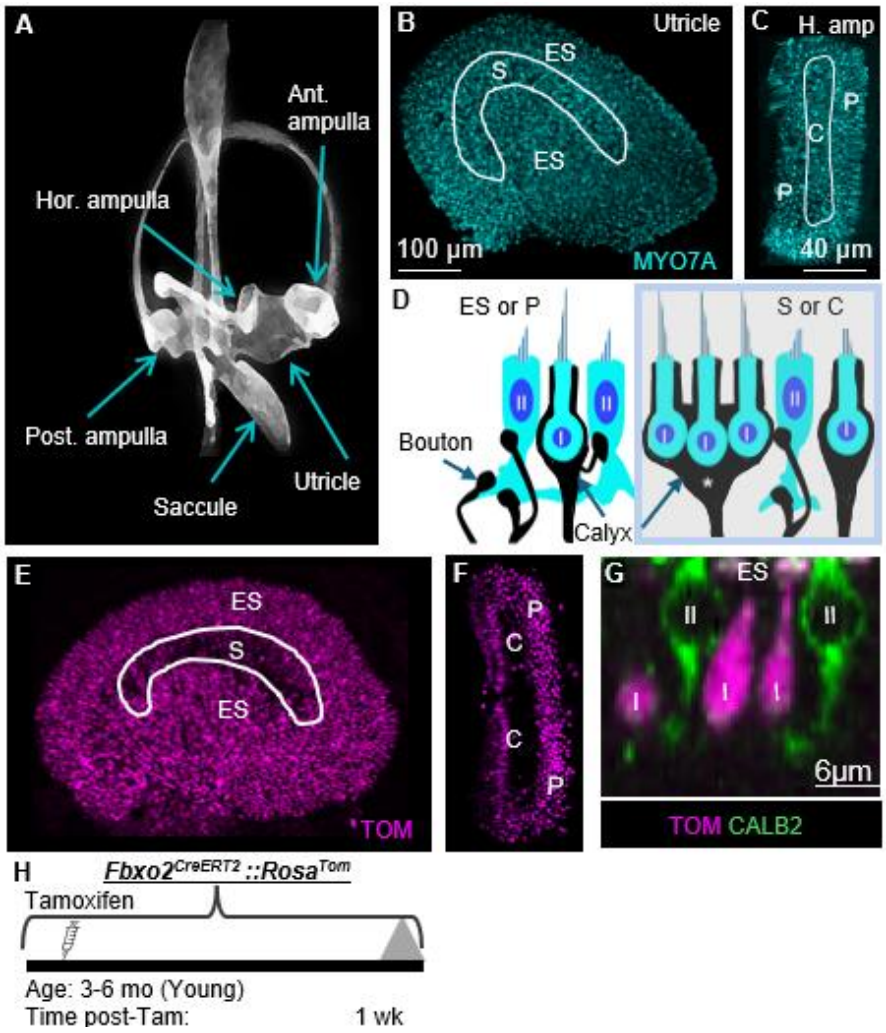

Figure 1. Tamoxifen-induced CreER activity in *Fbxo2*^{CreERT2}:: RosaTom **mice in peripheral type I hair cells across vestibular organs.**

A) Digitized version of a paintfill (generated prior to this study) illustrating the anatomical locations of the vestibular sensory epithelia. (A,B) Top-down confocal microscope images showing myosin VIIA (MYO7A) immunofluorescence in utricle (B) and horizontal ampulla (C). The different zones are shown for each epithelium: striolar (S) and extrastriolar (ES) for utricle in B, and central (C) and peripheral (P) for horizontal ampulla in C. D is an illustration of a transverse section through the type I and type II hair cells (cytoplasm, cyan; nucleus, cobalt blue) and their bouton and calyx afferents (black) in the analogous zones of sensory epithelium: extrastriolar (ES) and peripheral (P), as well as striolar (S) and central (C). (E–G) Confocal images showing tdTomato (TOM) fluorescence in utricle (E,G) and horizontal ampulla (F) at one week post tamoxifen in adult *Fbxo2*^{CreERT2}*::Rosa*^{Tom} mice. Note the high efficiency of TOM labeling in extrastriolar/peripheral zones and low efficiency in striolar/central zones (E,F) and in type I hair cells (G), which are CALB2-negative. (H) Schematic timeline illustrating tamoxifen delivery and subsequent tissue harvest (gray triangles) carried out one week after injection to validate TOM expression. Scale bar in B applies to E. Scale bar in C applies to F.

(**Fig1F, Table 1**). Only rare (5-15) supporting cells were TOM-positive in any organ. No TOM was seen in neurites in the epithelium, indicating that neither afferent neurons (VGNs) nor brainstem neurons projecting to epithelium had CreER activity.

Next, we assessed if tamoxifen induced selective loss of extrastriolar/peripheral type I hair cells in the various organs of adult *Fbxo2*^{CreERT2}*::Rosa*^{DTA} (experimental) mice. We counted type I and II hair cells in each zone of every organ at 1 and 4 weeks post-tamoxifen, and in the utricle and horizontal crista at 1, 4, 6, and 8 weeks post-Tam. A summary of the experimental schedule is shown in **Fig. 2T** To classify each hair cell as type I or type II and to identify each epithelial zone as ES/S or P/C during cell counting, we used antibodies to the following proteins: SPP1, which is expressed in extrastriolar type I hair cells but not in other cell types (McInturff et al., 2018); ßIII tubulin (TUBB3), which is enriched in the calyx terminal surrounding type I hair cells in all regions (see Stone et al., 2021); CALB2, which is expressed in the cytoplasm and nucleus of nearly every type II hair cell and few or no type I hair cells, as well as in a subset of afferent calyces in the striolar/central regions (Desmadryl and Dechesne, 1992; Leonard and Kevetter, 2002; Desai et al., 2005a, 2005b; Hoffman et al., 2018) and OCM, which is expressed in the nucleus and cytoplasm of most type I hair cells and a few type II hair cells, only in the striola (Simmons et al., 2010; Hoffman et al., 2018).

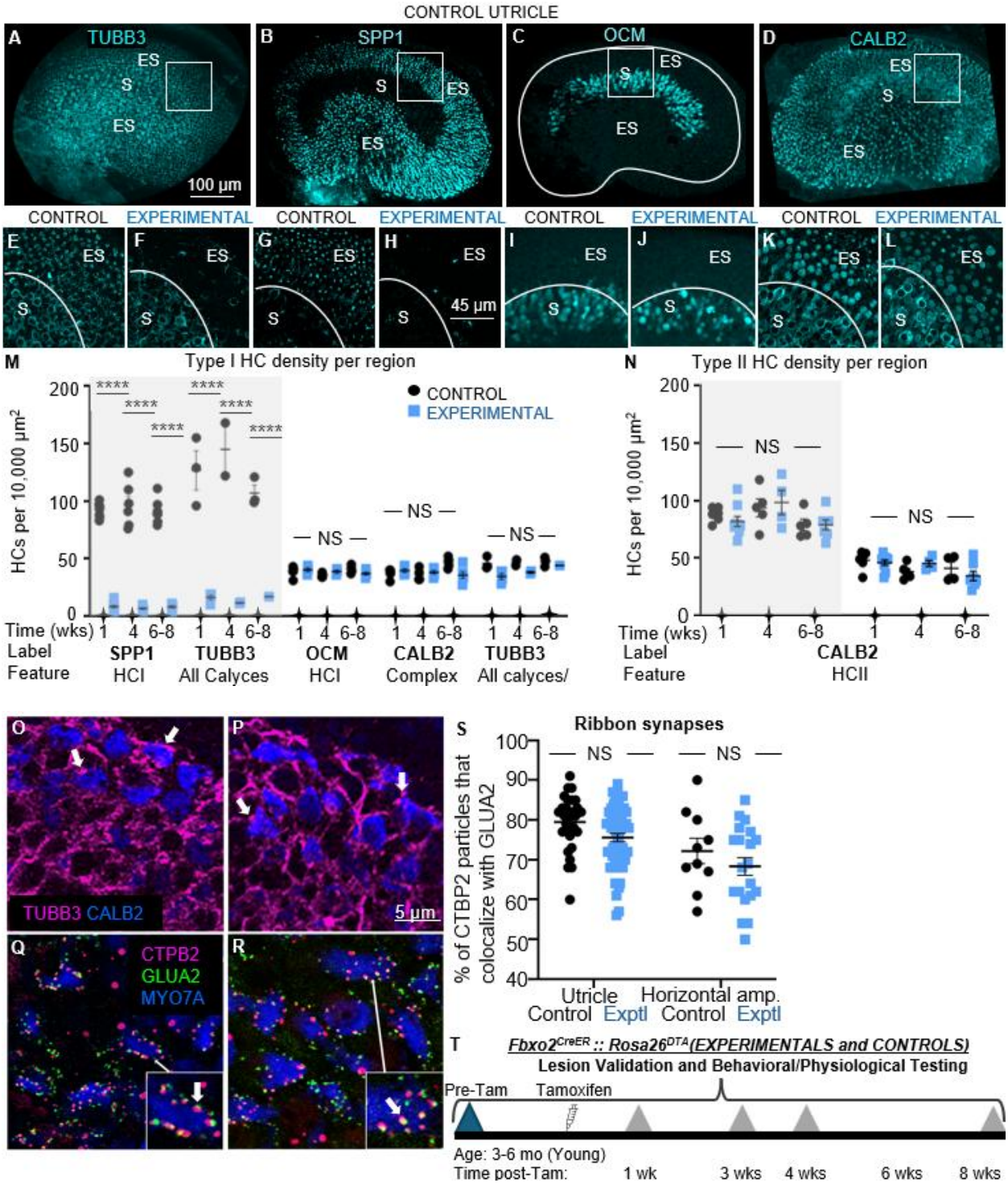
CONTROL UTRICLE
A TUBB3
B SPP1
C OCM
D CALB2
ES
S
100 µm
CONTROL EXPERIMENTAL CONTROL EXPERIMENTAL CONTROL EXPERIMENTAL CONTROL EXPERIMENTAL
E F G H I J K L
45 µm
M Type I HC density per region
N Type II HC density per region
HCs per 10,000 µm²
CONTROL
EXPERIMENTAL
****
NS
Time (wks)
Label
Feature
SPP1 HCI
TUBB3 All Calyces
OCM HCI
CALB2 Complex
TUBB3 All calyces/
CALB2 HCII
O P Q R
TUBB3 CALB2
CTPB2
GLUA2
MYO7A
5 µm
S Ribbon synapses
% of CTBP2 particles that colocalize with GLUA2
Utricle Horizontal amp.
Control Exptl Control Exptl
T Fbxo2CreER :: Rosa26DTA (EXPERIMENTALS and CONTROLS)
Lesion Validation and Behavioral/Physiological Testing
Pre-Tam
Tamoxifen
Age: 3-6 mo (Young)
Time post-Tam:
1 wk
3 wks
4 wks
6 wks
8 wks

Figure 2. Selective ablation of extrastriolar type I hair cells in the utricle

(A–D) Low-magnification confocal images of control utricles immunolabeled with markers to distinguish type I and type II hair cells: A) SPP1 (extrastriolar type I marker); B) TUBB3 (neuronal marker labeling calyceal afferents); C) CALB2 (type II hair cell marker and striolar calyx-only afferents); and D) OCM (striolar type I marker). (E–L) High-magnification images of each marker in A-D (cyan), showing a region spanning the striolar and extrastriolar zones in control (E,G,I,K) and experimental (F,H,J,L) utricles at 1 week post-tamoxifen. Note the near-complete loss of SPP1+ type I hair cells and TUBB3+ calyces in ES zones and the preservation of striolar type I hair cells (OCM+, CALB2+ calyces) and type II hair cells (CALB2+ cells) in both zones. (M) Quantification of type I hair cell density in each zone at different times post-tamoxifen. (N) Quantification of type II hair cell density in each zone at different times post-tamoxifen. M,N: Control = black circles; Experimental = blue squares. Each symbol is the mean from a single mouse. Graphs show mean number (± standard error of the mean, or SEM). Only the most pertinent significant differences are indicated; additional statistical results are presented in Table. ****$p \leq 0.0001$. *NS = not significant.* (O,P) Confocal images showing retention of TUBB3+ neurites (magenta) in extrastriolar zones and CALB2+ type II hair cells (blue) remaining after type I hair cell loss. (Q,R) High-magnification images of CTBP2 (magenta) and GLUA2 (green) immunolabeling reveal intact, closely apposed CTBP2-GLUA2 dyads on type II hair cells in both control and experimental utricles and horizontal ampullae (Hamp). (S) Quantification of the % of CTBP2+ particles that colocalized with GLUA2+ particles per hair cell (n= 2 experimental animals, n=1 control, each dot is a hair cell. 30 hair cells per utricle were counted.10 HCs per ampullae were counted. *NS = not significant*. Scale bar in A applies to B,C,D. Scale bar in E applies to F,G,H,I,J,K,L. Only the most pertinent significant differences are indicated; additional statistical results are presented in Table 2.

Examples of labeling for these markers in control utricles are shown at low magnification in **Fig. 2A-D** and for control and experimental utricles at higher magnification in the two zones in **Fig. 2E-L**. In experimental mice, the density of extrastriolar type I hair cells (counted as SPP1+ cells and as cells with a TUBB3+ calyx) was 5% of control mice by 1 week post-tamoxifen (compare **Fig. 2E,G,I,K** with **Fig. 2F,H,J,L,** and see graph in **Fig. 2M**), and HCI numbers didn't change over time. In contrast, there was no difference in the density of striolar type I hair cells (counted as OCM+ cells, cells with a CALB2+ calyx, and as cells in the striola with a TUBB3+ calyx) between experimental and control mice, even as late as 8 weeks post-tamoxifen. This was surprising because *Fbxo2*^{CreERT2} is expressed, albeit weakly, in the central zone. Furthermore, the density of type II hair cells (either extrastriolar or striolar) was not significantly different at 1, 4, or 8 weeks post-tamoxifen (compare **Figs. 2K** and **2L**, see graph in **Fig. 2N**). This was surprising because *Fbxo2*^{CreERT2} was expressed in the type II hair cells. While we are not sure how to interpret this finding, it is possible that we missed the timing of type II hair cell ablation and regeneration of those cells occurred, which happens in mature mice (e.g., Golub et al. 2012).

We considered the possibility that innervation of the type II hair cells in the extrastriola by VGNs may have changed in response to type I hair cell death because the neurons form synapses with both cell hair cell types. To address this, we labeled control and experimental utricles and horizontal ampullae at 4 weeks post-tamoxifen with antibodies to the type II maker CALB2 and the neurite marker TUBB3. We found that neurites were retained in the extrastriolar zone following type I hair cell ablation (compare **Fig. 2O and 2P**; utricles only are shown). Next, we labeled utricles and horizontal ampullae with antibodies to CTBP2, a marker of the presynaptic ribbons to which glutamate-filled vesicles attach, and to GLUA2, a postsynaptic glutamate receptor (González-Garrido et al., 2021; Schmitz et al., 2000; Matsubara et al., 1999). We identified hair cells using antibodies to MYO7A, and we defined synapses as dyads of closely apposed CTBP2 and GLUA2 labeling in the type II hair cell body, including in its basolateral processes (González-Garrido et al., 2021; Pujol et al., 2014). We observed no difference in ribbon synapses between extrastriolar or peripheral type II hair cells and VGNs following type I hair cell ablation in the utricle and horizontal ampullae (compare **Fig. 2Q and 2R)**. We found no significant difference in the % of CTBP2+ particles that were closely apposed to GLUA2+ particles. (**Fig. 2S)** supporting the idea that there was no substantial remodeling of the type II hair cell-VGN synapse after type I hair cell ablation.

These findings indicate although extrastriolar type I hair cells are lost, this zone's type II hair-cell circuitry remains intact. To determine whether a comparable pattern of selective loss and preservation extends beyond the utricle, we examined hair cell ablation in the horizontal cristae. Examples of labeling for these markers in control horizontal crista, shown at low magnification in **Fig. 3A-D** and for control and experimental cristae at higher magnification in the two zones in **Fig. 3E-L**. In experimental mice, the density of peripherally located type I hair cells (counted as SPP1+ cells) was 10% of control mice by 1 week post-tamoxifen (compare **Fig. 3E,G,I,K** with **Fig. 3F,H,J,L,** and see **Fig. 3M**), and type I hair cell numbers did not change over time. In contrast, there was no difference in the density of central type I hair cells (counted as OCM+ cells) between experimental and control mice, even as late as 8 weeks post-tamoxifen. Furthermore, similar to utricles, the density of type II hair cells in either zone did not change significantly between 1 and 8 weeks post-tamoxifen (compare **Figs. 3K** and **3L**, see **Fig. 3N**). Qualitative observations of the saccule, anterior crista, and posterior crista indicated similar hair cell loss (data not shown).

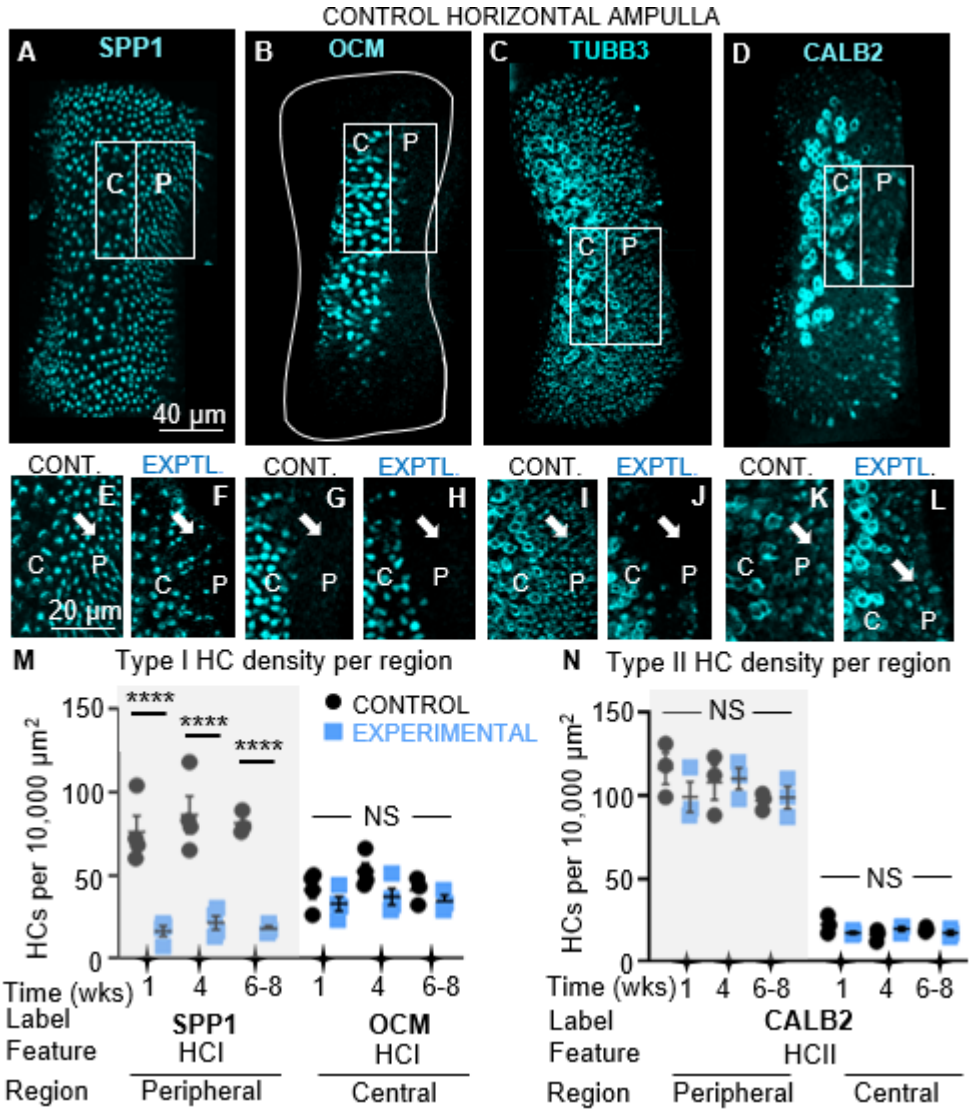

Figure 3. Selective ablation of peripheral type I hair cells in the horizontal ampulla. (A–D) Low-magnification images of control horizontal ampullae immunolabeled for SPP1, TUBB3, OCM, and CALB2 to distinguish hair cell types and zones. High-magnification images of each marker in A-D (cyan) showing a region spanning the striolar and extrastriolar zones in control (E,G,I,K) and experimental (F,H,J,L) horizontal ampullae at 1 week post-tamoxifen. Note the near-complete loss of SPP1+ peripheral type I hair cells and the preservation of central type I (OCM+) hair cells and type II (CALB2+) hair cells. (M) Quantification of type I hair cell density in each zone at different times post-tamoxifen. (N) Quantification of type II hair cell density in each zone in each zone at different times post-tamoxifen. M,N: Control = black circles; Experimental = blue squares. Each symbol is the mean from a single mouse. Graphs show mean number (± standard error of the mean, or SEM). Only the most pertinent significant differences are indicated; additional statistical results are presented in Table 3. ****$p \leq 0.0001$. Scale bar in A applies to B,C,D. Scale bar in E applies to F,G,H,I,J,K,L.

Together, these findings demonstrated that we could achieve targeted ablation of peripherally located type I hair cells in all vestibular organs, maintaining type II hair cells and their synapses in the same region, and not impacting type I or type II hair cells in the central zone.

Mice with peripheral type I hair cell ablation had significant impairments in motor coordination and balance

To assess the effect of ablating peripheral type I hair cells on motor functions that rely on the vestibular system, we subjected young adult mice to balance beam and rotarod testing. These tasks require mice to regulate posture, fine muscle movements, and balance. For the balance beam, we measured how long it took each mouse to walk across a slightly tilted, relatively thin beam to reach a goal box (**Fig. 4A**). Control mice completed 100% of the balance beam trials; they were able to traverse the bar to the goal box (**Fig. 4B**). On average, traversing the bar took 8-12 seconds (**Fig. 4C**). Prior to tamoxifen, experimental (*Fbxo2*^{CreERT2}*::Rosa*^{DTA}*)* mice performed similar to control mice. Within 1 week of tamoxifen treatment, none of the experimental mice could complete any trials, falling off the bar and into the net withing a few seconds (**Fig.4A-C**).

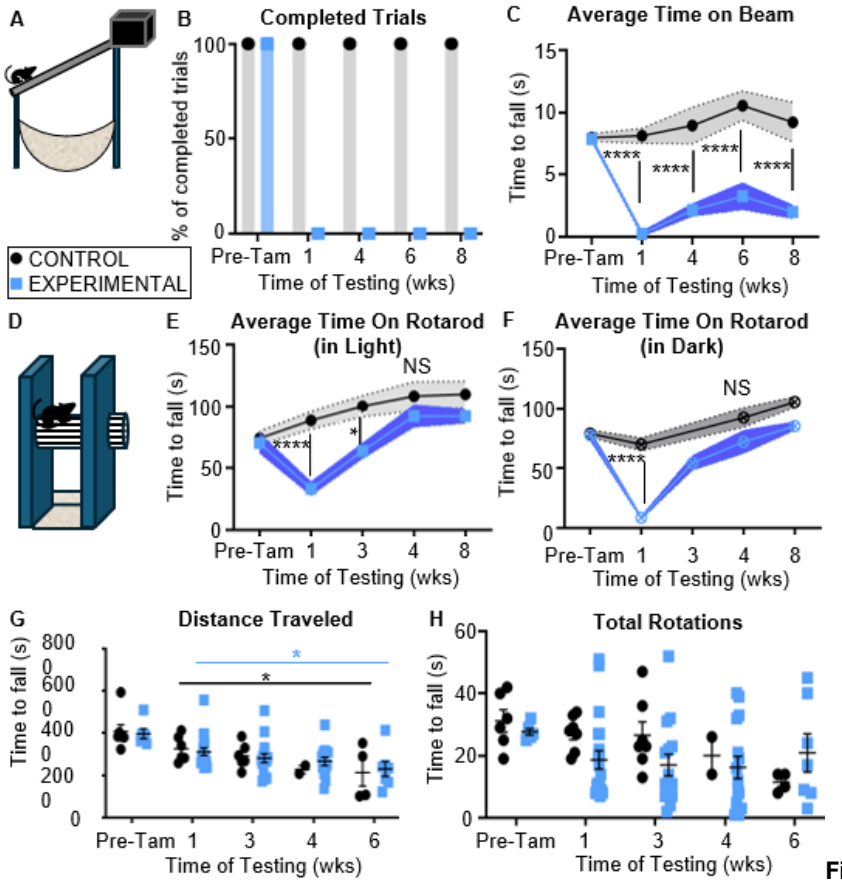

Figure 4. Ablation of peripheral type I hair cells impairs dynamic balance and coordination but preserves basic locomotor behaviors. (A) Schematic of the elevated balance beam apparatus. (B, C) Quantification of balance beam performance over time. (B) Percentage of completed trials (traversing across the full beam) before tamoxifen (Pre-Tam) and at 1, 4, 8 weeks post-tamoxifen. Experimental mice (blue squares) showed near-complete failure to complete trials by 1 week post-tamoxifen with no recovery up to 8 weeks, while control mice (black circles) consistently completed trials. (C) Average time on beam for completed trials. Asterisks indicate significant difference between experimental and control at each timepoint under the line. (D) Schematic of the rotarod apparatus. Mice were assessed both in normal room light and in darkness (relative darkness with red light). (E, F) Average latency to falling off of the rotarod across timepoints. (E) Performance in *light* conditions. (F) Performance in *dark* conditions. Control = black circles; Experimental = blue squares. For C-F, each symbol represents the average performance per group. The shaded area represents the SEM at each timepoint. Asterisks in graph represent significant difference between experimental and control at that time. *p ≤ 0.05, ***p ≤ 0.001, ****$p \leq 0.0001$. (G, H) Open field–style assessment of spontaneous locomotion in a novel, well-lit cage for 5 minutes. (G) Total distance traveled during the 5-minute testing period. (H) Total number of rotations during the 5-minute testing period. Both measures showed no significant differences between experimental and control groups at any timepoint. For G, H, each symbol represents a single mouse; Control = black circles; Experimental = blue squares. Each symbol is the mean from a single mouse. Graphs show mean (± standard error of the mean, or SEM). Asterisks in graph represent significant difference within experimental and control between 1 week and 6 weeks post-tamoxifen. For all graphs, only the most pertinent significant differences are annotated; additional comparisons in Tables 4, 5.

Next, we measured the mouse's ability to remain walking on the rotarod, which consists of a rotating rod whose speed increases over time (**Fig. 4D**). Initially, we performed this test in a bright room. Control mice were able to remain on the rotarod about 60 seconds or more, and their performance improved significantly at later times post-tamoxifen (**Fig. 4E**). This was expected based on previous studies on learned motor behavior in mammals (Buitrago et al., 2004; Pérez & Palmiter 2005; Babu et al., 2023; Costa et al., 2024). Before tamoxifen, experimental mice remained on the rotarod as long as control mice. However, by 1 week post-tamoxifen, experimental mice could not remain on the rotarod for more than a few seconds (**Fig. 4E**). Surprisingly, their performance improved over time, with the average time to fall resembling controls at 4 weeks post-tamoxifen. This improvement was surprising and could indicate adaption (e.g., recruitment of conserved type II or striolar type I HCs) or substitution (increased contributions by somatosensory and motor systems). Because experimental mice also regained much of their latency-to-fall by 4 weeks post-tamoxifen, we asked whether this improvement reflected true vestibular recovery or growing reliance on vision. We decided to test rotarod in the dark to see if there was any change in either group's performance. Dark conditions remove visual cues, placing a greater emphasis on mice proprioceptive and remaining vestibular sensory systems. Results are similar to what we saw in light conditions (compare **Fig. 4E** and **4F**); experimental mice performed similar to controls before tamoxifen, but 1 week later there is a significant decrease in experimental mice performance with an increase in performance at 4 weeks after tamoxifen. We observed that by 3-4 weeks post-tamoxifen, mice had learned to lean against the wall of the rotarod apparatus (not shown), potentially enabling them to stay on the rod longer using somatosensory or proprioceptive cue. This behavior was seen in some control mice from the 1 week post tamoxifen and onward, while in the experimental group, they learned this behavior weeks after the ablation. Although other studies have flagged potential coping strategies in which animals stop walking, brace themselves on the lane divider, or simply cling/lean so they can ride the rod instead of running (Keane et al., 2024), more research is needed to understand our results.

We were curious if the impacts of type I hair cell ablation upon mouse balance and motor coordination are worse during aging. We examined rotarod and balance beam performance in control and experimental mice at 16 months of age (**Supplemental Fig. 1A**). These mice are considered middle age (Shoji et al., 2016; Flurkey et al., 2007). First, we verified that these older mice experienced profound loss of

peripheral type I hair cell loss while preserving type II hair cells and striolar hair cells in utricles and horizontal cristae (**Supplemental Fig. 1B**). We next performed behavioral testing, before tamoxifen administration and at 1 and 4 weeks post-tamoxifen. On the balance beam, middle aged control animals were able to complete all of their trials but were significantly slower than the young adult controls starting from baseline (**Supplemental Fig. 1C-E, Table 6**). Similar to young adult mice, middle-aged experimental mice failed to complete any trials and fell off the balance beam almost immediately at 1 week post-tamoxifen (**Supplemental Fig. 1D,E**). Although not significant, they performed slightly worse than the young adult experimental mice at 4 weeks post-tamoxifen. On the rotarod, control middle-aged animals performed worse than the younger adults at baseline and over time (**Supplemental Fig.1F,G**). Middle-aged experimental mice also had worse performance at baseline. Strikingly, middle-aged experimental mice failed to improve performance over time (**Supplemental Fig.1F,G**) in contrast to the young adult cohorts. hese behavioral deficits in both young adult and middle-aged animals provided strong evidence that peripheral type I hair cells are required for motor coordination and balance.

Mice with peripheral type I hair cell loss did not exhibit overt changes in locomotor activity or exploratory behaviors

To further evaluate locomotor behaviors, young adult mice were placed in a new, clean cage for five minutes in bright light and their activity was videotaped for 5 minutes. Mice did not exhibit spinning or head-bobbing, which are present after near-complete hair cell destruction (e.g., Golub et al., 2012). By quantitatively analyzing videos using Ethovision software, we measured the total distance traveled and total rotations. We found no significant differences between control and experimental groups for both of these measures at any time point, indicating normal locomotion and exploration within the novel environments (**Fig. 4G**). For both control and experimental groups, the total distance traveled over time was significantly reduced over time, which was expected because mice reduce exploratory behaviors as they become accustomed to the testing cage environment. To verify our observations on spinning, we also measured the number of angular rotations using the Ethovision software. Although experimental mice exhibited a slight increase in angular rotations compared to controls, this trend was not statistically significant (**Fig. 4H**). These findings indicate that, although mice with peripheral type I hair cell loss had

clear deficits in complex motor tasks requiring balance and coordination, their normal locomotor and exploratory behaviors were not impacted.

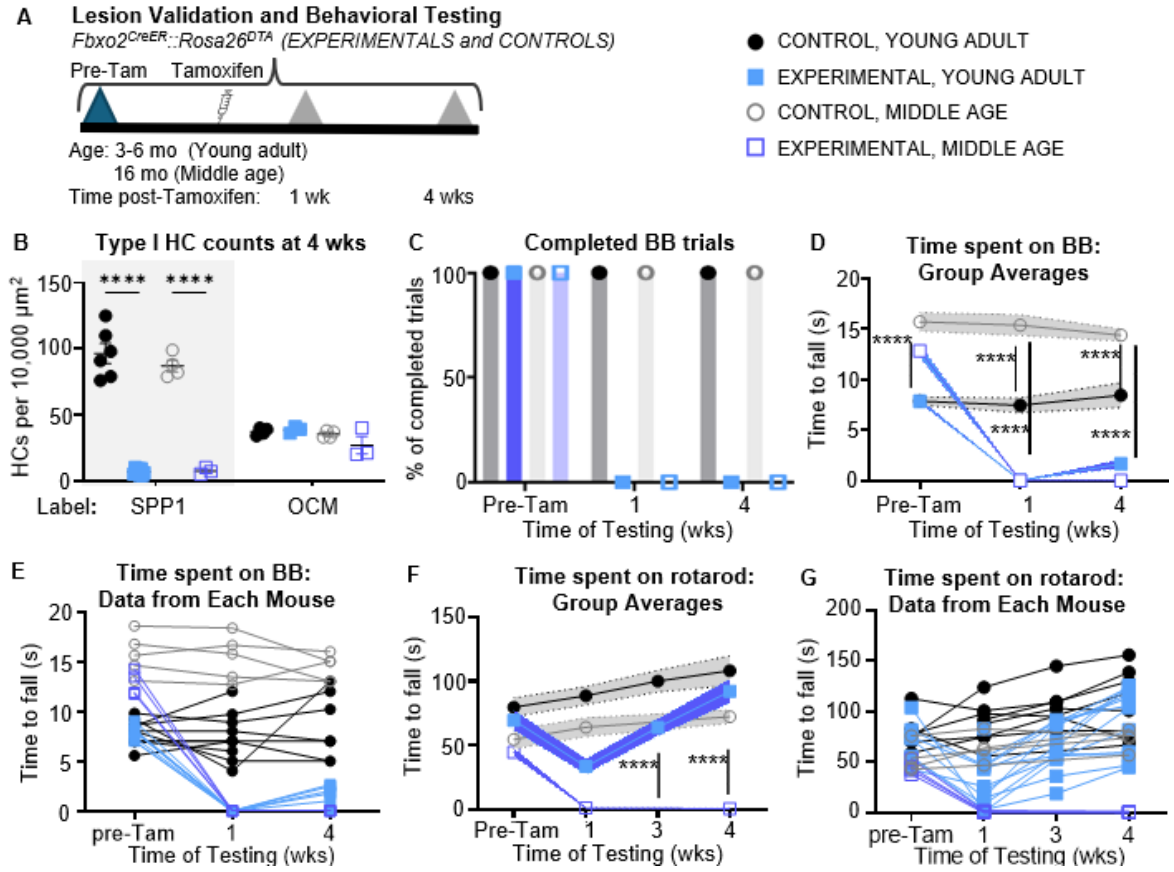

Supplemental Figure 1. Middle-aged mice exhibit more severely impaired balance following peripheral type I hair cell ablation.

(A) Experimental timeline for tamoxifen administration and behavioral testing in middle-aged (16–18 months) mice. (B) Quantification confirming substantial loss of peripheral type I hair cells in utricles and horizontal cristae of older experimental mice with preservation central type I hair cells. For B and other panels in this figure: CONTROL, YOUNG ADULT = black circles; CONTROL, MIDDLE-AGED = white circles with black outline; EXPERIMENTAL, YOUNG ADULT = blue squares, EXPERIMENTAL, MIDDLE-AGED = white squares with blue outline. (C) Percentage of completed trials (traversing across the full beam) before tamoxifen (Pre-Tam) and at 1, 4, weeks post-tamoxifen. (D) Group average time on beam for completed trials. (E) Average time on beam for completed trials. (E) Group average time on rotarod. (F) Individual average time on rotarod. Graph lines and bars coded by group (control: young = black circles; control: middle-aged = gray circles; experimental: young = blue squares, experimental: middle-aged =open blue squares). Graphs (B, C, E) show mean number (± standard error of the mean, or SEM). Only the most pertinent significant differences are shown; additional significant differences are presented in Tables 6. *Significance indicators: *p ≤ 0.05, **p ≤ 0.01, ***p ≤ 0.001, ****$p \leq 0.0001$.

Following peripheral type I hair cell loss, VOR gains were significantly diminished

Because whole-body balance tasks integrate visual, proprioceptive, and vestibular cues, we needed a reflex-level readout that isolates the direct contribution of canal hair-cell input to motor output. We analyzed head-free hVOR gains of control and experimental young adult mice during sinusoidal head motions in the dark at frequencies ranging from 0.3 to 1.0 Hz (**Fig. 5A**). Measuring hVOR gains allowed us to ask whether the behavioral deficits we observed stemmed from a primary loss of vestibular signal. Control mice had average hVOR gains (i.e., the velocity of slow phase eye motion divided by the velocity of head motion) at 0.35 to 0.40 at each frequency. These gains were comparable to those measured in our prior study of young adult C57Bl6/J mice (Jáuregui et al., 2024). Compared to controls, experimental mice had significantly reduced gains at all frequencies by 1 week post-tamoxifen, when peripheral type I hair cells had been ablated. At later times post-tamoxifen, VOR gains remained significantly reduced at all frequencies tested, except for at 6 weeks at 0.3 Hz. This finding indicates that peripheral type I hair cells are required to maintain normal hVOR gains.

Mice with ablation of peripheral type I hair cells failed to upregulate CFOS in vestibular nucleus neurons after off-axis sinusoidal centrifugation

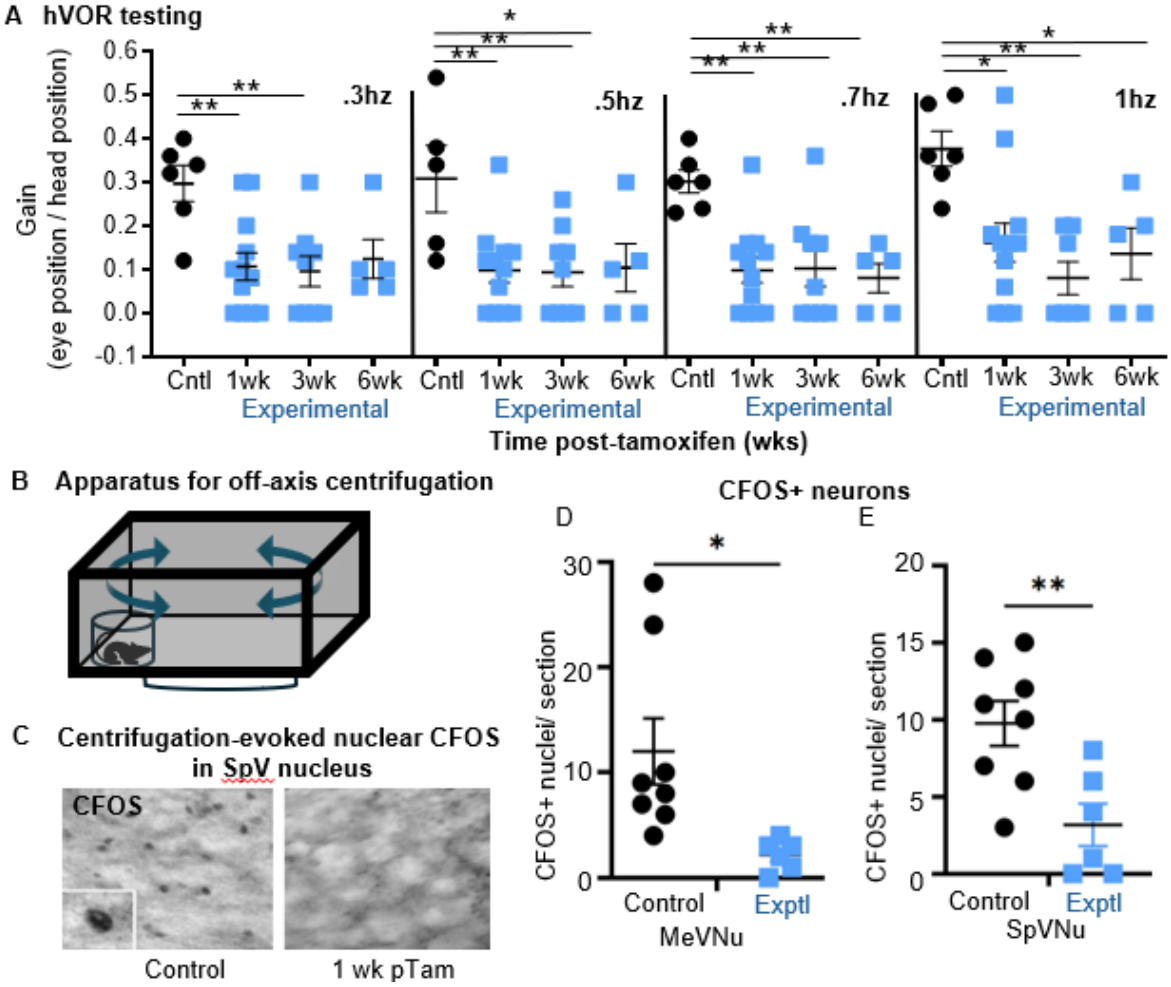

Figure 5. Peripheral type I hair cell ablation reduces hVOR gains and blunts vestibular nucleus neuronal activation following vestibular stimulation. (A) Quantification of horizontal vestibulo-ocular reflex (hVOR) gains across stimulus frequencies (0.3–1.0 Hz) in control and experimental mice. Control = black circles; experimental = blue squares, each dot represents one animal. Graphs show mean number (± standard error of the mean, or SEM). (B) Diagram of off-axis sinusoidal centrifugation apparatus. (C) Representative confocal images of CFOS immunolabeling in MeVNu and SpVNu at 45 minutes after centrifugation. (D,E) Quantification of CFOS-positive nuclei in MeVNu and SpVNu at 1 wk confirms significant reduction in experimental animals in each vestibular brainstem nucleus. Graphs show number of nuclei per region (± 1 standard error of the mean, or SEM). Asterisks in graph represent significant difference between experimental and control. *p ≤ 0.05., **p≤ 0.01

The changes that we noted in motor behaviors and hVOR gains after ablation of peripheral type I hair cells prompted us to explore if a vestibular stimulus could still alter the activity of vestibular nucleus neurons under these conditions. Both control and experimental mice at 1 week post-tamoxifen were

subjected to off-axis sinusoidal centrifugation for 10 minutes while they were free to move within a small beaker (Fig. **5B**). This stimulus likely alters hair cell activity in all vestibular sensory organs to some degree. Our prior study (Jáuregui et al., 2024) showed that, in normal mice, this stimulus upregulates CFOS expression in neurons of the medial (MedVNu) and spinal (SpVNu) vestibular nuclei, which receive inputs from hair cells via VGNs. 45 minutes after centrifugation, mice were killed and perfused before fixation in paraformaldehyde, before staining with the CFOS antibody.

We found that centrifugation evoked nuclear CFOS in control mice (without type I hair cell ablation)(**Fig. 5C**). In contrast, mice with peripheral type I hair cell ablation showed little or no change in nuclear CFOS expression in either the SpVNu or the MedVNu after off-axis centrifugation at 1 week post-tamoxifen (**Fig. 5C-E**). These differences between control and experimental mice were significantly different in both regions (**Fig. 5E**). These observations suggest that loss of type I hair cells significantly alters inputs to vestibular brainstem neurons, which could account in part for the reduction in hVOR gains and the loss of some motor skills.

Changes in mouse behavior and physiology are likely not due to off-target central effects of tamoxifen administration to *Fbxo2^{CreERT2}::Rosa^{Tom}* mice

To assess if the behavioral and physiological changes that we observed in mice with peripheral type I hair cell ablation could be due to off-target DTA expression, we assessed CreER activity at 4 weeks post-tamoxifen in VGNs and in neurons in key brain regions of *Fbxo2^{CreERT2}::Rosa^{Tom}* mice (**Supplemental Fig. 2**). We found no evidence of TOM labeling in neurons or glia in the vestibular ganglion, MeVNu, SpVNu, inferior olive, deep cerebellar nuclei, or oculomotor nuclei (see vestibular nucleus in **Supplemental Fig. 2A-A2**). In the cerebellum, only a few scattered TOM+ nuclei were observed in the vestibular pathway (see cerebellum in **Supplemental Fig. 2B-B2**). This restricted TOM expression is consistent with the interpretation that the primary underlying cause of the motor dysfunctions we observed, including reduction in VOR gains, is the loss of peripheral type I hair cells, rather than off-target killing of neurons of the vestibular pathway(s).

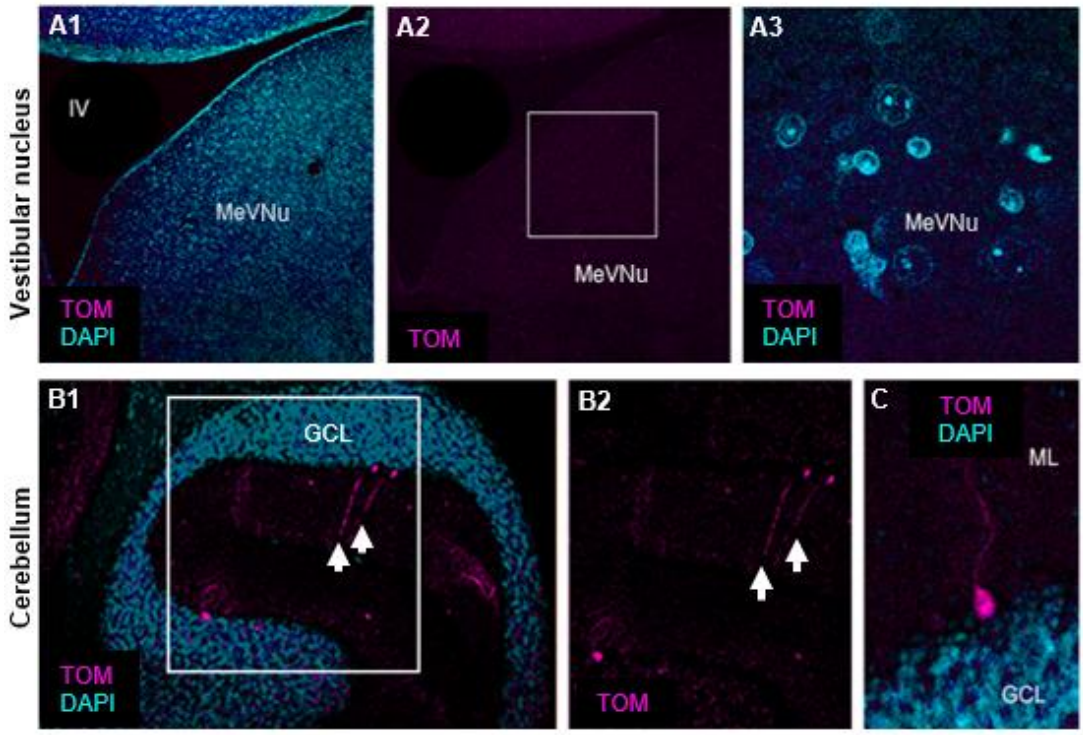

Supplemental Figure 2. Assessment of off-target CreER activity in *Fbxo2^{CreERT2}::RosaTOM* mice following tamoxifen treatment. (A1–A3) Confocal images of a brainstem slice at 4 weeks post-tamoxifen administration demonstrate absence of tdTomato (TOM, magenta) expression in neurons of the medial vestibular nucleus (MeV) this needs to be changed to the same name as in Fig 5 - MedVNu, indicating no recombination in key central vestibular relay regions. (A1) Low-magnification view showing TOM fluorescence (magenta) and DAPI labeling (cyan). IV = fourth ventricle. (A2) Same region as A1, showing TOM only. Box indicates area shown at higher magnification in (A3). Boxed region in A2. (B1,B2) Sagittal cerebellar sections from the same animal as for A1-A3 revealing sparse TOM-positive (magenta) nuclei primarily localized to the flocculus. (B1) Low-magnification view showing the granule cell layer (GCL) and molecular layer (ML) with scattered TOM-positive cell bodies and processes (arrows indicate labeled cells). (B2) TOM label only from boxed region in (B1). (C) An image from another slice showing a TOM-positive Purkinje neuron extending processes into the ML.

Discussion

The main finding of this study was that ablating the vast majority of type I hair cells from the peripheral zone of vestibular organs in young adult mice (3-5 months) caused persistent deficits in the vestibulo-ocular reflex (hVOR) and in behaviors that require motor coordination and balance (navigating the rotarod and the balance beam).

This is the first study to selectively ablate type I hair cells in any species. Prior studies in mice induced vestibular hair cell lesions by administering ototoxins such as aminoglycoside antibiotics (Nagato et al., 2018; Kim et al., 2005; Monzack et al., 2015; Kawamoto et al., 2009), IDPN (iminodipropionitrile)(Zeng et al., 2020), or cisplatin (Kim et al., 2008; Monzack et al., 2015; Callejo et al., 2017), or injecting diphtheria toxin in *Pou4f3*^{DTR} mice (Golub et al., 2012), but these methods caused widespread loss without specifically targeting type I cells in a given zone. By giving tamoxifen to adult *Fbxo2*^{CreERT2}*::Rosa*^{DTA} mice, we eliminated over 90% of type I hair cells in the peripheral zones in all vestibular organs in each ear within 1 week. The number of type I hair cells in the peripheral zone did not increase over time. This observation aligns with prior findings in adult rodents showing that type I hair cells are not regenerated (e.g., Forge et al., 1993; Kawamoto et al., 2009; Sayyid et al., 2019; Golub et al., 2012).

We detected no significant loss of type II hair cells or central type I hair cells. These observations were surprising because tamoxifen induced some CreER activity in those cells (**Fig. 1,** and McGovern et al., 2022). One potential explanation for the lack of type I hair cell loss in the central zone is that TOM fluorescence (and by logic, CreER activity) was weaker there.

We lack insight into why we saw no loss of type II hair cells at 1 week post-tamoxifen; 25% of them were strongly TOM-positive, so they should have died after tamoxifen administration. We considered that regeneration of type II hair cells may have obscured evidence of their loss. In adult mice, killing large numbers of hair cells triggers adjacent supporting cells to transdifferentiate into new hair cells (Kawamoto et al., 2009; Sayyid et al., 2019; Golub et al., 2012; Bucks et al., 2017). However, there was no change in the density of peripherally located type II numbers relative to controls at 4-8 weeks post-tamoxifen, suggesting that neither loss nor regeneration had occurred. We thought we might have seen some regeneration of type II hair cells upon type I ablation because we had reduced the total hair cell density by about half in the peripheral zone upon ablating type I hair cells. Our observations to the contrary suggest that significant loss of type II hair cells specifically, and/or loss of a higher number of hair cells in general, is necessary to trigger supporting cells to generate new type II hair cells in adult mice.

We wondered if the dimorphic afferent synapses with type II hair cells might undergo remodeling after losing calyceal inputs from type I hair cells. However, we found no significant change in the density or

distribution of ribbon synapses on type II hair cells in the extrastriola, which suggested that the signaling between these type II hair cells and vestibular afferent neurons remained intact throughout the course of the experiment.

We did not detect significant CreER-driven TOM expression in neurons in vestibular circuits, including VGNs, vestibular nucleus neurons. Purkinje cells or granule cells in the vestibular cerebellum, neurons of the oculomotor nuclei, inferior olive, or deep cerebellar nuclei. These observations increase confidence that the cellular ablation in the vestibular system we induced was largely limited to type I hair cells and that the vestibular and motor dysfunction we detected is due to the targeted removal of peripheral type I hair cells and not to off-target killing of neurons in the vestibular pathway.

Gains of the horizontal vestibulo-ocular reflex (hVOR) were significantly reduced after peripheral type I hair cell ablation

Ablation of peripheral type I hair cells resulted in significant and persistent reduction in gains of the hVOR across frequencies ranging from 0.3 to 1.0 Hz at 1 week after ablation, although the reflex was not abolished altogether. VOR gains showed no significant recovery, even as late as 8 weeks post-tamoxifen. Notably, this reflex impairment occurred despite the preservation of central (striolar) type I hair cells and all type II hair cells. Therefore, neural signaling deriving from peripheral type I hair cells are required to maintain normal hVOR gains, at least for the moderate head rotation frequencies and the amplitude tested.

Our findings build upon our understanding of how hair cells across the vestibular organs regulate the VOR. Ono et al. (2020) found that preventing differentiation of the central (striolar) zone in mouse maculae during development did not significantly impact hVOR gains between 0.3 Hz and 1 Hz. Before that, Minor and Goldberg (1991) selectively silenced irregular, central vestibular nerve fibers in squirrel monkey applying galvanic currents to the vestibule, leaving regular, peripheral afferents active. This functional ablation caused no significant change in VOR gains for sinusoidal head rotations at 0.5 and 4 Hz. The authors concluded that that the central zone is largely dispensable for the VOR and that peripheral type I and II hair cells are sufficient to drive the reflex under those conditions. Our finding that

peripheral type I hair cells are required for the VOR is consistent with this interpretation. We did see some preservation of the VOR when type I hair cells were killed, suggesting that peripheral type II hair cells are sufficient to drive the VOR to some degree. At this point, it remains unknown if inputs from central regions are sufficient for the VOR. This would need to be tested by ablating all hair cells in the periphery.

Balance and motor coordination deficits after type I hair cell loss

After losing peripheral type I hair cells, mice could not remain on the balance beam or the rotarod for more than a few seconds. These mice rapidly lost their ability to remain upright on the balance beam, often grasping or hanging from it prior to falling onto the foam below. These findings suggest that a severe deficit in dynamic equilibrium occurred upon loss of peripheral type I hair cells. This could be due to impaired regular afferent activity, which could maintain posture and fine-tune limb positions and movements over time (Sadeghi et al., 2007; Goldberg & Fernandez, 1971), and/or it may be attributable to the loss of type I hair cells, which may be best suited to detect sudden changes in head motions that could occur during these tasks (Eatock, 2018; Eatock and Songer, 2011; Goldberg, 2000; Baird et al., 1988; Goldberg et al., 1990).

We found no improvement in balance beam performance up to 8 weeks post-tamoxifen. In contrast, mice became able to stay on the rotarod significantly longer by 3 weeks post-tamoxifen. This improvement occurred under both light and dark conditions, indicating that visual input was not essential for this recovery. We observed mice in both the control and experimental groups leaning against the wall of the rotarod apparatus. We suspect that this behavior, which relies on proprioception, was the key factor enabling mice with ablation of peripheral type I hair cells to improve their rotarod performance over time. Interestingly, we found that middle-aged mice had a similar response as young adult mice to peripheral type I hair cell ablation, with one exception: they were unable to improve their ability to stay on the rotarod over time. This finding could mean that middle-aged mice are unable to invoke somatosensory substitution or other adaptive methods to remain on the rotarod. These findings may reflect challenges that people can have in managing loss of vestibular function as they age.

It is notable that, after ablation of peripheral type I hair cells, young adult mice did not exhibit abnormal behaviors such as repeated circling/spinning or head bobbing, which occur after near-complete killing of vestibular hair cells or after mutations that abolish vestibular hair cell function (Golub et al. 2012; Pan et al. 2012; Geng et al., 2009) Likewise, basic locomotor activity (distance traveled and average velocity of locomotion) was unchanged. These findings indicate that ablation of a larger population of hair cells beside peripheral type I hair cells–such as central type I hair cells and type II hair cells–is required to disrupt routine locomotor activities and/or to cause severe motor phenotypes.

Implications for vestibular hair cell regeneration

The findings in this study underscore the importance of protecting or restoring peripherally located type I hair cells for attaining normal vestibular function. This point is echoed in other studies in mice. For instance, Wan et al. (2019), who identified a correlation between the loss of calyces in the peripheral regions of vestibular organs and impaired vestibular functions in aging mice. Furthermore, adult rodents can regenerate up to about half of their type II hair cells after extensive hair cell loss, but no type I hair cells are replaced (Forge et al., 1993; 1998; Kawamoto et al., 2009; Golub et al., 2012; Bucks et al., 2017; Sayyid et al. 2019; Hicks et al., 2020; Ciani Berlingeri et al., 2022; Jauregui et al. 2024). Mice with this degree of hair cell regeneration do not regain normal VOR gains (Jauregui et al. 2024) or VsEP thresholds (Sayyid et al., 2019). In birds, both type I and type II hair cells are naturally replaced, but recovery of vestibular functions is correlated temporally with only type I hair cell replacement (Carey et al., 1996; Zakir & Dickman, 2006; Haque et al., 2008). Collectively, these findings suggest that regeneration of type I hair cells is likely necessary for restoring vestibular function in rodents, and eventually in humans. In support of this idea, preserving half of type I hair cells in parallel with type II regeneration in adult mice improves hVOR gains significantly (Jauregui et al. 2024). We found here that ablating most peripheral type I hair cells significantly reduced vestibular stimulus-evoked CFOS in vestibular nucleus neurons, indicating that, at least for off-axis centrifugation, peripheral type I hair cells are essential for altering neural activity in the central vestibular pathway. These findings, from our group and others', provide strong motivation to determine ways to coax regeneration of type I hair cells and their calyceal innervation in mammals after hair cell destruction or degeneration.

TABLE 1

UTRICLE HAIR CELL COUNTS- Tom+

GROUP	AVG % of Tom+ HCs	N
CONTROL 1 wk ES type I hair cells	92	2
CONTROL 1 wk ES type II hair cells	30	2
CONTROL 1 wk S type II hair cells	29	2
CONTROL 1 wk S type I hair cells	30	2

AMPULLAE HAIR CELL COUNTS- Tom+

GROUP	AVG % of Tom+ HCs	N
CONTROL 1 wk P type I hair cells	95	2
CONTROL 1 wk P type II hair cells	25	2
CONTROL 1 wk C type II hair cells	28	2
CONTROL 1 wk C type I hair cells	24	2

TABLE 2

2A. UTRICLE HAIR CELL COUNTS – SPP1+ HCs

GROUP	AVG # OF SPP1+ HCS	N	SEM	SIGDIF PER TWO-WAY ANOVA	NOTES
CONTROL 1 wk	92	9	2	<0.0001	**** FOR EXPERIMENTAL 1 wk, 4 wk, 6-8 wk
CONTROL 4 wk	97	6	8	<0.0001	**** FOR EXPERIMENTAL 1 wk, 4 wk, 6-8 wk
CONTROL 6-8 wk	91	6	4	<0.0001	**** FOR EXPERIMENTAL 1 wk, 4 wk, 6-8 wk
EXPERIMENTAL 1 wk	8	9	1	<0.0001	**** FOR CONTROL 1 wk, 4 wk, 6-8 wk
EXPERIMENTAL 4 wk	6	5	1	<0.0001	**** FOR CONTROL 1 wk, 4 wk, 6-8 wk
EXPERIMENTAL 6-8 wk	8	5	1	<0.0001	**** FOR CONTROL 1 wk, 4 wk, 6-8 wk

2B. UTRICLE HAIR CELL COUNTS – TUBB3 es CALYX

GROUP	AVG # OF TUBB3 es CALYX	N	SEM	SIGDIF PER TWO-WAY ANOVA	NOTES
CONTROL 1 wk	127	3	17	<0.001	*** FOR EXPERIMENTAL 1 wk, <.001 (**) FOR 4 wk
CONTROL 4 wk	145	2	23	<.05	* FOR EXPERIMENTAL 6-8 WEEK .01
CONTROL 6-8 wk	107	3	7	<0.001	***
EXPERIMENTAL 1 wk	16	3	2	<0.001	*** FOR CONTROL 1 wk
EXPERIMENTAL 4 wk	24	2	1		
EXPERIMENTAL 6-8 wk	17	1			

2C. UTRICLE HAIR CELL COUNTS – OCM HC

GROUP	AVG # OF OCM HC	N	SEM	SIGDIF PER TWO-WAY ANOVA
CONTROL 1 wk	39	4	2	ns
CONTROL 4 wk	36	3	1	ns
CONTROL 6-8 wk	41	4	2	ns
EXPERIMENTAL 1 wk	40	3	2	ns
EXPERIMENTAL 4 wk	41	3	1	ns
EXPERIMENTAL 6-8 wk	38	3	3	ns

2D. UTRICLE HAIR CELL COUNTS – CALB2 CALYX

GROUP	AVG # OF CALB2 CALYX	N	SEM	SIGDIF PER TWO-WAY ANOVA	NOTES
CONTROL 1 wk	37	3	2		
CONTROL 4 wk	36	3	1		
CONTROL 6-8 wk	47	4	2	0	** FOR EXPERIMENTAL 6-8 wk
EXPERIMENTAL 1 wk	40	4	2		
EXPERIMENTAL 4 wk	38	4	2		
EXPERIMENTAL 6-8 wk	38	4		0	** FOR CONTROL 6-8 wk

2E. UTRICLE HAIR CELL COUNTS – TUBB3+ S HC

GROUP	AVG # OF TUBB3+ S HC	N	SEM	SIGDIF PER TWO-WAY ANOVA
CONTROL 1 wk	48	3	3	ns
CONTROL 4 wk	47	2	3	ns
CONTROL 6-8 wk	47	3	2	ns
EXPERIMENTAL 1 wk	35	4	3	ns
EXPERIMENTAL 4 wk	38	2	1	ns
EXPERIMENTAL 6-8 wk	44	1		ns

2F. UTRICLE HAIR CELL COUNTS – CALB2 HC ES

GROUP	AVG # OF CALB2 HC ES	N	SEM	SIGDIF PER TWO-WAY ANOVA
CONTROL 1 wk	88	6	3	ns
CONTROL 4 wk	94	5	8	ns
CONTROL 6-8 wk	79	5	5	ns
EXPERIMENTAL 1 wk	82	8	4	ns
EXPERIMENTAL 4 wk	98	4	11	ns
EXPERIMENTAL 6-8 wk	79	1	4	ns

2G. UTRICLE HAIR CELL COUNTS – CALB2 HC S

GROUP	AVG # OF CALB2 HC S	N	SEM	SIGDIF PER TWO-WAY ANOVA
CONTROL 1 wk	48	6	3	ns
CONTROL 4 wk	38	5	3	ns
CONTROL 6-8 wk	41	4	5	ns
EXPERIMENTAL 1 wk	46	8	2	ns
EXPERIMENTAL 4 wk	45	4	3	ns
EXPERIMENTAL 6-8 wk	34	7	4	ns

TABLE 3

3A. HORIZTONTAL AMPULLAE HAIR CELL COUNTS – SPP1+ HCs

GROUP	AVG # OF peripheral SPP1+ HCS	N	SEM	SIGDIF PER TWO-WAY ANOVA	NOTES
CONTROL 1 wk	76	4	10	<0.0001	**** FOR EXPERIMENTAL 1 wk, 4 wk, 6-8 wk
CONTROL 4 wk	86	4	11	<0.0001	**** FOR EXPERIMENTAL 4 wk, 6-8 wk
CONTROL 6-8 wk	81	3	4		****
EXPERIMENTAL 1 wk	16	4	3	<0.0001	****
EXPERIMENTAL 4 wk	21	4	4	<0.0001	****
EXPERIMENTAL 6-8 wk	18	3	2	<0.0001	****

3B. HORIZTONTAL AMPULLAE HAIR CELL COUNTS – OCM+ HCs

GROUP	AVG # OF central OCM+ HCS	N	SEM	SIGDIF PER TWO-WAY ANOVA
CONTROL 1 wk	41	4	5	ns
CONTROL 4 wk	52	4	5	ns
CONTROL 6-8 wk	41	3	5	ns
EXPERIMENTAL 1 wk	32	4	4	ns
EXPERIMENTAL 4 wk	37	4	5	ns
EXPERIMENTAL 6-8 wk	34	3	4	ns

3C. HORIZTONTAL AMPULLAE HAIR CELL COUNTS – CALB2+ HCs

GROUP	AVG # OF peripheral CALB2+ HCS	N	SEM	SIGDIF PER TWO-WAY ANOVA
CONTROL 1 wk	116	4	9	ns
CONTROL 4 wk	108	4	2	ns
CONTROL 6-8 wk	97	3	26	ns
EXPERIMENTAL 1 wk	99	4	9	ns
EXPERIMENTAL 4 wk	110	4	6	ns
EXPERIMENTAL 6-8 wk	99	3	7	ns

TABLE 4

BALANCE BEAM – EXPERIMENTAL YOUNG

TIMEPOINT	AVG TIME SPENT ON BEAM (S)	N	SEM	SIGDIF PER TWO-WAY ANOVA	NOTES
pre-Tam	8	7	0	<.0001	FOR EXPERIMENTAL 1 wk, 4 wk, 6 wk, 8 wk
1	0	7	0	<.0001	FOR CONTROL 1 wk, 4 wk, 6 wk, 8 wk
4	2	7	1	<.001	FOR CONTROL 4 wk, 6 wk, 8 wk
6	3	4	1	<.001	FOR CONTROL 6 wk
8	2	3	1	<.001	FOR CONTROL 8 wk

BALANCE BEAM – CONTROL YOUNG

TIMEPOINT	AVG TIME SPENT ON BEAM (S)	N	SEM	SIGDIF PER TWO-WAY ANOVA	NOTES
pre-Tam	8	7	0	<.0001	FOR EXPERIMENTAL 1 wk, 4 wk, 6 wk, 8 wk
1	7	5	0	<.001	FOR EXPERIMENTAL 1 wk 4 wk, 6 wk, 8 wk
4	7	5	1	<.01	FOR EXPERIMENTAL 4 wk, 6 wk, 8 wk
6	9	2	2	<.0001	FOR EXPERIMENTAL 6 wk, 8 wk
8	8	2	1	<.0001	FOR EXPERIMENTAL 8 wk

TABLE 5

ROTAROD LIGHT – CONTROL

TIMEPOINT	AVG TIME SPENT ON ROD (S)	N	SEM	SIGDIF PER TWO-WAY ANOVA	NOTES
pre-Tam	69	11	4	<0.001	FOR CONTROL 1 wk, 3 wk, 4 wk, 8 wk, EXPERIMENTAL 4 wk
1	43	19	7	<0.001	FOR CONTROL 1 wk, 3 wk, 4 wk, 8 wk, EXPERIMENTAL 4 wk
3	75	16	7	<0.001	.05 FOR 3 wk, .01 FOR 4 wk, 8 wk
4	94	13	9	ns	
8	97	4	6	ns	

ROTAROD LIGHT – EXPERIMENTAL

TIMEPOINT	AVG TIME SPENT ON ROD (S)	N	SEM	SIGDIF PER TWO-WAY ANOVA	NOTES
pre-Tam	74	13	6	<0.001	FOR EXPERIMENTAL 1 wk
1	89	8	7	ns	
3	100	8	9	ns	
4	108	8	12	ns	
8	110	6	11	ns	

ROTAROD DARK – EXPERIMENTAL

TIMEPOINT	AVG TIME SPENT ON ROD (S)	N	SEM	SIGDIF PER TWO-WAY ANOVA	NOTES
pre-Tam	78	6	5	<0.0001	FOR CONTROL 1 wk
1	9	6	2	<0.001	FOR CONTROL 1 wk, 3 wk, 4 wk, 8 wk, EXPERIMENTAL 4 wk, 8 wk
3	54	4	6	ns	
4	72	6	10	ns	
8	85	3	4	ns	

ROTAROD DARK – CONTROL

TIMEPOINT	AVG TIME SPENT ON ROD (S)	N	SEM	SIGDIF PER TWO-WAY ANOVA	NOTES
pre-Tam	77	8	3	<0.0001	FOR EXPERIMENTAL 1 wk
1	66	8	5	ns	
3	45	8	5	ns	
4		8	8	ns	
8	105	3	4	ns	

TABLE 6

BALANCE BEAM – CONTROL OLD

TIMEPOINT	AVG TIME SPENT ON BEAM (S)	N	SEM	SIGDIF PER TWO-WAY ANOVA	NOTES
pre-Tam	16	5	1	<.0001	FOR CONTROL YOUNG AND OLD PRE-TAM, 1 wk, AND EXPERIMENTAL
1	15	5	1	<.0001	FOR CONTROL AND EXPERIMENTAL PRE-TAM, 1 wk, 4 wk
4	14	5	1	<.0001	FOR CONTROL AND EXPERIMENTAL PRE-TAM, 1 wk, 4 wk

BALANCE BEAM – EXPERIMENTAL OLD

TIMEPOINT	AVG TIME SPENT ON BEAM (S)	N	SEM	SIGDIF PER TWO-WAY ANOVA	NOTES
pre-Tam	13	4	1	<.0001	FOR CONTROL YOUNG PRE-TAM, 1 wk, AND EXPERIMENTAL YOUNG
1	0	4	0	<.0001	FOR CONTROL AND EXPERIMENTAL PRE-TAM, 1 wk, 4 wk
4	0	3	0	<.0001	FOR CONTROL AND EXPERIMENTAL PRE-TAM, 1 wk, 4 wk

ROTAROD – CONTROL OLD

TIMEPOINT	AVG TIME SPENT ON BEAM (S)	N	SEM	SIGDIF PER TWO-WAY ANOVA	NOTES
pre-Tam	16	5	1	<.0001	FOR CONTROL YOUNG AND OLD PRE-TAM, 1 wk, AND EXPERIMENTAL
1	15	5	1	<.0001	FOR CONTROL AND EXPERIMENTAL PRE-TAM, 1 wk, 4 wk
4	14	5	1	<.0001	FOR CONTROL AND EXPERIMENTAL PRE-TAM, 1 wk, 4 wk

ROTAROD – EXPERIMENTAL OLD

TIMEPOINT	AVG TIME SPENT ON BEAM (S)	N	SEM	SIGDIF PER TWO-WAY ANOVA	NOTES
pre-Tam	13	4	2	<.0001	FOR CONTROL YOUNG PRE-TAM, 1 wk, AND EXPERIMENTAL YOUNG
1	0	4	0	<.0001	FOR CONTROL AND EXPERIMENTAL PRE-TAM, 1 wk, 4 wk
4	0	3	0	<.0001	FOR CONTROL AND EXPERIMENTAL PRE-TAM, 1 wk, 4 wk

---

Chapter 5: Thesis Discussion

This thesis includes three complementary studies about the adult vestibular system in mice: (1) *Sox2* conditional knockout experiments to analyze supporting cell regenerative capacity; (2) single-nucleus RNAseq profiling of adult utricles defined hair cell subtype molecular identities and markers; and (3) selective ablation of peripheral type I hair cells to test their functional roles in adult balance and reflexes. Together, the findings presented in this thesis collectively advance our understanding of how vestibular hair cell identity, survival, and regenerative potential are governed in the adult mammalian inner ear.

Limits on Supporting Cell–Mediated Regeneration

By defining the essential role of *Sox2* in enabling supporting cell-mediated regeneration, characterizing hair cell subtypes, and establishing the functional indispensability of peripheral type I cells, this work provides new insights into why balance function is so difficult to restore after vestibular injury and what biological levers might eventually be manipulated to change that. Taken together, these studies show that while supporting cells retain limited regenerative potential via *Sox2*, this regeneration is biased towards type II-like hair cell fate and fails to reproduce critical type I populations whose loss causes lasting functional deficits. Our transcriptomic atlas provides a framework for understanding this limitation, revealing distinct molecular programs in type I hair cells that may be inaccessible to adult supporting cells due to epigenetic silencing. Factors like *Sox2* may maintain known regenerative abilities, but are

insufficient to unlock the specific type I programs without signals from other genes, possibly like *Bmp2* or *Paqr9*. This integration of molecular, functional, and regenerative perspectives suggests that future research needs to target not just hair cell numbers but also subtype identification and their connectivity.

A central implication of this work is that spontaneous regeneration in the adult vestibular system, while limited, is not fundamentally absent, but it is highly restricted in scope. The observation that regenerated hair cells are uniformly type II-like suggests that supporting cells either lack access to type I-specific gene regulatory programs or are actively prevented from expressing them. This could also indicate that a different population of supporting cells, which require activation, could be necessary to regenerate type I-like hair cells or more type II-like hair cells. This raises key questions for future work: are there subpopulations of supporting cells, are the molecular determinants of type I identity permanently silenced in adult supporting cells, or could they be reactivated under permissive conditions? Identifying how type II-like these regenerated cells truly are and what are the underlying supporting cell populations, are two fundamental questions that need to be explored.

Molecular Specialization of Hair Cell Subtypes

The single-nucleus RNAseq analysis provides a starting point to begin to understand the molecular differences in vestibular cells. Our data identified five transcriptomically unique hair cell subtypes in the adult mouse utricles. Genes that are selectively expressed in hair cell subtypes could serve as markers, regulators of the hair cell or afferent neural (calyx) phenotype, and mechanisms to target gene misexpression to type I hair cells. The distinct gene expression signatures uncovered in type I versus type II hair cells, particularly those enriched in peripheral versus central zones, offer candidate transcriptional regulators that might also control cell fate commitment during development and reemerge (or fail to) during regeneration. For example, genes like *Mgat4c*, and *Paqr9* were highly specific to extrastriolar and striolar type I hair cell subtypes respectively, and could serve as both markers and mechanistic targets. The two clusters of extrastriolar type I hair cells found in our data are interesting. Xia et al (2025) showed *Aglb1* is expressed in extrastriolar type I hair cells. In our data, *Agbl1* shows very specific expression in only one of our extrastriolar type I hair cell clusters. The *Agbl1*-negative extrastriolar type I cluster has some transcriptional similarities to both the OCM+, striolar type I cluster as well as the other extrastriolar

type I cluster. This could indicate that this group of type I hair cells could be an intermediary group of hair cells with a different developmental trajectory or represent an edge-zone cell, potentially with dual molecular identity and or occupy a transitional spatial zone or state. The few mRNA probes we tried to distinguish regional variability of these two extrastriolar clusters showed broad expression in extrastriolar type I hair cells. These markers may have a gradient rather than strict zonation differences, have transcriptomic but not translational specificity, or the spatial expression patterns might be modulated post-transcriptionally. Although the rest of our results align with prior evidence for zonal subtypes, studies like Hoffman et al., (2018) and Desai et al. (2005a,b) already describe physiological and synaptic differences between central (striolar) and peripheral zones, more work needs to be done to understand the differences between these two extrastriolar type I hair cell groups. Comparing transcriptomic differences in hair cells pre- and post-injury, future studies could also identify key genes in hair cell degeneration and injury response. This could identify different mechanisms to protect hair cells and give us insights into hair cell regeneration.

Hair Cell Degeneration and Aging

Another compelling direction lies in understanding the signaling events that precede and accompany hair cell degeneration. Although this thesis focused on regeneration after experimentally induced ablation, it remains unclear how natural degeneration unfolds over time in damage contexts, aging, or disease. Is type I hair cell loss in older adults driven by intrinsic cellular aging, loss of afferent support, metabolic stress, or inflammatory signaling? Each of these possibilities could initiate distinct molecular cascades that either trigger apoptotic pathways or disrupt the niche environment required for hair cell maintenance. Experimental models using inducible degeneration or longitudinal sequencing and imaging of early-stage damage could help elucidate which signaling pathways mark hair cells for death over survival.

Our adult transcriptomic data aligns with morphological evidence that hair cell bodies remain stable through mid-life (Wan et al., 2019), even though synaptic loss occurs with age. Our data adds evidence that in young adult mice, hair cell identity is also preserved at the molecular level. This could indicate that age-related vestibular decline may involve changes at the synaptic level instead of loss of hair cell subtype identity. Under normal physiological conditions and after damage, type II hair cells are replaced

(Forge et al., 1993; 1998; Kawamoto et al., 2009; Golub et al., 2012; Bucks et al., 2017; Sayyid et al. 2019; Hicks et al., 2020; Ciani Berlingeri et al., 2022; Jauregui et al. 2024). This replacement could help maintain hair cell number over time.

Although our transcriptomic results revealed subtype-specific markers, it provides only a static temporal snapshot and may exclude rare transitional states or dynamic responses. Recently, Xia et al. (2025), used single-nucleus RNA sequencing to examine aging-related transcriptomic changes in the mouse inner ear, including the utricle. They showed clear transcriptomic changes, especially in one of their type I hair cell groups, as animals aged from 6 – 24 months (Xia et al., 2025). Our study, focusing on the young adult window (6-22 weeks), does not show any strong evidence of age-related shifts in marker expression or cluster proportions. Interestingly, many of our genes of interest per each hair cell cluster were not the differentially expressed genes of interest they identified in their study in older adults over time (Xia et al., 2025). This could show that these genes are stable hair cell identifiers in adult mice. In addition to Xia et al., our data suggest that major aging-associated transcriptomic reprogramming most likely emerges later in life, after a period of relative stability.

Understanding death signals may also inform how to modulate survival preemptively. For example, if type I cells are more vulnerable due to their metabolic demands or reliance on calyx innervation, enhancing trophic support or stabilizing synaptic interactions might delay degeneration in progressive conditions. Conversely, if cell death is required to trigger regeneration, as appears to be the case in some systems, then learning to fine-tune this process could allow for regeneration without catastrophic sensory loss. These ideas align with the broader question of whether “regeneration” must always follow destruction, or whether partial de-differentiation and reprogramming within surviving cells could enable functional repair.

Intrinsic Properties of Supporting Cells and Their Diversity as a Population

The requirement of *Sox2* in supporting cells for successful hair cell regeneration is particularly thought-provoking. *Sox2*’s continued expression in mature supporting cells has been interpreted as a vestige of their developmental history, but my work shows it plays an active, dosage-sensitive role in enabling plasticity after injury. Removal of *Sox2* in supporting cells, using our methods, did not appear to change the cells, but is required for the transdifferentiation into type II-like hair cells. This dual role as both a

gatekeeper of cell identity and a facilitator of transdifferentiation makes *Sox2* a potential focal point for regenerative manipulation. Whether its downstream effectors overlap with known developmental regulators like Atoh1, Gfi1, or Pou4f3, or involve unique adult-specific pathways, remains to be determined. Moving beyond the hair cells, by comparing transcriptomic differences in supporting cells pre- and post-injury, future studies could also identify whether key type I enhancers remain latent or are actively repressed in the adult epithelia. Jen et al., (2019) found adult utricular supporting cells retain open chromatin at hair-cell loci, keeping them potentially primed for regeneration. Studies on the developing vestibular epithelia that use multiomics-transcriptomics and epigenomics, are also needed to understand how supporting cells give rise to distinct hair cell types and establish the proper innervation (calyx terminals). These results could inform us on how to drive supporting cells to form new, functional type I hair cells.

Importantly, this work also highlights the need to study vestibular supporting cells more deeply, not only as latent progenitors, but as a heterogeneous population with distinct regional identities, gene expression programs, and epigenetic landscapes. It remains unclear whether all supporting cells share equal regenerative potential, or whether subsets (e.g., striolar vs. extrastriolar, utricle vs. ampulla) are more responsive to damage. Additionally, supporting cells contribute to hair cell maintenance, debris clearance, and homeostasis even in the absence of regeneration (Forge, A., & Li, L. 2000; Wan et al., 2013; Hirose et al., 2017). Exploring their non-regenerative roles and defining their interactions with neighboring hair cells, immune cells, and afferents could reveal new targets for preserving vestibular integrity before damage occurs. Technologies like spatial transcriptomics, single-nucleus multi-omics, and in vivo lineage tracing will be instrumental in dissecting the functional diversity of supporting cells and understanding how they can be coaxed toward more substantial repair. We could continue this work by sequencing these supporting cells and fate mapping their transdifferentiation at a molecular level as well as analyze what is happening to degenerative hair cells concurrently. Are hair cells expressing anything that signals supporting cells to transdifferentiate? Are all supporting cells capable of transdifferentiating? The mouse line we used as a control with the TOM reporter in supporting cells could be used to answer these questions and others.

Functional Consequences of Peripheral Type I Hair Cell Loss

Finally, the persistent behavioral deficits following peripheral type I hair cell ablation, even in the presence of intact type II and central type I hair cells, highlight that functional recovery will require not just regeneration of hair cells but regeneration of the right types in the right places. This adds evidence for premise that regenerative strategies should not simply aim to only increase total hair cell counts after damage but should also prioritize restoring the appropriate cellular architecture and circuit connectivity that underlie specific vestibular functions. This is especially relevant given the aging population and the growing recognition that vestibular dysfunction contributes to falls, cognitive decline, and loss of independence in older humans. After damage, adult mice do not regain normal VOR gains (Jauregui et al. 2024) or VsEP thresholds (Sayyid et al., 2019) upon type II hair cell replacement. Wan et al., (2019) demonstrated that deterioration of extrastriolar calyceal synapses could change reflex responses to head motions, due to loss of their non-quantal transmission resulting in impaired balance function in aged mice. In birds, both type I and type II hair cells are naturally replaced, but recovery of vestibular functions is correlated temporally with restoration of type I hair cell numbers (Carey et al., 1996; Zakir & Dickman, 2006; Haque et al., 2008). These findings suggest that peripheral replacing type I hair cells and their synaptic connections are necessary for restoring normal vestibular function in mammals. In support of this idea, preserving half of type I hair cells in parallel with type II regeneration in adult mice improves hVOR gains significantly (Jauregui et al., 2024). My findings address the importance of type I hair cells and the necessity of their regeneration for restoring vestibular-dependent motor functions and reflexes. Although my transcriptomics work has given us an in-depth look at the molecular identities of adult vestibular hair cells, further investigation is necessary to understand the functional roles of the different populations of hair cells before we can employ functional regeneration.

Limitations and future directions

While this thesis defines molecular subtypes and essential roles of vestibular hair cell subtypes in adult mice, more research is needed to understand what is required for functional regeneration. For now, we still do not know how to regenerate type I hair cells in mammals, and the molecular barriers in supporting cells that limit type I fate are also unknown. The discrete functions of each hair cell subtype also need to

be tested. Although advancement is limited due to the lack of tools available to elucidate the functional differences of each population of hair cells, I have started by identifying some of the peripheral type I hair cell functions. Hopefully, the transcriptomic data from my work will help to generate new ways of studying vestibular hair cells and their functions. Also, now that we identified utricular hair cell subtypes, we should continue transcriptomic profiling of all vestibular end organs.

Another limitation of this thesis is the lack of direct afferent characterization via recordings from vestibular neurons. Vestibular evoked recordings after peripheral type I hair cell ablation would be a great addition. Performing electrophysiological experiments such as patchseq could help to identify not only the regional and molecular information about each hair cell, but also electrophysiological signatures (e.g. loss of tonic firing) which currently remain inferred in my behavioral study. The behavioral testing explained in chapter 4 also only went up to 8 weeks post-ablation, leaving the question of whether longer-term compensation, adaptation, or substitution could eventually emerge. We know normal regeneration in adult mice results in type II-like hair cells and only 20% of them regenerate over a 60-day period with no functional regeneration ever occurring (Golub et al., 2012; Hicks et al., 2020). This led me to believe that 8 weeks (~56 days) would be long enough to see any differences in hair cells and potential functional restoration. The rotarod data suggests animals could adapt in some way as quickly as 4 weeks post ablation of peripheral type I hair cells. Other tests could take longer to improve, and the additional of older animals would allow for a more systematic analysis of these hair cells and their functions over time.

The same can be said for the transcriptomics study. We only included the transcriptomic results from 6-22 weeks (1.5-4 months) of age. A pseudotime analysis of our data, developmental data (Jan et al., 2021; Burns et al., 2015; Scheffer et al., 2015), as well as the aging data from Xia et al., 2025, could result in a complete developmental trajectory and maturation, as well as insights into degeneration. Also, analysis of crista data has been published previously which could be combined and compared with our utricle data to analyze a more complete understanding of vestibular end organs in mice, although the oldest age was P7 (Wilkerson et al., 2021). However, sequencing all separate organs at one age has not been done, leaving the possibility that chosen molecular markers are not generalized to the whole system. Additionally,

increasing throughput of sequenced utricular epithelia would provide a better representation of the genetic makeup of this each tissue.

While mouse models approximate human patterns, direct translation is limited and may differ. I also did not formally compare male vs female differences in any of my studies. Hormonal status and other sex-based differences may influence balance recovery or regeneration potential.

Building on current knowledge and the findings of this thesis, we could investigate many promising avenues for future work. Understanding the molecular mechanisms restricting type I hair cell regeneration is critical. The specific expression of genes like *Bmp2* and *Paqr9* could be functionally tested in supporting cells using gene delivery or CRISPR-based approaches for now, until potential Cre-lines are generated. Expansion of single-cell transcriptomic profiling to other vestibular organs would allow for the construction of a comprehensive molecular atlas of the adult vestibular system. Implementing spatial transcriptomics and lineage tracing will help map supporting cell heterogeneity and fate decisions, while patch-seq electrophysiology could link gene expression to functional properties. By employing next generation sequencing methods such as Flex-Seq and multiplexed library construction, we could uncover the entirety of vestibular sensory epithelia transcriptomics over particular time points simultaneously while increasing throughput and lowering costs. Expanding the behavioral tests to include VsEP thresholds could validate how specific subtypes contribute to circuit dynamics and behavior. Further work on how aging affects function and molecular identity also needs to be explored. The insights from this thesis inform regenerative strategies aiming to restore not just hair cell numbers but subtype specific identities and synaptic architecture necessary for meaningful recovery of vestibular function.

In conclusion, this work highlights the molecular specificity and functional necessity of vestibular hair cell subtypes in adult mice and opens several avenues for future exploration. By integrating insights from developmental biology, regenerative medicine, and systems neuroscience, future efforts may yet overcome the longstanding challenge of restoring vestibular function in the damaged inner ear.

Conclusion and Thesis Overview

In summary, the work presented in this thesis addresses three complementary aspects of vestibular hair cell biology; cell-type-specific functional importance, molecular identity, and capacity for regeneration, to build a more comprehensive understanding of how these sensory cells operate and how we might restore them after loss. By analyzing the role of *Sox2* in supporting cell transdifferentiation, I identified a crucial molecular mechanism governing hair cell regeneration: supporting cells must retain *Sox2* to regenerate lost hair cells. This finding not only helps explain why spontaneous vestibular hair cell regeneration in adult mammals is so limited but also highlights a potential target for enhancing regeneration. By selectively ablating peripheral type I hair cells in adult mice, I established that this subpopulation of type I hair cells is needed for certain vestibular-dependent reflexes and behaviors, confirming a functional specialization among hair cell types that had long been hypothesized but not previously proven. Through transcriptomic profiling of adult vestibular hair cells, I delineated the gene expression signatures that define type I and type II hair cells, uncovering molecular distinctions and subtypes that could underlie their physiological differences. This provided new molecular markers (and potential genetic tools) for each hair cell type and a baseline for investigating pathological or regenerative changes. Together, these studies advance our understanding of vestibular hair cell function, resilience, and plasticity. They highlight the necessity of peripheral type I hair cells for high-demand vestibular reflexes and balance tasks, define the previously unknown transcriptional diversity among adult vestibular hair cell subtypes from 6-22 wks of age, and reveal the essential role of *Sox2* in enabling supporting cell-to-hair cell transdifferentiation after damage. By linking the functional significance of specific hair cell types to their unique molecular profiles and regenerative capacity, this body of work lays important groundwork for future strategies to protect or restore vestibular function—for instance, by guiding regenerative therapies to produce the appropriate hair cell types, or by designing interventions that reactivate specific hair cell subtype genes like *Bmp2* or *Paqr9* in a controlled manner. Ultimately, a deeper knowledge of the functional, molecular, and regenerative mechanisms of vestibular hair cells is essential for combating vestibular disorders and improving balance health in aging and disease.

Bibliography for full thesis

Anniko, M. (1983). The aging vestibular hair cell. American Journal of Otolaryngology, 4(3), 151–160. https://doi.org/10.1016/S0196-0709(83)80037-4

Agrawal, Y., Carey, J. P., Della Santina, C. C., Schubert, M. C., & Minor, L. B. (2009). Disorders of Balance and Vestibular Function in US Adults: Data From the National Health and Nutrition Examination Survey, 2001-2004. Archives of Internal Medicine, 169(10), 938. https://doi.org/10.1001/archinternmed.2009.66

Agarwal, S., Mishra, A., Jagade, M., Kasbekar, V., & Nagle, S. K. (2013). Effects of Hypertension on Hearing. Indian Journal of Otolaryngology and Head & Neck Surgery, 65(3), 614–618. https://doi.org/10.1007/s12070-013-0630-1

Atkinson, P. J., Dong, Y., Gu, S., Liu, W., Najarro, E. H., Udagawa, T., & Cheng, A. G. (2018). Sox2 haploinsufficiency primes regeneration and Wnt responsiveness in the mouse cochlea. American Society for Clinical Investigation. https://doi.org/10.1172/JCI97248

Babu, V., Bahari, R., Laban, N., Kulaga, J., Abdul, Z., Zakkar, B., Al-Najjar, A., Lesus, J., Al-Rifai, A.-R., Sattar, H., Irukulla, S., Gunniya, P., Requena, T., & Lysakowski, A. (2023). RotaRod and acoustic startle reflex performance of two potential mouse models for Meniere's disease. European Journal of Neuroscience, 58(3), 2708–2723. https://doi.org/10.1111/ejn.16083

Baird, R. A., Desmadryl, G., Fernandez, C., & Goldberg, J. M. (1988). The vestibular nerve of the chinchilla. II. Relation between afferent response properties and peripheral innervation patterns in the semicircular canals. Journal of Neurophysiology. https://doi.org/10.1152/jn.1988.60.1.182

Bermingham, N. A., Hassan, B. A., Price, S. D., Vollrath, M. A., Ben-Arie, N., Eatock, R. A., Bellen, H. J., Lysakowski, A., & Zoghbi, H. Y. (1999). Math1: An essential gene for the generation of inner ear hair cells. Science (New York, N.Y.), 284(5421), 1837–1841. https://doi.org/10.1126/science.284.5421.1837

Bremer, H. G., Versnel, H., Hendriksen, F. G. J., Topsakal, V., Grolman, W., & Klis, S. F. L. (2014). Does Vestibular End-Organ Function Recover after Gentamicin-Induced Trauma in Guinea Pigs? Audiology and Neurotology, 19(2), 135–150. https://doi.org/10.1159/000357587

Brooker, R., Hozumi, K., & Lewis, J. (2006). Notch ligands with contrasting functions: Jagged1 and Delta1 in the mouse inner ear. Development, 133(7), 1277–1286. https://doi.org/10.1242/dev.02284

Bucks, S. A., Cox, B. C., Vlosich, B. A., Manning, J. P., Nguyen, T. B., & Stone, J. S. (2017). Supporting cells remove and replace sensory receptor hair cells in a balance organ of adult mice. eLife, 6, e18128. https://doi.org/10.7554/eLife.18128

Buitrago, M. M., Schulz, J. B., Dichgans, J., & Luft, A. R. (2004). Short and long-term motor skill learning in an accelerated rotarod training paradigm. Neurobiology of Learning and Memory, 81(3), 211–216. https://doi.org/10.1016/j.nlm.2004.01.001

Burns, J. C., Cox, B. C., Thiede, B. R., Zuo, J., & Corwin, J. T. (2012). In Vivo Proliferative Regeneration of Balance Hair Cells in Newborn Mice. Journal of Neuroscience, 32(19), 6570–6577. https://doi.org/10.1523/JNEUROSCI.6274-11.2012

Burns, J. C., & Corwin, J. T. (2014). Responses to Cell Loss Become Restricted as the Supporting Cells in Mammalian Vestibular Organs Grow Thick Junctional Actin Bands That Develop High Stability. Journal of Neuroscience, 34(5), 1998–2011. https://doi.org/10.1523/JNEUROSCI.4355-13.2014

Burns, J. C., Kelly, M. C., Hoa, M., Morell, R. J., & Kelley, M. W. (2015). Single-cell RNA-Seq resolves cellular complexity in sensory organs from the neonatal inner ear. Nature Communications, 6(1), 8557. https://doi.org/10.1038/ncomms9557

Bylund, M., Andersson, E., Novitch, B. G., & Muhr, J. (2003). Vertebrate neurogenesis is counteracted by Sox1–3 activity. Nature Neuroscience, 6(11), 1162–1168. https://doi.org/10.1038/nn1131

Cai, Tiantian, and Andrew K. Groves. (2015). The Role of Atonal Factors in Mechanosensory Cell Specification and Function. Molecular Neurobiology 52, no. 3: 1315–29. https://doi.org/10.1007/s12035-014-8925-0.

Callejo A., Durochat A., Bressieux S., Saleur A., Chabbert C., Domènech Juan I., Llorens J., Gaboyard Niay S. (2017). Dose dependent cochlear and vestibular toxicity of trans tympanic cisplatin in the rat. Neurotoxicology, 60, 1 9. https://doi.org/10.1016/j.neuro.2017.02.007

Carey, J. P., Fuchs, A. F., & Rubel, E. W. (1996). Hair cell regeneration and recovery of the vestibuloocular reflex in the avian vestibular system. Journal of Neurophysiology, 76(5), 3301–3312. https://doi.org/10.1152/jn.1996.76.5.3301

Ciani Berlingeri, A. N., Pujol, R., Cox, B. C., & Stone, J. S. (2022). Sox2 is required in supporting cells for normal levels of vestibular hair cell regeneration in adult mice. Hearing Research, 426, 108642. https://doi.org/10.1016/j.heares.2022.108642

Contini, D., Holstein, G. R., & Art, J. J. (2024). Simultaneous recordings from vestibular Type I hair cells and their calyceal afferents in mice. Frontiers in Neurology, 15, 1434026. https://doi.org/10.3389/fneur.2024.1434026

Contini, D., Holstein, G. R., & Art, J. J. (2020). Synaptic cleft microenvironment influences potassium permeation and synaptic transmission in hair cells surrounded by calyx afferents in the turtle. The Journal of Physiology, 598(4), 853–889. https://doi.org/10.1113/JP278680

Contini, D., Price, S.D. and Art, J.J. (2017), Accumulation of K+ in the synaptic cleft modulates activity by influencing both vestibular hair cell and calyx afferent in the turtle. J Physiol, 595: 777-803. https://doi.org/10.1113/JP273060

Contini, D., Zampini, V., Tavazzani, E., Magistretti, J., Russo, G., Prigioni, I., & Masetto, S. (2012). Intercellular K+ accumulation depolarizes Type I vestibular hair cells and their associated afferent nerve calyx. Neuroscience, 227, 232–246. https://doi.org/10.1016/j.neuroscience.2012.09.051

Corey, D. P., & Hudspeth, A. J. (1983). Kinetics of the receptor current in bullfrog saccular hair cells. The Journal of neuroscience : the official journal of the Society for Neuroscience, 3(5), 962–976. https://doi.org/10.1523/JNEUROSCI.03-05-00962.1983

Corwin, J. T., & Cotanche, D. A. (1988). Regeneration of sensory hair cells after acoustic trauma. Science (New York, N.Y.), 240(4860), 1772–1774. https://doi.org/10.1126/science.3381100

Costa, R. M., Cohen, D., & Nicolelis, M. A. L. (2004). Differential corticostriatal plasticity during fast and slow motor skill learning in mice. Current Biology: CB, 14(13), 1124–1134. https://doi.org/10.1016/j.cub.2004.06.053

Coto, J., Alvarez, C. L., Cejas, I., Colbert, B. M., Levin, B. E., Huppert, J., Rundek, T., Balaban, C., Blanton, S. H., Lee, D. J., Loewenstein, D., Hoffer, M., & Liu, X. Z. (2021). Peripheral vestibular system: Age-related vestibular loss and associated deficits. Journal of Otology, 16(4), 258–265. https://doi.org/10.1016/j.joto.2021.06.001

Curthoys, I. S., Kim, J., McPhedran, S. K., and Camp, A. J. (2006). Bone conducted vibration selectively activates irregular primary otolithic vestibular neurons in the guinea pig. Exp. Brain Res. 175, 256–267. doi: 10.1007/s00221-006-0544-1

Curthoys, I. S. (2019). Concepts and Physiological Aspects of the Otolith Organ in Relation to Electrical Stimulation. Audiology and Neurotology, 25(1–2), 25–34. https://doi.org/10.1159/000502712

Dabdoub, A., Puligilla, C., Jones, J. M., Fritzsch, B., Cheah, K. S. E., Pevny, L. H., & Kelley, M. W. (2008). Sox2 signaling in prosensory domain specification and subsequent hair cell differentiation in the developing cochlea. Proceedings of the National Academy of Sciences, 105(47), 18396–18401. https://doi.org/10.1073/pnas.0808175105

Dechesne, C. J., & Thomasset, M. (1988). Calbindin (CaBP 28 kDa) appearance and distribution during development of the mouse inner ear. Developmental Brain Research, 40(2), 233–242. https://doi.org/10.1016/0165-3806(88)90135-6

Demêmes, D., Lleixa, A., & Dechesne, C. J. (1995). Cellular and subcellular localization of AMPA-selective glutamate receptors in the mammalian peripheral vestibular system. Brain Research, 671(1), 83–94. https://doi.org/10.1016/0006-8993(94)01322-9

Desai, S. S., Ali, H., & Lysakowski, A. (2005a). Comparative Morphology of Rodent Vestibular Periphery. II. Cristae Ampullares. Journal of Neurophysiology, 93(1), 267–280. https://doi.org/10.1152/jn.00747.2003

Desai, S. S., Zeh, C., & Lysakowski, A. (2005b). Comparative Morphology of Rodent Vestibular Periphery. I. Saccular and Utricular Maculae. Journal of Neurophysiology, 93(1), 251–266. https://doi.org/10.1152/jn.00746.2003

Desmadryl, G., & Dechesne, C. J. (1992). Calretinin immunoreactivity in chinchilla and guinea pig vestibular end organs characterizes the calyx unit subpopulation. Experimental brain research, 89(1), 105–108. https://doi.org/10.1007/BF00229006

Eatock, R. A. (2018). Specializations for Fast Signaling in the Amniote Vestibular Inner Ear. Integrative and Comparative Biology, 58(2), 341–350. https://doi.org/10.1093/icb/icy069

Eatock, R. A., & Songer, J. E. (2011). Vestibular hair cells and afferents: Two channels for head motion signals. Annual Review of Neuroscience, 34, 501–534. https://doi.org/10.1146/annurev-neuro-061010-113710

El-Amraoui, A., Cohen-Salmon, M., Petit, C., & Simmler, M.-C. (2001). Spatiotemporal expression of otogelin in the developing and adult mouse inner ear. Hearing Research, 158(1), 151–159. https://doi.org/10.1016/S0378-5955(01)00312-4

Fernández, C., Baird, R. A., & Goldberg, J. M. (1988). The vestibular nerve of the chinchilla. I. Peripheral innervation patterns in the horizontal and superior semicircular canals. Journal of Neurophysiology, 60(1), 167–181. https://doi.org/10.1152/jn.1988.60.1.167

Fernández, C., & Goldberg, J. M. (1976). Physiology of peripheral neurons innervating otolith organs of the squirrel monkey. I. Response to static tilts and to long-duration centrifugal force. Journal of Neurophysiology, 39(5), 970–984. https://doi.org/10.1152/jn.1976.39.5.970

Fernandez, C., Goldberg, J. M., & Baird, R. A. (1990). The vestibular nerve of the chinchilla. III. Peripheral innervation patterns in the utricular macula. Journal of Neurophysiology. https://doi.org/10.1152/jn.1990.63.4.767

Fernandez, C., Lysakowski, A., & Goldberg, J. M. (1995). Hair-cell counts and afferent innervation patterns in the cristae ampullares of the squirrel monkey with a comparison to the chinchilla. Journal of Neurophysiology, 73(3), 1253–1269. https://doi.org/10.1152/jn.1995.73.3.1253

Flurkey, Kevin & Currer, Joanne & Harrison, David. (2007). The Mouse in Aging Research. The Mouse in Biomedical Research. 3. 10.1016/B978-012369454-6/50074-1.

Forge, A., & Li, L. (2000). Apoptotic death of hair cells in mammalian vestibular sensory epithelia. Hearing Research, 139(1), 97–115. https://doi.org/10.1016/S0378-5955(99)00177-X

Forge, A., Li, L., Corwin, J. T., & Nevill, G. (1993). Ultrastructural Evidence for Hair Cell Regeneration in the Mammalian Inner Ear. Science, 259(5101), 1616–1619. http://www.jstor.org/stable/2880671

Forge, A., Li, L., & Nevill, G. (1998). Hair cell recovery in the vestibular sensory epithelia of mature guinea pigs. Journal of Comparative Neurology, 397(1), 69–88. https://doi.org/10.1002/(SICI)1096-9861(19980720)397:1<69::AID-CNE6>3.0.CO;2-G

Geng, R., Geller, S. F., Hayashi, T., Ray, C. A., Reh, T. A., Bermingham-McDonogh, O., Jones, S. M., Wright, C. G., Melki, S., Imanishi, Y., Palczewski, K., Alagramam, K. N., & Flannery, J. G. (2009). Usher syndrome IIIA gene clarin-1 is essential for hair cell function and associated neural activation. Human Molecular Genetics, 18(15), 2748–2760. https://doi.org/10.1093/hmg/ddp210

Gillespie, P. G., & Müller, U. (2009). Mechanotransduction by Hair Cells: Models, Molecules, and Mechanisms. Cell, 139(1), 33–44. https://doi.org/10.1016/j.cell.2009.09.010

Gleeson, M., & Felix, H. (1987). A comparative study of the effect of age on the human cochlear and vestibular neuroepithelia. Acta Oto-Laryngologica. Supplementum, 436, 103–109.

Goldberg, J. M., & Fernández, C. (1977). Conduction times and background discharge of vestibular afferents. Brain research, 122(3), 545–550. https://doi.org/10.1016/0006-8993(77)90465-6

Goldberg, J. M., Desmadryl, G., Baird, R. A., & Fernández, C. (1990). The vestibular nerve of the chinchilla. V. Relation between afferent discharge properties and peripheral innervation patterns in the utricular macula. Journal of neurophysiology, 63(4), 791–804. https://doi.org/10.1152/jn.1990.63.4.791

Goldberg, J. M. (2000a). Afferent diversity and the organization of central vestibular pathways. Experimental Brain Research. Experimentelle Hirnforschung. Experimentation Cerebrale, 130(3), 277–297. https://www.ncbi.nlm.nih.gov/pmc/articles/PMC3731078/

González-Garrido, A., Pujol, R., López-Ramírez, O., Finkbeiner, C., Eatock, R. A., & Stone, J. S. (2021). The Differentiation Status of Hair Cells That Regenerate Naturally in the Vestibular Inner Ear of the Adult Mouse. Journal of Neuroscience, 41(37), 7779–7796. https://doi.org/10.1523/JNEUROSCI.3127-20.2021

Golub, J., Tong, L., Ngyuen, T., Hume, C., Palmiter, R. D., Rubel, E. W., & Stone, J. S. (2012). Hair cell replacement in adult mouse utricles after targeted ablation of hair cells with diphtheria toxin. Journal of Neuroscience, 32(43), 15093–15105.

Graham, V., Khudyakov, J., Ellis, P., & Pevny, L. (2003). SOX2 Functions to Maintain Neural Progenitor Identity. Neuron, 39(5), 749–765. https://doi.org/10.1016/S0896-6273(03)00497-5

Hasson, T., Gillespie, P. G., Garcia, J. A., MacDonald, R. B., Zhao, Y., Yee, A. G., Mooseker, M. S., & Corey, D. P. (1997). Unconventional myosins in inner-ear sensory epithelia. The Journal of Cell Biology, 137(6), 1287–1307. https://doi.org/10.1083/jcb.137.6.1287

Haque, A., Zakir, M., & Dickman, J. D. (2008). Recovery of Gaze Stability During Vestibular Regeneration. Journal of Neurophysiology, 99(2), 853–865. https://doi.org/10.1152/jn.01038.2007

Hartman, B. H., Böscke, R., Ellwanger, D. C., Keymeulen, S., Scheibinger, M., & Heller, S. (2018). Fbxo2VHC mouse and embryonic stem cell reporter lines delineate in vitro-generated inner ear sensory epithelia cells and enable otic lineage selection and Cre-recombination. Developmental Biology, 443(1), 64–77. https://doi.org/10.1016/j.ydbio.2018.08.013

Hicks, K. L., Wisner, S. R., Cox, B. C., & Stone, J. S. (2020). Atoh1 is required in supporting cells for regeneration of vestibular hair cells in adult mice. Hearing Research, 385, 107838. https://doi.org/10.1016/j.heares.2019.107838

Highstein, S. M., & Holstein, G. R. (2006). The anatomy of the vestibular nuclei. Progress in brain research, 151, 157–203. https://doi.org/10.1016/S0079-6123(05)51006-9

Hirose, K., Rutherford, M. A., & Warchol, M. E. (2017). Two cell populations participate in clearance of damaged hair cells from the sensory epithelia of the inner ear. Hearing Research, 352, 70–81. https://doi.org/10.1016/j.heares.2017.04.006

Hoffman, L. F., Choy, K. R., Sultemeier, D. R., & Simmons, D. D. (2018). Oncomodulin Expression Reveals New Insights into the Cellular Organization of the Murine Utricle Striola. JARO: Journal of the Association for Research in Otolaryngology, 19(1), 33–51. https://doi.org/10.1007/s10162-017-0652-6

Hoffman, L. F., Ross, M. D., Varelas, J., Jones, S. M., & Jones, T. A. (2006). Afferent synapses are present in utricular hair cells from otoconia-deficient mice. Hearing Research, 222(1–2), 35–42. https://doi.org/10.1016/j.heares.2006.05.013

Holt, J. C., Xue, J. T., Brichta, A. M., & Goldberg, J. M. (2006). Transmission between type II hair cells and bouton afferents in the turtle posterior crista. Journal of neurophysiology, 95(1), 428–452. https://doi.org/10.1152/jn.00447.2005

Holt, J. C., Chatlani, S., Lysakowski, A., & Goldberg, J. M. (2007). Quantal and nonquantal transmission in calyx-bearing fibers of the turtle posterior crista. Journal of Neurophysiology, 98(3), 1083–1101. https://doi.org/10.1152/jn.00332.2007

Hudspeth A. J. (1997). How hearing happens. Neuron, 19(5), 947–950. https://doi.org/10.1016/s0896-6273(00)80385-2

Hume, C. R., Bratt, D. L., & Oesterle, E. C. (2007). Expression of LHX3 and SOX2 during mouse inner ear development. Gene Expression Patterns, 7(7), 798–807. https://doi.org/10.1016/j.modgep.2007.05.002

Iwasaki S, Yamasoba T. (2015). Dizziness and Imbalance in the Elderly: Age-related Decline in the Vestibular System. Aging Dis. 2014 Feb 9;6(1):38-47. doi: 10.14336/AD.2014.0128. PMID: 25657851; PMCID: PMC4306472.

Jáuregui, E. J., Scheinman, K. L., Bibriesca Mejia, I. K., Pruett, L., Zaini, H., Finkbeiner, C., Phillips, J. A., Gantz, J. A., Nguyen, T. B., Phillips, J. O., & Stone, J. S. (2024). Sensorineural correlates of failed functional recovery after natural regeneration of vestibular hair cells in adult mice. Frontiers in Neurology, 15, 1322647. https://doi.org/10.3389/fneur.2024.1322647

Jan, T. A., Eltawil, Y., Ling, A. H., Chen, L., Ellwanger, D. C., Heller, S., & Cheng, A. G. (2021). Spatiotemporal dynamics of inner ear sensory and non-sensory cells revealed by single-cell transcriptomics. Cell Reports, 36(2), 109358. https://doi.org/10.1016/j.celrep.2021.109358

Jen, H.-I., Hill, M. C., Tao, L., Sheng, K., Cao, W., Zhang, H., Yu, H. V., Llamas, J., Zong, C., Martin, J. F., Segil, N., & Groves, A. K. (2019). Transcriptomic and epigenetic regulation of hair cell regeneration in the mouse utricle and its potentiation by Atoh1. eLife, 8, e44328. https://doi.org/10.7554/eLife.44328

Jones, S. M., & Jones, T. A. (2014). Genetics of Peripheral Vestibular Dysfunction: Lessons from Mutant Mouse Strains. Journal of the American Academy of Audiology, 25(3), 289–301. https://doi.org/10.3766/jaaa.25.3.8

Kawamoto, K., Izumikawa, M., Beyer, L. A., Atkin, G. M., & Raphael, Y. (2009). Spontaneous hair cell regeneration in the mouse utricle following gentamicin ototoxicity. Hearing Research, 247(1), 17–26. https://doi.org/10.1016/j.heares.2008.08.010

Keane, S. P., Chadman, K. K., Gomez, A. R., & Hu, W. (2024). Pros and cons of narrow- versus wide-compartment rotarod apparatus: An experimental study in mice. Behavioural Brain Research, 463, 114901. https://doi.org/10.1016/j.bbr.2024.114901

Kempfle, J. S., Turban, J. L., & Edge, A. S. B. (2016). Sox2 in the differentiation of cochlear progenitor cells. Scientific Reports, 6(1), 23293. https://doi.org/10.1038/srep23293

Kevetter, G. A., & Perachio, A. A. (1986). Distribution of vestibular afferents that innervate the sacculus and posterior canal in the gerbil. The Journal of comparative neurology, 254(3), 410–424. https://doi.org/10.1002/cne.902540312

Kiernan, A. E., Pelling, A. L., Leung, K. K. H., Tang, A. S. P., Bell, D. M., Tease, C., Lovell-Badge, R., Steel, K. P., & Cheah, K. S. E. (2005). Sox2 is required for sensory organ development in the mammalian inner ear. Nature, 434(7036), 1031–1035. https://doi.org/10.1038/nature03487

Kim, H.-J., So, H.-S., Lee, J.-H., Park, C., Lee, J.-B., Youn, M.-J., Kim, S.-J., Yang, S.-H., Lee, K.-M., Kwon, K.-B., Park, B.-H., & Park, R. (2008). Role of proinflammatory cytokines in cisplatin-induced vestibular hair cell damage. Head & Neck, 30(11), 1445–1456. https://doi.org/10.1002/hed.20892

Kim, T.-S., Nakagawa, T., Kitajiri, S., Endo, T., Takebayashi, S., Iguchi, F., Kita, T., Tamura, T., & Ito, J. (2005). Disruption and restoration of cell-cell junctions in mouse vestibular epithelia following aminoglycoside treatment. Hearing Research, 205(1–2), 201–209. https://doi.org/10.1016/j.heares.2005.03.017

Lahlou H., Zhu H., Zhou W., Edge A.S.B. (2024). Pharmacological regeneration of sensory hair cells restores afferent innervation and vestibular function. Journal of Clinical Investigation, 134 (22): e181201. doi: 10.1172/JCI181201

Leonard, R. B., & Kevetter, G. A. (2002). Molecular probes of the vestibular nerve. I. Peripheral termination patterns of calretinin, calbindin and peripherin containing fibers. Brain research, 928(1-2), 8–17. https://doi.org/10.1016/s0006-8993(01)03268-1

Li, A., Xue, J., & Peterson, E. H. (2008). Architecture of the Mouse Utricle: Macular Organization and Hair Bundle Heights. Journal of Neurophysiology, 99(2), 718–733. https://doi.org/10.1152/jn.00831.2007

Li, L., & Forge, A. (1997). Morphological evidence for supporting cell to hair cell conversion in the mammalian utricular macula. International Journal of Developmental Neuroscience: The Official Journal of the International Society for Developmental Neuroscience, 15(4–5), 433–446. https://doi.org/10.1016/s0736-5748(96)00102-5

Liberman, L. D., Wang, H., & Liberman, M. C. (2011). Opposing Gradients of Ribbon Size and AMPA Receptor Expression Underlie Sensitivity Differences among Cochlear-Nerve/Hair-Cell Synapses. The Journal of Neuroscience, 31(3), 801–808. https://doi.org/10.1523/JNEUROSCI.3389-10.2011

Lin, F. R., & Ferrucci, L. (2012). Hearing Loss and Falls Among Older Adults in the United States. Archives of Internal Medicine, 172(4), 369–371. https://doi.org/10.1001/archinternmed.2011.728

Lin, V., Golub, J. S., Nguyen, T. B., Hume, C. R., Oesterle, E. C., & Stone, J. S. (2011). Inhibition Of Notch Activity Promotes Nonmitotic Regeneration of Hair Cells in the Adult Mouse Utricles. Journal of Neuroscience, 31(43), 15329–15339. https://doi.org/10.1523/JNEUROSCI.2057-11.2011

Llorens, J., Crofton, K. M., & Peele, D. B. (1994). Effects of 3,3′-iminodipropionitrile on acquisition and performance of spatial tasks in rats. Neurotoxicology and Teratology, 16(6), 583–591. https://doi.org/10.1016/0892-0362(94)90036-1

Llorens, J., & Demêmes, D. (1994). Hair cell degeneration resulting from 3,3’-iminodipropionitrile toxicity in the rat vestibular epithelia. Hearing Research, 76(1–2), 78–86. https://doi.org/10.1016/0378-5955(94)90090-6

Luong, T. N., Carlisle, H. J., Southwell, A., & Patterson, P. H. (2011). Assessment of Motor Balance and Coordination in Mice using the Balance Beam. JoVE (Journal of Visualized Experiments), 49, e2376. https://doi.org/10.3791/2376

Lysakowski, A., Minor, L. B., Fernandez, C., & Goldberg, J. M. (1995). Physiological identification of morphologically distinct afferent classes innervating the cristae ampullares of the squirrel monkey. Journal of Neurophysiology. https://doi.org/10.1152/jn.1995.73.3.1270

Lysakowski, A., & Goldberg, J. M. (1997). A regional ultrastructural analysis of the cellular and synaptic architecture in the chinchilla cristae ampullares. The Journal of Comparative Neurology, 389(3), 419–443. https://doi.org/10.1002/(sici)1096-9861(19971222)389:3<419::aid-cne5>3.0.co;2-3

Lysakowski, A., & Goldberg, J. M. (2008). Ultrastructural Analysis of the Cristae Ampullares in the Squirrel Monkey (Saimiri sciureus). The Journal of Comparative Neurology, 511(1), 47–64. https://doi.org/10.1002/cne.21827

Madisen, L., Zwingman, T. A., Sunkin, S. M., Oh, S. W., Zariwala, H. A., Gu, H., Ng, L. L., Palmiter, R. D., Hawrylycz, M. J., Jones, A. R., Lein, E. S., & Zeng, H. (2010). A robust and high-throughput Cre reporting and characterization system for the whole mouse brain. Nature Neuroscience, 13(1), 133–140. https://doi.org/10.1038/nn.2467

Ma, E. Y., Rubel, E. W., & Raible, D. W. (2008). Notch signaling regulates the extent of hair cell regeneration in the zebrafish lateral line. The Journal of neuroscience : the official journal of the Society for Neuroscience, 28(9), 2261–2273. https://doi.org/10.1523/JNEUROSCI.4372-07.2008

Matsubara, A., Laake, J. H., Davanger, S., Usami, S., & Ottersen, O. P. (1996). Organization of AMPA receptor subunits at a glutamate synapse: a quantitative immunogold analysis of hair cell synapses in the rat organ of Corti. The Journal of neuroscience : the official journal of the Society for Neuroscience, 16(14), 4457–4467. https://doi.org/10.1523/JNEUROSCI.16-14-04457.1996

McGovern MM, Hartman B, Thawani A, Maunsell H, Zhang H, Yousaf R, Heller S, Stone J, Groves AK. Fbxo2CreERT2: A new model for targeting cells in the neonatal and mature inner ear. Hear Res. 2023 Feb;428:108686. doi: 10.1016/j.heares.2022.108686. Epub 2022 Dec 27. PMID: 36587458; PMCID: PMC9840692.

McInturff, S., Burns, J. C., & Kelley, M. W. (2018). Characterization of spatial and temporal development of Type I and Type II hair cells in the mouse utricle using new cell-type-specific markers. Biology Open, 7(11). https://doi.org/10.1242/bio.038083

Millimaki, B. B., Sweet, E. M., & Riley, B. B. (2010). Sox2 is required for maintenance and regeneration, but not initial development, of hair cells in the zebrafish inner ear. Developmental Biology, 338(2), 262–269. https://doi.org/10.1016/j.ydbio.2009.12.011

Minor, L. B., & Goldberg, J. M. (1991). Vestibular-nerve inputs to the vestibulo-ocular reflex: A functional-ablation study in the squirrel monkey. Journal of Neuroscience, 11(6), 1636–1648. https://doi.org/10.1523/JNEUROSCI.11-06-01636.1991

Monzack, E. L., May, L. A., Roy, S., Gale, J. E., & Cunningham, L. L. (2015). Live imaging the phagocytic activity of inner ear supporting cells in response to hair cell death. Cell Death and Differentiation, 22(12), 1995–2005. https://doi.org/10.1038/cdd.2015.48

Nagato, S., Sugahara, K., Hirose, Y., Takemoto, Y., Hashimoto, M., Fujii, H., & Yamashita, H. (2018). Oral administration of geranylgeranylacetone to protect vestibular hair cells. Auris Nasus Larynx, 45(3), 412–416. https://doi.org/10.1016/j.anl.2017.07.006

Nakayama, M., Helfert, R. H., Konrad, H. R., & Caspary, D. M. (1994). Scanning Electron Microscopic Evaluation of Age-Related Changes in the Rat Vestibular Epithelium. Otolaryngology—Head and Neck Surgery. https://doi.org/10.1177/019459989411100617

Neves, J., Uchikawa, M., Bigas, A., & Giraldez, F. (2012). The Prosensory Function of Sox2 in the Chicken Inner Ear Relies on the Direct Regulation of Atoh1. PLOS ONE, 7(1), e30871. https://doi.org/10.1371/journal.pone.0030871

Neves, J., Vachkov, I., & Giraldez, F. (2013). Sox2 regulation of hair cell development: Incoherence makes sense. Hearing Research, 297, 20–29. https://doi.org/10.1016/j.heares.2012.11.003

Oesterle, E. C., Campbell, S., Taylor, R. R., Forge, A., & Hume, C. R. (2008). Sox2 and JAGGED1 expression in normal and drug-damaged adult mouse inner ear. Journal of the Association for Research in Otolaryngology: JARO, 9(1), 65–89. https://doi.org/10.1007/s10162-007-0106-7

Ohlemiller, K. K., Jones, S. M., & Johnson, K. R. (2016). Application of Mouse Models to Research in Hearing and Balance. Journal of the Association for Research in Otolaryngology, 17(6), 493–523. https://doi.org/10.1007/s10162-016-0589-1

Ono, K., Keller, J., López Ramírez, O., González Garrido, A., Zobeiri, O. A., Chang, H. H. V., Vijayakumar, S., Ayiotis, A., Duester, G., Della Santina, C. C., Jones, S. M., Cullen, K. E., Eatock, R. A., & Wu, D. K. (2020a). Retinoic acid degradation shapes zonal development of vestibular organs and sensitivity to transient linear accelerations. Nature Communications, 11(1), Article 1. https://doi.org/10.1038/s41467-019-13710-4

Ono, K., Sandell, L. L., Trainor, P. A., & Wu, D. K. (2020b). Retinoic acid synthesis and autoregulation mediate zonal patterning of vestibular organs and inner ear morphogenesis. Development, 147(15), dev192070. https://doi.org/10.1242/dev.192070

Orvis, J., Gottfried, B., Kancherla, J., Adkins, R. S., Song, Y., Dror, A. A., Olley, D., Rose, K., Chrysostomou, E., Kelly, M. C., Milon, B., Matern, M. S., Azaiez, H., Herb, B., Colantuoni, C., Carter, R. L., Ament, S. A., Kelley, M. W., White, O., … Hertzano, R. (2021). gEAR: Gene Expression Analysis Resource portal for community-driven, multi-omic data exploration. Nature Methods, 18(8), 843–844. https://doi.org/10.1038/s41592-021-01200-9

Pan, N., Kopecky, B., Jahan, I., & Fritzsch, B. (2012). Understanding the evolution and development of neurosensory transcription factors of the ear to enhance therapeutic translation. Cell and Tissue Research, 349(2), 415–432. https://doi.org/10.1007/s00441-012-1454-0

Park, J. C., Hubel, S. B., & Woods, A. D. (1987). Morphometric analysis and fine structure of the vestibular epithelium of aged C57BL/6NNia mice. Hearing Research, 28(1), 87–96. https://doi.org/10.1016/0378-5955(87)90156-0

Park, J. J., Tang, Y., Lopez, I., & Ishiyama, A. (2001). Age-related change in the number of neurons in the human vestibular ganglion. Journal of Comparative Neurology, 431(4), 437–443. https://doi.org/10.1002/1096-9861(20010319)431:4<437::AID-CNE1081>3.0.CO;2-P

Pastras, C. J., Curthoys, I. S., Asadnia, M., McAlpine, D., Rabbitt, R. D., & Brown, D. J. (2023a). Evidence That Ultrafast Nonquantal Transmission Underlies Synchronized Vestibular Action Potential Generation. The Journal of Neuroscience, 43(43), 7149–7157. https://doi.org/10.1523/JNEUROSCI.1417-23.2023

Pastras, C. J., Curthoys, I. S., Asadnia, M., McAlpine, D., Rabbitt, R. D., & Brown, D. J. (2023b). Evidence That Ultrafast Nonquantal Transmission Underlies Synchronized Vestibular Action Potential Generation. The Journal of Neuroscience, 43(43), 7149–7157.

Perez, F. A., & Palmiter, R. D. (2005). Parkin-deficient mice are not a robust model of parkinsonism. Proceedings of the National Academy of Sciences, 102(6), 2174–2179. https://doi.org/10.1073/pnas.0409598102

Pevny, L. H., & Nicolis, S. K. (2010). Sox2 roles in neural stem cells. The International Journal of Biochemistry & Cell Biology, 42(3), 421–424. https://doi.org/10.1016/j.biocel.2009.08.018

Pujol, R., Pickett, S. B., Nguyen, T. B., & Stone, J. S. (2014). Large basolateral processes on type II hair cells are novel processing units in mammalian vestibular organs. Journal of Comparative Neurology, 522(14), 3141–3159. https://doi.org/10.1002/cne.23625

Puligilla, C., & Kelley, M. W. (2016). Dual role for Sox2 in specification of sensory competence and regulation of Atoh1 function. Developmental Neurobiology, 77(1), 3–13. https://doi.org/10.1002/dneu.22401

Purcell, I. M., & Perachio, A. A. (2001). Peripheral patterns of terminal innervation of vestibular primary afferent neurons projecting to the vestibulocerebellum in the gerbil. Journal of Comparative Neurology, 433(1), 48–61. https://doi.org/10.1002/cne.1124

Rauch, S. D., Velazquez-Villaseñor, L., Dimitri, P. S., & Merchant, S. N. (2006). Decreasing Hair Cell Counts in Aging Humans. Annals of the New York Academy of Sciences, 942(1), 220–227. https://doi.org/10.1111/j.1749-6632.2001.tb03748.x

Rosenhall, U., & Rubin, W. (1975). Degenerative changes in the human vestibular sensory epithelia. Acta Oto-Laryngologica, 79(1–2), 67–80. https://doi.org/10.3109/00016487509124657

Rüsch, Alfons, Anna Lysakowski, and Ruth Anne Eatock. (1998). Postnatal Development of Type I and Type II Hair Cells in the Mouse Utricle: Acquisition of Voltage-Gated Conductances and Differentiated Morphology. Journal of Neuroscience 18, no. 18: 7487–7501. https://doi.org/10.1523/JNEUROSCI.18-18-07487.1998.

Ryals, B. M., & Rubel, E. W. (1988). Hair cell regeneration after acoustic trauma in adult Coturnix quail. Science (New York, N.Y.), 240(4860), 1774–1776. https://doi.org/10.1126/science.3381101

Sadeghi, S. G., Minor, L. B., & Cullen, K. E. (2007). Response of vestibular-nerve afferents to active and passive rotations under normal conditions and after unilateral labyrinthectomy. Journal of neurophysiology, 97(2), 1503–1514. https://doi.org/10.1152/jn.00829.2006

Sayyid, Z. N., Wang, T., Chen, L., Jones, S. M., & Cheng, A. G. (2019). Atoh1 Directs Regeneration and Functional Recovery of the Mature Mouse Vestibular System. Cell Reports, 28(2), 312-324.e4. https://doi.org/10.1016/j.celrep.2019.06.028

Scheffer, D. I., Shen, J., Corey, D. P., & Chen, Z.-Y. (2015). Gene Expression by Mouse Inner Ear Hair Cells during Development. Journal of Neuroscience, 35(16), 6366–6380. https://doi.org/10.1523/JNEUROSCI.5126-14.2015

Schlecker, C., Praetorius, M., Brough, D. E., Presler, R. G., Hsu, C., Plinkert, P. K., & Staecker, H. (2011). Selective atonal gene delivery improves balance function in a mouse model of vestibular disease. Gene Therapy, 18(9), 884–890. https://doi.org/10.1038/gt.2011.33

Schmitz, F., Königstorfer, A., & Südhof, T. C. (2000). RIBEYE, a component of synaptic ribbons: a protein's journey through evolution provides insight into synaptic ribbon function. Neuron, 28(3), 857–872. https://doi.org/10.1016/s0896-6273(00)00159-8

Shaham, O., Smith, A. N., Robinson, M. L., Taketo, M. M., Lang, R. A., & Ashery-Padan, R. (2009). Pax6 is essential for lens fiber cell differentiation. Development, 136(15), 2567–2578. https://doi.org/10.1242/dev.032888

Shiga, A., Nakagawa, T., Nakayama, M., Endo, T., Iguchi, F., Kim, T.-S., Naito, Y., & Ito, J. (2005). Aging Effects on Vestibulo-Ocular Responses in C57BL/6 Mice: Comparison with Alteration in Auditory Function. Audiology and Neurotology, 10(2), 97–104. https://doi.org/10.1159/000083365

Shoji, H., Takao, K., Hattori, S., & Miyakawa, T. (2016). Age-related changes in behavior in C57BL/6J mice from young adulthood to middle age. Molecular Brain, 9, 11. https://doi.org/10.1186/s13041-016-0191-9

Shou J, Zheng JL, Gao WQ (2003) Robust generation of new hair cells in the mature mammalian inner ear by adenoviral expression of Hath1. Mol Cell Neurosci 23(2):169-79. doi: 10.1016/s1044-7431(03)00066-6.PMID: 12812751

Simmons, D. D., Tong, B., Schrader, A. D., & Hornak, A. J. (2010). Oncomodulin identifies different hair cell types in the mammalian inner ear. Journal of Comparative Neurology, 518(18), 3785–3802. https://doi.org/10.1002/cne.22424

Slowik, A. D., & Bermingham-McDonogh, O. (2013). Hair cell generation by notch inhibition in the adult mammalian cristae. Journal of the Association for Research in Otolaryngology: JARO, 14(6), 813–828. https://doi.org/10.1007/s10162-013-0414-z

Slowik, A. D., & Bermingham-McDonogh, O. (2013-REVIEW). Notch signaling in mammalian hair cell regeneration. Trends in Developmental Biology, 7, 73–89. https://www.ncbi.nlm.nih.gov/pmc/articles/PMC4199338/

Songer, J. E., & Eatock, R. A. (2013). Tuning and Timing in Mammalian Type I Hair Cells and Calyceal Synapses. Journal of Neuroscience, 33(8), 3706–3724. https://doi.org/10.1523/JNEUROSCI.4067-12.2013

Soto, E., Vega, R., & Budelli, R. (2002). The receptor potential in type I and type II vestibular system hair cells: A model analysis. Hearing Research, 165(1–2), 35–47. https://doi.org/10.1016/s0378-5955(01)00418-x

Spaiardi, P., Marcotti, W., Masetto, S., & Johnson, S. L. (2022). Signal transmission in mature mammalian vestibular hair cells. Frontiers in Cellular Neuroscience, 16. https://doi.org/10.3389/fncel.2022.806913

Staecker, H., Praetorius, M., Baker, K., & Brough, D. E. (2007). Vestibular Hair Cell Regeneration and Restoration of Balance Function Induced by Math1 Gene Transfer. Otology & Neurotology, 28(2), 223. https://doi.org/10.1097/MAO.0b013e31802b3225

Steevens, A. R., Glatzer, J. C., Kellogg, C. C., Low, W. C., Santi, P. A., & Kiernan, A. E. (2019). SOX2 is required for inner ear growth and cochlear nonsensory formation before sensory development. Development, 146(13). https://doi.org/10.1242/dev.170522

Stone, J. S., Pujol, R., Nguyen, T. B., & Cox, B. C. (2021). The transcription factor Sox2 is required to maintain the cell type-specific properties and innervation of type II vestibular hair cells in adult mice. The Journal of Neuroscience: The Official Journal of the Society for Neuroscience, 41(29), 6217–6233. https://doi.org/10.1523/JNEUROSCI.1831-20.2021

Stone, J. S., Wisner, S. R., Bucks, S. A., Mellado Lagarde, M. M., & Cox, B. C. (2018). Characterization of Adult Vestibular Organs in 11 CreER Mouse Lines. Journal of the Association for Research in Otolaryngology, 19(4), 381–399. https://doi.org/10.1007/s10162-018-0676-6

Takahashi, Kazutoshi, and Shinya Yamanaka. (2006). Induction of Pluripotent Stem Cells from Mouse Embryonic and Adult Fibroblast Cultures by Defined Factors.” Cell 126, no. 4: 663–76. https://doi.org/10.1016/j.cell.2006.07.024.

Taylor, R. R., Filia, A., Paredes, U., Asai, Y., Holt, J. R., Lovett, M., & Forge, A. (2018). Regenerating hair cells in vestibular sensory epithelia from humans. eLife, 7, e34817. https://doi.org/10.7554/eLife.34817

Taylor, R. R., Jagger, D. J., Saeed, S. R., Axon, P., Donnelly, N., Tysome, J., Moffatt, D., Irving, R., Monksfield, P., Coulson, C., Freeman, S. R., Lloyd, S. K., & Forge, A. (2015). Characterizing human vestibular sensory epithelia for experimental studies: New hair bundles on old tissue and implications for therapeutic interventions in ageing. Neurobiology of Aging, 36(6), 2068–2084. https://doi.org/10.1016/j.neurobiolaging.2015.02.013

Tong, L., Strong, M. K., Kaur, T., Juiz, J. M., Oesterle, E. C., Hume, C., Warchol, M. E., Palmiter, R. D., & Rubel, E. W. (2015). Selective Deletion of Cochlear Hair Cells Causes Rapid Age-Dependent Changes in Spiral Ganglion and Cochlear Nucleus Neurons. Journal of Neuroscience, 35(20), 7878–7891. https://doi.org/10.1523/JNEUROSCI.2179-14.2015

Tung, V. W. K., Burton, T. J., Dababneh, E., Quail, S. L., & Camp, A. J. (2014). Behavioral Assessment of the Aging Mouse Vestibular System. JoVE (Journal of Visualized Experiments), 89, e51605. https://doi.org/10.3791/51605

Wan, G., Corfas, G., & Stone, J. S. (2013). Inner ear supporting cells: rethinking the silent majority. Seminars in cell & developmental biology, 24(5), 448–459. https://doi.org/10.1016/j.semcdb.2013.03.009

Wan, G., Ji, L., Schrepfer, T., Gong, S., Wang, G.-P., & Corfas, G. (2019). Synaptopathy as a Mechanism for Age-Related Vestibular Dysfunction in Mice. Frontiers in Aging Neuroscience, 11. https://doi.org/10.3389/fnagi.2019.00156

Wang, G.-P., Chatterjee, I., Batts, S. A., Wong, H. T., Gong, T.-W., Gong, S.-S., & Raphael, Y. (2010). Notch signaling and Atoh1 expression during hair cell regeneration in the mouse utricle. Hearing Research, 267(1), 61–70. https://doi.org/10.1016/j.heares.2010.03.085

Wang, T., Chai, R., Kim, G. S., Pham, N., Jansson, L., Nguyen, D.-H., Kuo, B., May, L. A., Zuo, J., Cunningham, L. L., & Cheng, A. G. (2015). Lgr5+ cells regenerate hair cells via proliferation and direct transdifferentiation in damaged neonatal mouse utricle. Nature Communications, 6(1), 6613. https://doi.org/10.1038/ncomms7613

Wang, T., Niwa, M., Sayyid, Z. N., Hosseini, D. K., Pham, N., Jones, S. M., Ricci, A. J., & Cheng, A. G. (2019). Uncoordinated maturation of developing and regenerating postnatal mammalian vestibular hair cells. PLOS Biology, 17(7), e3000326. https://doi.org/10.1371/journal.pbio.3000326

Wang, T., Yang, T., Kedaigle, A., Pregernig, G., McCarthy, R., Holmes, B., Wu, X., Becker, L., Pan, N., So, K., Chen, L., He, J., Mahmoudi, A., Negi, S., Kowalczyk, M., Gibson, T., Druckenbrod, N., Cheng, A. G., & Burns, J. (2024). Precise genetic control of ATOH1 enhances maturation of regenerated hair cells in the mature mouse utricle. Nature communications, 15(1), 9166. https://doi.org/10.1038/s41467-024-53153-0

Warchol, M. E., Lambert, P. R., Goldstein, B. J., Forge, A., & Corwin, J. T. (1993). Regenerative proliferation in inner ear sensory epithelia from adult guinea pigs and humans. Science, 259(5101), 1619–1622. https://doi.org/10.1126/science.8456285

Wersall, J. (1956). Studies on the structure and innervation of the sensory epithelium of the cristae ampulares in the guinea pig; a light and electron microscopic investigation. Acta Oto-Laryngologica Supplementum, 126, 1–85.

Wu, J., Li, W., Lin, C., Chen, Y., Cheng, C., Sun, S., Tang, M., Chai, R., & Li, H. (2016). Co-regulation of the Notch and Wnt signaling pathways promotes supporting cell proliferation and hair cell regeneration in mouse utricles. Scientific Reports, 6(1), 29418. https://doi.org/10.1038/srep29418

Xia, Mingyu, Feng Zhang, Jiaoyao Ma, et al. “Single-Nucleus Profiling of Mouse Inner Ear Aging Uncovers Cell Type Heterogeneity and Hair Cell Subtype-Specific Age-Related Signatures.” Cell Reports 44, no. 6 (2025): 115781. https://doi.org/10.1016/j.celrep.2025.115781.

Xu, J.-C., Huang, D., Hou, Z.-H., Guo, W.-W., Sun, J.-H., Zhao, L.-D., Yu, N., Young, W.-Y., He, D. Z.-Z., & Yang, S.-M. (2012). Type I hair cell regeneration induced by Math1 gene transfer following neomycin ototoxicity in rat vestibular sensory epithelium. Acta Oto-Laryngologica, 132(8), 819–828. https://doi.org/10.3109/00016489.2012.673233

Zakir, M., & Dickman, J. D. (2006). Regeneration of Vestibular Otolith Afferents after Ototoxic Damage. Journal of Neuroscience, 26(11), 2881–2893. https://doi.org/10.1523/JNEUROSCI.3903-05.2006

Zeng, S., Ni, W., Jiang, H., You, D., Wang, J., Lu, X., Liu, L., Yu, H., Wu, J., Chen, F., Li, H., Wang, Y., Chen, Y., & Li, W. (2020). Toxic Effects of 3,3 ′-Iminodipropionitrile on Vestibular System in Adult C57BL/6J Mice In Vivo. Neural Plasticity, 2020(1), 1823454. https://doi.org/10.1155/2020/1823454